CRACK IDENTIFICATION IN AN OFFSHORE STRUCTURAL FRAME THROUGH STATIC SUBSTRUCTURING AND FINITE ELEMENT METHOD

MD. RABIUL ALAM

Crack Identification in an Offshore Structural Frame through Static Substructuring and Finite Element Method

by

© Md. Rabiul Alam, B. Sc. Eng.

A thesis submitted to the School of Graduate Studies

in partial fulfillment of the requirements for the degree of

Master of Engineering

Faculty of Engineering and Applied Science

Memorial University of Newfoundland

September, 2001

St. John's Newfoundland Canada

Abstract

Identification of crack in an offshore structural frame using static substructuring and finite element approach was carried out by comparing local stresses, strains and global displacement results between uncracked and cracked structures. For simplicity of calculation and reduction of computational time and resources, a two-dimensional plane frame instead of the actual three-dimensional space frame structure was used in the numerical analysis; substructuring technique in finite element method was utilized as the numerical analysis methodology. In order to develop finite element meshes of this plane frame, eight noded degenerate isoparametric shell elements with reduced Gaussian integration points were used over the entire structure. ABAQUS finite element software was used to solve the problem and process all information relating to the above-mentioned global and local responses. Numerical results obtained in the analysis have been verified (for correctness) by using earlier published information and comparison with those obtained using other types of elements available in ABAQUS.

From the analysis mentioned above, it was observed that the rate of change of normalized global displacements of a cracked structure becomes a maximum within the crack region; in addition, enormous changes in normalized local strains develop around the crack region. These parameters could be used to detect the crack and its position in real structures by the processing of information obtained from installed sensors (triaxial strain gauges, LVDTs and accelerometers) at various critical regions of the structure.

Acknowledgement

This thesis was completed under the supervision of Dr. A. S. J. Swamidas, Professor, Faculty of Engineering and Applied Science, Memorial University of Newfoundland, St. John's, Canada. My heartiest gratitude and sincere appreciation to him for his affectionate guidance, helpful suggestions, continuous supervision, sympathetic cooperation and expert counsel at all stages of the development of this thesis.

I would like to thank Dr. M. R. Haddara, Associate Dean, Faculty of Engineering and Applied Science, and Dr. R. Seshadri, Dean of the Faculty of Engineering and Applied Science, who provided all the necessary facilities for me to pursue Master's degree in this university.

I am also deeply grateful to all teachers who taught theory courses during my graduate days. Finally, I would like to thank to my friends Mr. Md. Ahsan Shamim and Mr. Li Pan, for their help in using computer and valuable discussions during my research time.

Contents

List of Tables and Figures

List of Tables

List of Figures

List of Symbols

CPU	Central processing unit
c	Length of the crack
D	Chord diameter
DOF	Degree of freedom
[D]	Elasticity matrix
d	Brace diameter
E	Modulus of elasticity
h_i	directional thickness at node i
[J]	Jacobian matrix
K_I	Mode I stress intensity factor
K_{II}	Mode II stress intensity factor
K_{III}	Mode III stress intensity factor
[K]	Stiffness matrix
$[K]^e$	Element stiffness matrix
$[K_r]$	Reduced or condensed stiffness matrix
L	Chord length
l_{3i}, m_{3i}, n_{3i}	directional cosine of the vector V_{3i}
MPC	Multi-point Constraints
[N]	Shape function matrix
N_i	Shape function at node i

$\{P\}$	Force vector
$\{P_r\}$	Reduced force vector
r	Radius of the brace member
SCF	Stress concentration factor
S11, S22	Stresses in local 1- and 2- directions
[S]	Element properties matrix
T	Chord thickness
t	Brace thickness
$\{u\}$	Degrees of freedom vector
$\{u_e\}$	Eliminated degrees of freedom
$\{u_r\}$	Retained degrees of freedom
u, v, w	displacements in the global x, y, z directions
u_i, v_i, w_i	displacements in the global x, y, z directions at node i
u', v', w'	displacements in the local x',y',z' directions
v_1, v_2, v_3	unit vectors in the x_1', x_2' and x_3' directions, respectively
$\mathbf{V}_{1i}$,$\mathbf{V}_{2i}$,$\mathbf{V}_{3i}$	Vectors along the nodal co-ordinate axes
$\hat{v}_{1i}$, $\hat{v}_{2i}$, $\hat{v}_{3i}$	unit vectors in the direction of $\mathbf{V}_{1i}$, $\mathbf{V}_{2i}$ and $\mathbf{V}_{3i}$
x, y, z	Global Cartesian co-ordinates
x_i, y_i, z_i	Cartesian co-ordinates of node i
x_1', x_2', x_3'	Local Cartesian co-ordinates
x', y', z'	Local Cartesian co-ordinates
α_i, β_i	Rotations of normal at node i

γ_e	Surface energy per unit crack area
$\gamma_{x'y'}, \gamma_{x'z'}$ $\gamma_{y'z'}$	Shearing strain in local x′, y′ and z′ axes, respectively
$\{\delta\}$	Vector of the element nodal variables
ε	Strain
$\varepsilon_{11}, \varepsilon_{22}$	Strains in local 1- and 2- directions
$\varepsilon_{x'}, \varepsilon_{y'}$	Normal strain in local x′ and y′ axes, respectively
$\{\varepsilon'\}$	Strain vector in local co-ordinate system
ζ, η, ξ	Curvilinear co-ordinates set
$[\theta]$	Directional cosine matrix
κ	Shear deformation correction factor
ν	Poisson's ratio
σ	Applied nominal stress
σ_{crit}	Critical stresses for plane stress and plane strain condition
$\sigma_{x'}, \sigma_{y'}$	Stresses in local x′ and y′ axes, respectively
τ	Nominal shearing stress
$\tau_{x'y'}, \tau_{x'z'}$ $\tau_{y'z'}$	Shearing stresses in local x′, y′ and z′ axes, respectively

Chapter 1

Introduction

1.1 General

Natural sources of energy such as oil and gas are abundant in many offshore regions of the world. The demand for exploration and production of these resources has increased worldwide during the last few decades. A large number structures of various types and sizes have been installed in many offshore regions around the world, mainly for production and processing of oil and gas. Steel jacket structure is one of the structures that is used widely for the construction of offshore platforms (Figure 1.1). These jacket structures are fabricated by joining together steel tubular members using welding procedures. Any welded joint in a complex structure like a steel jacket structure is a potential failure site. Damage can be initiated at any of these critical points in spite of taking proper care in the design and fabrication of the joints. Hence, the long-term integrity of the welded joints of these structures must be maintained to ensure their safe and reliable operation.

Offshore structural applications in hostile environments require high performance joints made of tubular members. Due to severe corrosion and random cyclic loadings, fatigue cracking of structures is one of the main problems that causes degradation of the long-term integrity of offshore structures. Various kinds of flaws ranging from microscopic

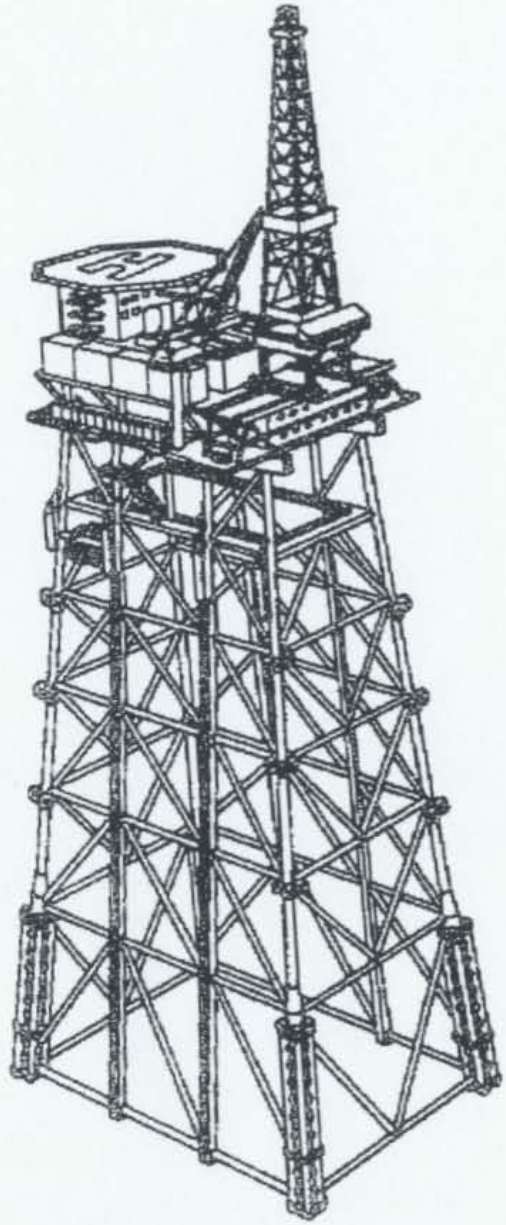

Figure 1.1: An offshore jacket structure (Dover and Rao 1996)

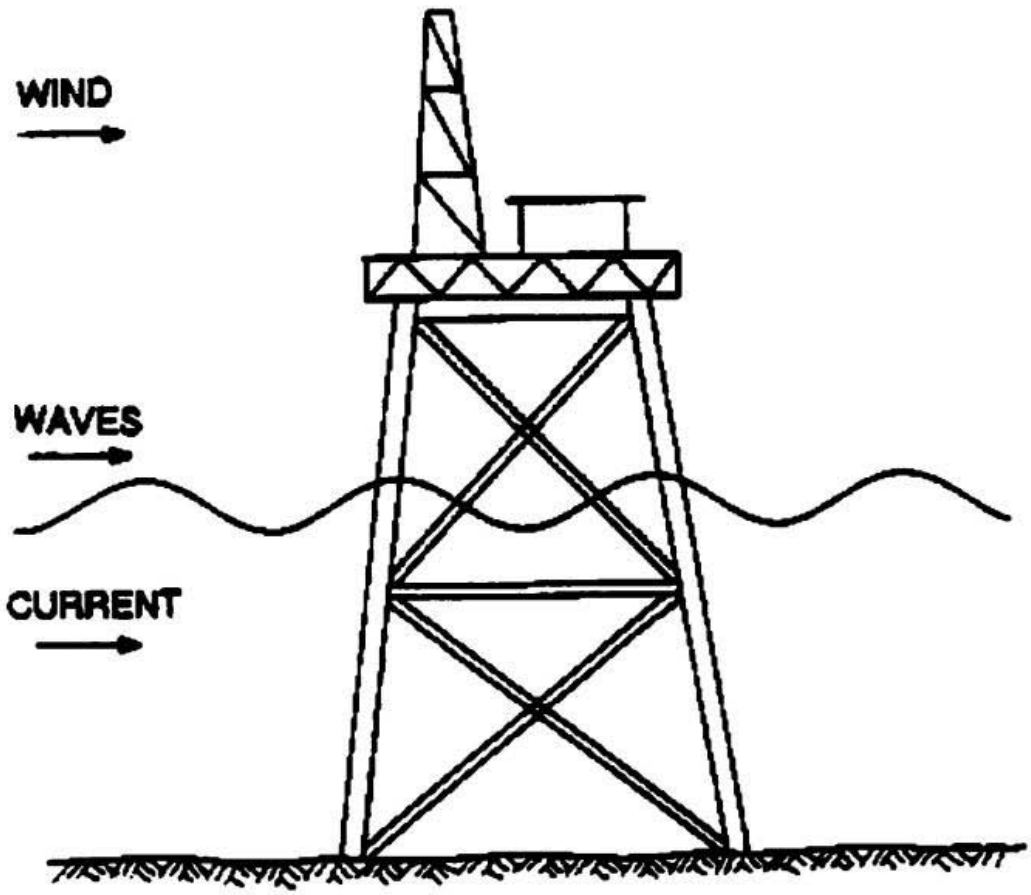

Figure 1.2: Environmental loading on a steel jacket offshore platform (Nwosu 1993).

material defects to macroscopic geometric imperfections (due to fabrication and construction processes) are contained in steel jacket structures. Crack can develop from such flaws due to the combined cyclic action of wind, wave, and current loadings (shown in Figure 1.2) exerted by the harsh and hostile offshore environment. Besides the above,

degradation of structural materials due to corrosion is also not negligible. Corrosion affects offshore steel structures due to their constant exposure to seawater action.

Offshore structures, in general, are likely to suffer fatigue cracking during their service lives that would affect their overall performance; in addition, if any one of the crack sizes becomes very large, then the structure may also experience catastrophic failure. For this reason, continuous monitoring of the structural performance is essential to prevent such catastrophic occurrences. When any fault such as cracking, delamination, debonding, or loosening of a part occurs in the structure, it will cause a decrease in stiffness (and perhaps an increase in damping), in a local region of the structure; this will affect the structural properties locally as well as globally. While the global effects due to the presence of a small crack at a local region are marginal and almost insignificant, the local effects around the crack zone will be significant and noticeable.

Conventionally the steel jacket structure of an offshore platform is modeled, using planar/spatial beam elements (having hollow tubular cross sections), in finite element analysis. The advantages in the choice of this section are: (i) high-torsional rigidity; (ii) symmetry of sectional properties; (iii) same omnidirectional property with respect to fluid flow in horizontal direction; (iv) simplicity of shape; and (v) pleasing appearance. It also possesses great structural advantages (relative bending strength and stiffness properties) as structural elements, but the intersection becomes quite complex when it is joined to other tubular members. In recent years, researchers have been able to overcome this difficulty due to well developed intersecting techniques and refined welding processes.

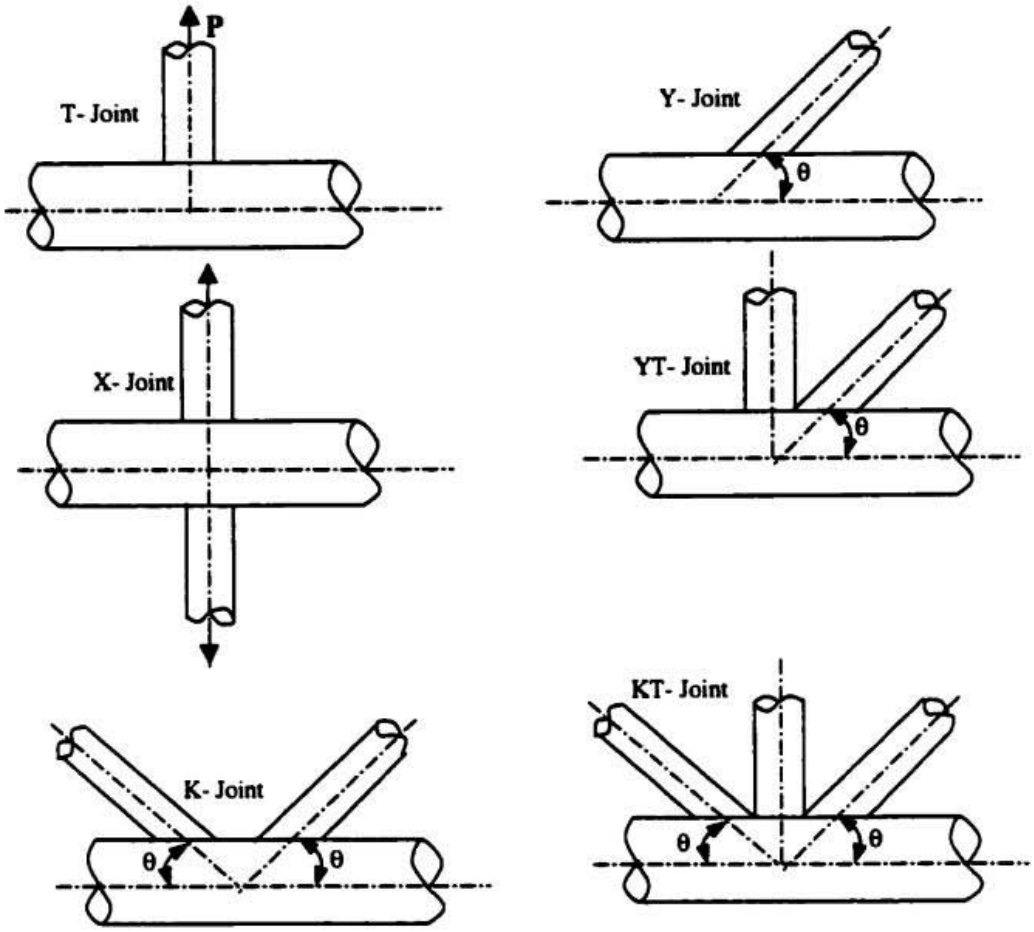

Figure 1.3: Different types offshore structure tubular joints (Dover and Rao 1996).

The three-dimensional geometry of an offshore structure tubular joint has a large number of configurations; even two-dimensional in-plane connections have many configurations. Normally T, Y, K, KT, X, and L type connections are used in plane frame structures made up of tubular members (Figure 1.3). The types of connection used depend on the position of the braces. In case of static vertical load transfer, brace members do not carry much loads. Most of the loads are carried by the main chord members. But in case of

horizontal dynamic loading (due to the wave and wind environment) brace members are fully active in transferring loads from chord to brace. Due to the abrupt changes in geometry and presence of welded seams severe stress concentrations occur at the intersection of brace and chord. At certain critical locations it could be several times higher (nearly 30 to 40 times) than that occurring in the original structure without welded seams and geometric changes. The location of the maximum stress, where cracking is most likely to initiate, will most probably be around the junctions of tubular members which are subjected to axial forces and in-plane/out-of-plane bending moments. The crack may be initiated at the saddle or crown or any other locations around the hot spot region, depending on the nature of loading in members mating at the joint (Berge 1996).

In this study dealing with the analysis of an offshore plane frame structure with or without crack, the frame is subdivided into a number of substructures, called super elements, and the connectivity matrices that join these super elements are retained for global analysis. Once the global analysis has been carried out, the local responses in each of the super elements are examined for the presence of any possible cracking. When the pre- and post- damaged regions are superposed and examined for anomalies, then the crack region will become obvious. Thus the crack region could be monitored in a continuous manner. This thesis discusses the growth of a through-thickness crack around the hot spot region of a tubular joint, using superelements and finite element analysis procedure; it also details the various changes that occur around the welded seams and these changes are used in laying out a procedure to locate and detect cracking in tubular-jointed plane frame structures.

1.2 Scope of the Thesis

Up to date numerous research investigations have been carried out for determining the stress and strain state around the crack regions for a single-jointed configuration such as T-, Y-, TK- or others. No studies have been reported (to the best of the author's knowledge), in open literature, on the computation of stress-strain information of the entire structure containing cracks in the critical hot spot region of welded joints. In the present study, the global displacements and local stress-strain variations of a tubular jointed structure containing one or two cracks have been analyzed.

1.3 Organization of the Thesis

The following outline provides a brief description of the contents of the thesis:

Chapter 2 covers the literature survey based on cracked structural analysis from the aspects of classical approaches, application of line spring elements in cracked structures, and use of 3-D solid elements & plane plate elements with quarter point node shifting. The influence of cracks on the static and dynamic behaviour is also presented in this Chapter; in addition, it also covers the literature survey based on the development of substructure finite element method, and its application to the analysis of large structures.

Chapter 3 deals with the theory regarding the degenerate isoparametric shell elements, which have been used to model the structure. It also covers the theory related to the effect of shifting the mid-point node to quarter point in isoparamtric shell elements and the use of substructuring and superelement techniques.

Chapter 4 deals with the modeling procedures used for the entire tubular-jointed plane frame structure without and with a crack. It gives the results of detailed analyses of uncracked and cracked plane frame structures considering the influence of different crack modelling, in the near and far-fields of the crack region.

The variation of stresses and strains in elements near and far away from the crack zone due to the extension of crack around the hot spot region of the tubular-jointed structure, has been discussed in Chapter 5. Conclusions drawn from this thesis investigation, as well as areas for further research, are discussed in Chapter 6.

Chapter 2

Literature Review

2.1 General

The exploration for offshore oil and gas was begun in the Gulf of Mexico after 1947 and in the North Sea during the 1966. Number of offshore platforms have been installed in various water depths, starting from a modest depth of 6 m in 1947 to 310 m by 1978 (Cognac) and 412 m by 1988 (Bullwinkle). Since most of the natural resources are available in the deeper continental shelf and slope regions of the world, oil and gas industry has always attempted to install large platforms in the deep waters of the ocean. Due to recent innovations in structural concepts and fabrication technology, the installation of deep water structures has been quite successful, even in 600 m to 2000 m deep waters. One such structure is the Roseau Tower proposed for installation in 1000 m of water (Reddy and Arockiasamy 1991). Most of these structures are constructed of tubular-jointed steel frames, using medium strength weldable steels.

Sea environment is a hostile one for the recovery of oil and gas and always generates forces which are cyclic in nature. Due to the repeated nature of loading, fatigue cracking is likely to be developed at the critical locations of welded junctions of tubular members.

A recent study has identified that the main cause of repair to North Sea offshore platform structures is fatigue (Dover and Rao 1996). Besides these types of flaws, dents in structural members due to ship collisions, loosening of structural parts during in-service operation, debonding and delamination during fabrication/construction, operations, etc., also occur in structures.

It has been recognized that small cracks could propagate under fatigue loading and spread along the intersection before proceeding through the thickness and causing failure of the joint or even catastrophic failure of the entire structure (Paranavitana 1996). When any of these flaws are developed at any location on the structure, it will change the platform's structural properties; in addition, it will also change the stress distributions around the crack region, shifting energy from the crack region and to the crack tip region. In order to predict stress distributions accurately in the critical regions of the offshore structural joints, numerous research investigations have been carried out during the last four decades. In analyzing the stress fields around a complex and cracked tubular joint, finite element method and fracture mechanics approach have been used successfully with some degree of sophistication. The precise mathematical derivation of the stress and strain fields in and around the weld is precluded due to the complex geometry of the joint configuration. Currently two methods are widely used in offshore industries for the estimation of stress-strain distribution around the critical regions of cracked tubular joints as well as to compute the fatigue life of the structure. These two methods are based on S-N (stress-life) and fracture mechanics approaches.

For the detection of any type of cracks in an offshore structure, numerous techniques based on structural vibration concepts have been developed. Non-destructive inspection techniques have been used to detect and identify anomalies between cracked and uncracked structures without damaging the actual structure. Vibration measurements are effective, inexpensive and fast procedures for non-destructive examination of a structure (Gdoutos 1993). Vibration techniques, which use sensitive and accurate instruments (accelerometers and signal analyzers) that are integrated with detailed mathematical analysis of response data, measure quantitatively the changes in vibration responses and these are used for evaluating the entire condition of the structure. A brief discussion of these methods is given in the subsequent section of this thesis.

2.2 Classical Analysis of Cracked Structures

When any fault such as cracking, delamination, debonding, etc., is developed in the structure, it changes its local and global stiffnesses and perhaps the damping of the structure. Since damping phenomena is very much sensitive to the environmental condition, detection of a crack considering change in damping is almost impossible. Most of the research studies related to crack analysis have been carried out considering the change in stiffness before and after cracking of the structure. Crack can be developed in the structure as an open crack or breathing crack. Open crack is a simplifying assumption made in representing a cracked region; the crack always remain open both during the opening and closing cycle of the vibrating motion of the structure. Breathing (open and close) cracks develop due to the effect of cyclic loading on the structure. Fatigue cracking

is an example of this type. Crack opens in the structure when the load produces a tensile strain around the crack region and closes when the reverse phenomena occurs. Most of the researchers have used open crack model for the static and dynamic analyses of a cracked structure. In order to investigate the change in stiffness due to cracking of a structural member, different kinds of open crack models have been used by a number of researchers. Some of them are, short beam, linear spring, reduced Young's modulus, reduced moment of inertia and fracture mechanics models. Brief descriptions of these models are given below.

Short beam model: Before mid-seventies, many researchers were using this model for the analysis of a cracked structure. The advantages of this model are that the analytical solution using finite element analysis can be established easily. In this model, cracked regions are isolated from the main structure and this isolated region is considered as a short beam with lesser moment of inertia. Thomson and Madison (1949) used this model for the determination of the effect of a narrow crack on flexural, longitudinal and torsional vibrations of a slander bar. The analytical expression between the short beam length and the depth of a symmetric discontinuity (or crack) and its location along a longitudinally uniform beam has been developed by Springer et al (1987). In spite of the various advantages of this model, it can not be used exactly as an alternate form for the actual crack influence. The variation of stresses in this model around the cracked regions will be quite different in comparison with the real situation.

Linear Spring Model: When any crack is developed in the structure, it reduces the stiffness of the structure. In linear spring model, this reduced stiffness, in a cracked portion, is idealized to a linear spring. Many researchers have used this model for various purposes. Haisty and Springer (1985) used linear spring elements as a substitute for crack in the investigation of the longitudinal vibration of a uniform beam containing two symmetrical cracks. They obtained the equivalent spring stiffness using fracture mechanics concept. The same authors developed spring stiffness of a beam with a double-sided open crack for tensile, bending and torsional loading (1988). Since the presence of cracks in the structure changes its natural frequencies, some researchers have used this concept to detect crack. Gomes and Silva (1991) investigated this change in natural frequency using a flexural spring model. Despite the various uses of the linear spring model, it has also some additional disadvantages. This model cannot properly incorporate the damping influence; in addition the stress distribution near the crack region would also be quite different from the actual state of stress in the region.

Reduced Young's Modulus and Moment of Inertia Models: Crack in a structural member reduces the local cross sectional area of a structure. For this reason, moment of inertia in the cracked portion decreases as the crack grows. It is well known that the stiffness matrix of different kinds of elements is completely dependent on the material and geometric properties of the elements used in finite element method. Sometimes Young's modulus controls the material properties and moment of inertia (bending behaviour) and cross sectional area (axial behaviour) controls the geometric properties. In finite element modelling, it is easier to assume a change in Young's modulus to represent

the presence of a crack than a change in the moment of inertia. In actuality, Young's modulus is not affected by cracking occurring in the structure; but the apparent change in Young's modulus is assumed as an equivalent and simpler alternative to represent the change in stiffness that occurs due to cracking. It has one advantage that no new elements are required to model the cracking.

2.3 Basic Fracture Mechanics Approach for a Cracked Structure

The analysis of stress and displacement fields, along with a postulate predicting the structural failure causing cracking, is essential for the mechanical design of engineering structures. To obtain information about deformation as well as the stress and strain fields of cracked structures, engineers normally use fracture mechanics approach and finite element method. The objective of fracture mechanics approach is to determine the load-carrying capacity of structures in the presence of cracks, voids or inclusions (which can also be modelled as a dominant crack (Gdoutos 1993). The other objective of this approach, which is applicable for engineering design, is the determination of critical load of a structure by considering the size and location of an initial flaw. The engineering design based on fracture mechanics needs knowledge of critical crack size and behavior during crack extension. Two kinds of strength failures, such as brittle and ductile failures from the macroscopic point of view, are usually considered in fracture mechanics approaches. The brittle failure causes only small deformations, and usually is sudden in nature. On the other hand, ductile failure causes large deformations over a relatively long time period and is associated with yielding or plastic flaw and high energy dissipation

rates. A great number of structures have been lost due to brittle failure over the centuries, resulting in loss of human lives and enormous wealth.

The fracture of a solid depends on a variety of factors such as macroscopic effect, microscopic phenomena and the composition of the material. Few of the fracture mechanisms that occur at different scale levels are shown in Figure 2.1. For the study of rupture of cohesive bond in a solid, principle of quantum mechanics should be used. In case of a homogeneous continuum material, continuum mechanics and classical thermodynamic concepts are required. These two cases deal with the movement of dislocations, formation of sub-grain boundary precipitates and slip band, grain inclusions and voids (Gdoutos 1993).

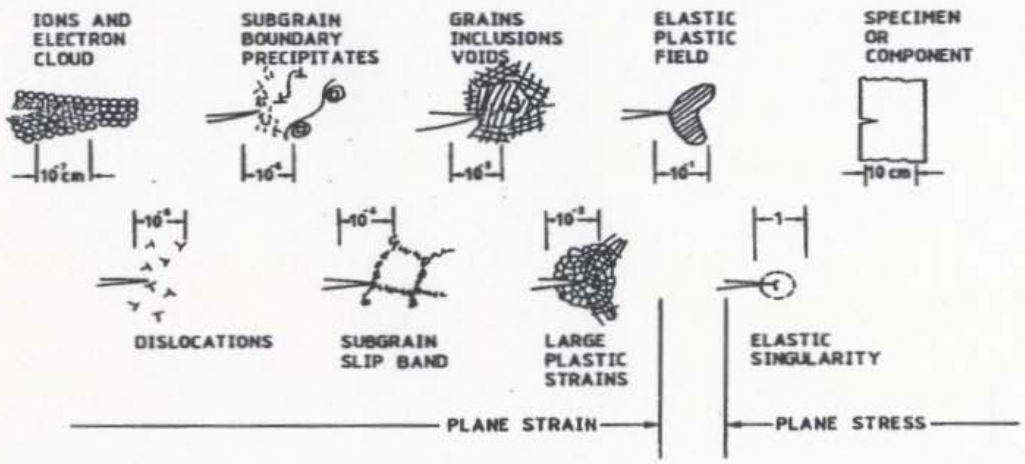

Figure 2.1. Fracture mechanisms at different scale levels (Gdoutos 1993).

Crack driving force is an important parameter in fracture mechanics studies. This force is a function of material behavior, crack size, structural geometry and loading conditions. The critical value of this force is called fracture toughness and it indicates the ability of material to resist fracture in the presence of cracks. In structural applications, lower fracture toughness is essential for most of the design cases where small initial cracks exist. In this case a higher yield strength material should be used. However, when the size of crack is large, higher fracture toughness would be preferable (Gdoutos 1993). Earliest theoretical work on the elastic stress distribution surrounding a crack in a stressed plate was published by Inglis (1913). He also showed that for a given particular crack size, there is a critical value of stress above which unstable fracturing of material will occur. Later on the weakening effect of cracks produced in a material was identified properly by Griffith (1920). The results of both Inglis and Griffith studies show that the stresses ultimately tend to infinity at the crack tip, due to a steep stress gradient near the crack tip. Using energy balance assumption, Griffith developed a fracture criterion. This criterion is written as,

$$\sigma\sqrt{a} = \left(\frac{2\gamma_e E}{\pi}\right)^{1/2} \tag{2.1}$$

where 'σ' is the applied nominal stress, 'a' is the crack length and γ_e is the surface energy per unit crack area. Griffith energy balance assumption was that the energy required to create new surfaces in the material was proportional to the fracture area from which energy is released. Griffith also discovered that the fracture strength is inversely proportional to the square root of the crack size for brittle fracture behavior.

According to Griffith criterion, the critical stresses for plane stress and plane strain condition can be written as

$$\sigma_{crit.} = \left(\frac{2\gamma_e E}{\pi a}\right)^{1/2} \qquad \textit{Plane stress}$$

$$\sigma_{crit.} = \left(\frac{2\gamma_e E}{\pi a(1-\nu^2)}\right)^{1/2} \qquad \textit{Plane strain} \tag{2.2}$$

where E is the Young's modulus, and ν the Poisson's ratio.

2.4 Linear Elastic Stress Fields in Cracked Structures

When any crack is developed in a structure, it leads to high stresses near the crack tip. For this reason inelastic deformation and non-linear effects occur near the crack tip in a ductile material. The stress distribution in the cracked body can be linear or non-linear depending on the inelastic deformation and other nonlinear effects. When inelastic deformation and nonlinear effect are small with respect to crack length and other characteristic lengths of the body, linear elastic theory is adequate to calculate the stress distribution in the cracked structure; otherwise non-linear fracture mechanics theory becomes necessary.

Crack normally extends within the body according to three basic failure modes. These modes are, opening mode, sliding mode and tearing mode. In opening mode (I) crack surfaces separate symmetrically with respect to the crack plane, viz., along the plane perpendicular to crack plane. In sliding mode (II) crack surfaces slide relative to each

other symmetrically with respect to the plane perpendicular to the crack plane. In tearing mode (III) crack surfaces slide relative to each other skew-symmetrically with respect to both planes (Gdoutos 1993). These three modes are shown in Figure 2.2.

The stress and displacement fields are essential to describe the stresses and strains in the neighborhood of the crack tip, because these fields govern crack extension behavior near the crack tip. The stress fields of the above three deformation modes are given below. For the calculation of these fields, an infinite plate with a crack length of 2a subjected to equal stresses σ at infinity along both axes (shown in Figure 2.3) is considered.

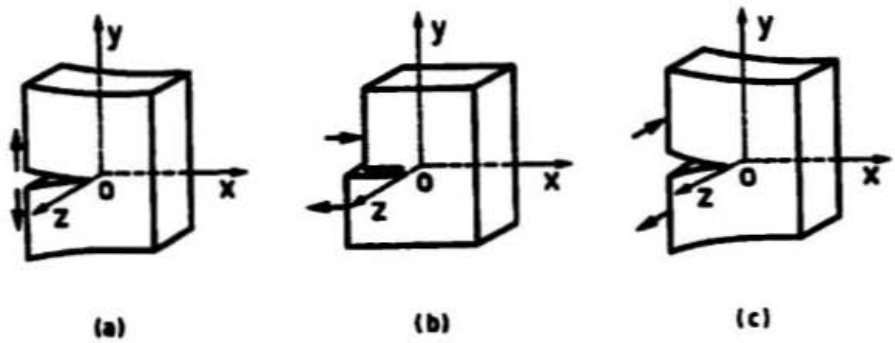

Figure 2.2: The three basic modes of crack extension; (a) Opening mode, I, (b) Sliding mode, II, and (c) Tearing (or antiplane) mode, III, (Gdoutos 1993)

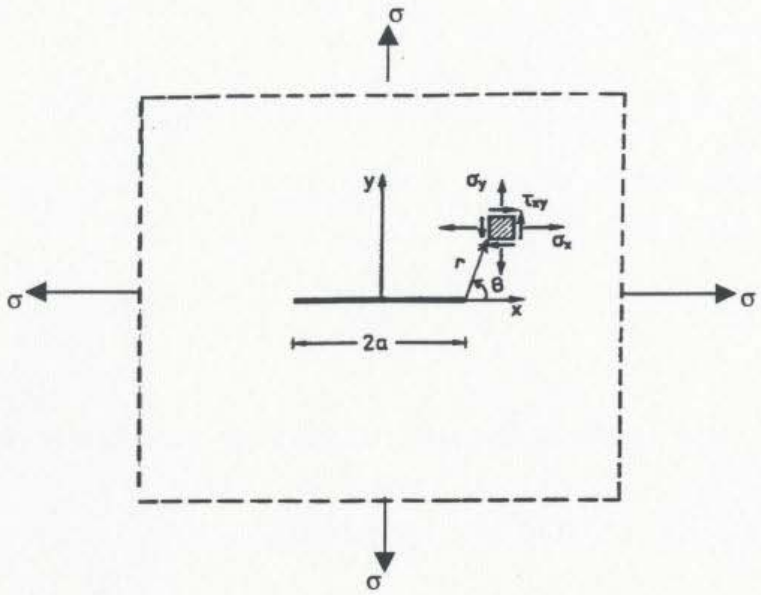

Figure 2.3: A crack of length 2a in an infinite plate subjected to a uniform stress σ at infinity, along both axes (Gdoutos 1993)

In opening mode (Mode I),

$$\sigma_x = \frac{K_I}{\sqrt{2\pi r}}\cos\frac{\theta}{2}\left(1-\sin\frac{\theta}{2}\sin\frac{3\theta}{2}\right)$$
$$\sigma_y = \frac{K_I}{\sqrt{2\pi r}}\cos\frac{\theta}{2}\left(1+\sin\frac{\theta}{2}\sin\frac{3\theta}{2}\right) \qquad (2.3)$$
$$\tau_{xy} = \frac{K_I}{\sqrt{2\pi r}}\cos\frac{\theta}{2}\sin\frac{\theta}{2}\sin\frac{3\theta}{2}$$

where K_I is the opening mode stress intensity factor and its value is given by,

$$K_I = \sigma\sqrt{\pi a} \qquad (2.4)$$

and r is the radial distance of the element, θ is the angle from x axes, and σ_x and σ_y are the normal stresses corresponding to plane x and y and τ_{xy} is the shear stress on those planes.

In sliding mode (Mode II), the stress field is given by,

$$\sigma_x = \frac{K_{II}}{\sqrt{2\pi r}} \sin\frac{\theta}{2}\left(2 + \cos\frac{\theta}{2}\cos\frac{3\theta}{2}\right)$$
$$\sigma_y = \frac{K_{II}}{\sqrt{2\pi r}} \sin\frac{\theta}{2}\cos\frac{\theta}{2}\cos\frac{3\theta}{2} \qquad (2.5)$$
$$\tau_{xy} = \frac{K_{II}}{\sqrt{2\pi r}} \cos\frac{\theta}{2}\left(1 - \sin\frac{\theta}{2}\sin\frac{3\theta}{2}\right)$$

where K_{II} is the sliding mode stress intensity factor and its value is given by,

$$K_{II} = \tau\sqrt{\pi a} \qquad (2.6)$$

In tearing mode (Mode III), the stresses σ_x, σ_y and τ_{xy} will be zero. The stress field for this mode is,

$$\tau_{xz} = -\frac{K_{III}}{\sqrt{2\pi r}} \sin\frac{\theta}{2}$$
$$\tau_{yz} = -\frac{K_{III}}{\sqrt{2\pi r}} \cos\frac{\theta}{2} \qquad (2.7)$$

where

$$K_{III} = \tau\sqrt{\pi a}$$

2.5 Influence of Cracks in a Steel Jacket Structure due to Dynamic Loading

As described earlier most of the offshore jacket structures are made of steel tubular members. Welding is usually used to connect brace and chord members. Due to severe environmental loading, geometric discontinuities of the members mating at a joint, weld zone inhomogeneity, etc., fatigue cracking is likely to occur at the junctions of tubular members. These cracks initiate first at the highly stressed regions as multiple cracks along the weld toe regions and they coalesce very fast to form a single crack; then the single crack starts to grow through the thickness of the chord or brace wall. From metallic engineering point of view, it is well known that severe failures of metallic structures occur due to cyclic loading. This type of loading reduces the strength of structures and causes cracking consisting of different phases such as crack initiation, coalescence, propagation, and catastrophic failure. Numerous research investigations based on theoretical and experimental studies have been carried out to predict the effects of these cracks before they lead to severe structural failures.

The conventional design approach for the prediction of fatigue life of the structure involves the use of (fatigue) stress-life (S-N) curves. This approach requires only the knowledge of the hot-spot stresses and strains and it does not take into account the presence of an initial crack (or cracks). For this reason, this method leads to an overestimation of life in case of real structures where crack initiation stage is small due to the pre-existing faults. Normally constant amplitude S-N data are used in the design for

fatigue in welded structures. However, an offshore structure will always experience random loading due to the real ocean wave environment. In the case of variable amplitude or random loading, Miner-Palmgren cumulative damage law is used to calculate the fatigue damage and it gives almost accurate results in conjunction with the fracture mechanics approach. This cumulative law is based on the assumption that the damage on the structure per cycle of loading is constant at a given stress range. Since it is difficult to distinguish between crack initiation and crack propagation in the conventional S-N method, development of fracture mechanics approach in conjunction with finite element analysis has made possible the prediction of fatigue life for any type of situation.

In fracture mechanics approach, the total fatigue life is divided into three characteristic stages. These stages are initiation, propagation and ultimate failure. The ultimate failure stage is not considered in most practical design cases, especially for offshore steel structures since it leads to a rapid brittle fracture. Microscopic level of cracking is considered as initiation stage and macroscopic level of cracking is considered as propagation stage. From the microscopic point of view, damage is associated with the process of nucleation and growth of micro-voids and cavities (Wang et al 1997). In these cases, the rupture of atomic bonds due to high local stresses causes material separation and this phenomena may be approached from different points of view, viz., either from on atomic approach (concept based on quantum mechanics) or continuum mechanics approach (Gdoutos 1993). In the atomic approach, material deformations are considered to occur within distances between the particles of the order of 10^{-7} cm; in continuum mechanics approach, it is considered for distances greater than 10^{-2} cm and the material is

considered to be a homogeneous continuum. The crack initiation life is normally calculated by the concept of local strain approach. In this method the material responses (of many components) at critical locations are strain or deformation dependent. It means that fatigue is a localized process and the regions of stress concentration in the structure are the most probable crack initiation zones. Due to the existence of the local plastic deformation, plasticity effects are considered in crack initiation stage explicitly. The equation of strain-life curves for the fatigue resistance of the structure, at the critical location, is given by:

$$\frac{\Delta\varepsilon}{2} = \frac{\sigma'_f}{E}(2N_f)^b + \varepsilon'_f(2N_f)^c \qquad (2.8)$$

where E = elastic modulus, σ'_f = fatigue strength coefficient, ε'_f = fatigue ductility coefficient, b = fatigue strength exponent, c = fatigue ductility exponent, and N_f = crack initiation life of the specimen.

During recent years, researchers have paid considerable attention to estimate the crack propagation life of offshore steel structures. To characterize the fracture behavior of the tubular joint, two parameters such as nominal hot spot stress and crack size are used. An analytical procedure based on stress field magnitude and stress distribution near the crack tip is used in linear elastic fracture mechanics approach. Due to stress concentration in the vicinity of a crack tip, large elastic stresses are developed near the crack tip for any small loading on the cracked body and these stresses are characterized by the stress intensity

factor. The deformations and stresses at the crack tip can be prescribed by one or a combination of the three modes of crack extension, described earlier in section 2.4. However it depends on the geometry and loading conditions of the cracked body. Fatigue crack propagation rate (da/dN) can also be related to the stress intensity factor range. A number of theories and empirical equations have been established regarding this relationship. The most common relationship that is used to calculate the fatigue life of a tubular joint is the Paris power law given by;

$$\frac{da}{dN} = C(\Delta K)^m \tag{2.9}$$

where C and m are material constants, and ΔK is the stress intensity factor (SIF) range.

From this equation, the propagation life is calculated by integrating from the initial flaw size (a_i) to the critical flaw size (a_c) as:

$$N_p = \int_{a_i}^{a_c} \frac{da}{C(\Delta K)^m} \tag{2.10}$$

The total fatigue life (N_T) is equal to the sum of the cycles during crack initiation (N_f) and cycles during crack propagation (N_p) and is expressed by,

$$N_T = N_f + N_p \tag{2.11}$$

Several researchers have determined the crack propagation life and total fatigue life of the tubular welded joint structure by using different methods. Nwosu (1993) worked on fatigue strength analysis of offshore tubular welded joints under constant amplitude loading. He used local stress-strain and linear elastic fracture mechanics approaches for the numerical investigation of the total fatigue life of offshore tubular welded joints, under the action of axial, in-plane and out-of-plane bending loads and compared his results with experimental results and parametric equations. He obtained a good agreement with the experimental results.

Qian (1996) used strain energy density factor theory to estimate of the propagation of surface crack in tubular T-joints. His study basically focused on the propagation direction of a surface crack in tubular T-joints and the surface crack profile. To obtain the variation of SIF along the crack fronts of prefabricated semi-elliptic surface cracks at the hot spots of tubular T-joints, he used photoelasticity and finite element method. He concluded that the crack is developed in tubular T-joints due to mixed-mode loading, and the distribution of SIF along the front edge of the crack depends not only on a/T, the ratio of crack depth to thickness of chord wall, but also on the crack shape ratio a/c (the ratio of depth of the crack 'a' to its length 'c'). From this study, it was concluded that a crack can be influenced by several factors such as geometry of the joint, size, shape and orientation of the crack, loading conditions, material properties etc.

2.6 Damage Identification Procedures

Identification of damage in a structure is an important research area in the civil, mechanical, and aerospace engineering communities. Damage in any kind of structure reduces its in-service capability, degrades its performance, and even could contribute to the loss of enormous wealth and human lives. Damage is defined as changes introduced into a system either intentionally or unintentionally that severely affects the present and future behaviour of that system. The identification of damage in any structure is almost impossible, if there is no idea about the original state of the intact structure. A number of methods have been developed for the identification of damage in a structure. These methods are classified herein as conventional methods and vibration based methods.

Conventional methods: These methods are essentially localized experimental measurement methods. They collect all the relevant local information of the structure and carry out detailed data analyses to identify damage in structures. The available conventional methods for the identification of damage in a structure are Visual Inspection, Liquid or Dye Penetrant Inspection, Magnetic Particle Inspection (MPI), Electromagnetic Techniques, Ultrasonic, Radiography, Alternating Current Potential Difference (ACPD) Technique, Eddy Current Technique, Alternating Current Field Measurement (ACFM) Technique and Acoustic Emission. All of these methods are only applicable if only portions of the structure are being inspected and as well they are readily accessible.

Visual inspection

The under-water inspection of offshore structures using this technique gives an overall notion of the general condition of the structure. This method is normally of two categories. One is the general visual inspection and the other is the close visual inspection. Marine growth, major physical defects, debris, scour and cathodic protection survey are assessed by the general visual inspection. The diver inspects all the configurations of the structure, which are underwater. Close circuit TV, video probes and still photograph are required to assist the diver in data acquisition and interpretation. No highly sophisticated instruments are needed for this survey. To carry out observation in the vicinity of a weld, the close visual inspection method (using video probes) is normally used. In this method, marine-growth-free and paint-coating-free surface is required to assess the image and weld conditions.

Magnetic Particle Inspection (MPI)

This method depends on the phenomena of magnetic flux leakage. The main idea of MPI method is, to induce magnetic flux lines in a ferro-magnetic material by applying external magnetic forces. When induced flux lines meet a defect and cross the defect, magnetic poles are formed, where they enter and leave the material. If very fine ferro-magnetic particles are passed in a carrier fluid to the area under inspection, it will be attracted by these poles. By observing particles' coalescence, defects can be found out in the structure. In case of underwater inspection, special lamps are used to produce ultra-violet light. The particles, which fluoresce under this light, are used to create visibility in underwater environment. This method is commonly used to identify and locate any surface crack

present in the structure. The disadvantages of this method are that it is applicable to ferro-magnetic material only and it is often very difficult to obtain a permanent record of the results.

Ultrasonic

The basic principle of this method is that, ultrasonic signals are generated by moving an ultrasonic probe containing a piezoelectric crystal that generates this signal over the surface of the body to be examined. The reflected waves from the examined body are also received by the same probe. The source of reflection and the position of defect can be located and identified by measuring the time delay between the emitted signal and the reception of each reflection. It is the most flexible, convenient and practical method to identify and locate any internal flaw present in the body, determine weld quality and assess the tube wall thickness.

Radiography

This method is actually used to detect the internal defects of a structural body. X-ray or γ-ray is passed through the surface of the examined body and observation is made on the absorbed amount of traversed waves. A defect absorbs less of the rays traversing it than a homogeneous material. The intensity variations due to flaw in the body are represented on the photographic film. Shadow picture image on the film indicates the defect. Permanent record of the inspection is possible in this method.

Alternating Current Potential Difference Technique

This technique is based on the principle of electric current flow. By using a simple relationship between the crack depth and the electrical potential difference, the crack depth for an infinitely long crack can be measured. For an infinitely long crack, crack depth = 0.5 D $\{(V_c/V_r) - 1\}$, where D is the probe electrode spacing, V_c is the potential difference measured across the crack and V_r is the reference potential difference measured in the uncracked body across the probes (Dover and Rao 1996). For a small crack depth, measurement does not give the true depth of crack. In this case a correction factor is required for the calculation of the true depth. This technique is used only for depth calculation of known surface breaking faults and also needs a coating-free surface.

Alternating Current Field Measurement (ACFM) Technique

In this technique, absolute quantities of surface magnetic fields that are produced from an induced magnetic field parallel to the crack are measured. The crack depth sizing is carried out by using the measurement of the components of magnetic field. The theory involved in this method is that when a current flows on the surface (X-Y plane) of a metallic structure, then the magnetic flux density in any direction (either X or Y) is proportional to the current in that perpendicular direction; the magnetic flux density in the Z- direction is proportional to the curvature of current in the X-Y plane (Dover and Rao 1996). In ACFM technique, application of uniform current flow into the specimen is required and measurement of magnetic field components in the air above the specimen is used. For a quick examination of the surface using single or multiple sensors, this method is especially useful.

Eddy Current Technique

Eddy current is induced when currents flow in an electrical conductor by the time and / or space variation of an applied magnetic field. The magnitude and phase of the induced eddy current are affected by a defect in the body. Eddy current instrument is used to convert AC signal from the coil to a DC signal that can be interpreted by the operator. This technique works by the measurement of change in impedance in a coil due to an induced voltage in a coil (Dover and Rao 1996). Impedance of signal (from induced voltage) is displayed directly in case of a general purpose eddy current instrument and shows a complete picture of what is going on in the coil. By using special probes and particular setting on the instrument, crack is detected in welds. Surface crack detection in conductors, sub-surface defect detection in non-magnetic conductors, tube and bar inspection, metal sorting and layer thickness measurement are carried out by this technique. Measurement of signal with phase information distinguishes it from ACFM. The advantages of this technique are that it can detect faults quickly without any surface contact and that it has a useful sizing capability for imperfect flaw detection.

2.7 Vibration-based Damage Detection Methods

The defect identification methods discussed in the previous section require the vicinity of the damage to be known and the portions of the structure being inspected to be readily accessible. To overcome these drawbacks, researchers have tried to develop a global damage detection method so that proper information about the damage of the structure could be easily obtained. In recent years, vibration-based damage detection technique has

been used to give information about the global behavior of the structure. Numerous research studies have been done in last three decades to establish this method. Sophisticated experimental techniques such as modal testing have been developed and firmed up. Other methods such as Wavelet Techniques and Laser-based Vibration Procedures have also been developed to enhance crack detection in the high frequency ranges and in a remote non-contact manner. It is well known that when any fault occurs in a structure, it will change the stiffness properties and perhaps damping of the structure. This concept is utilized in modal testing. From a theoretical point of view, it is known that modal parameters such as natural frequencies, mode shapes and modal damping are functions of the physical properties (mass, damping and stiffness) of the structure. Therefore, changes in the physical properties will cause noticeable changes in these modal parameters. These parameters can be used as indicators for the identification of damage in a structure. Roitman et al (1991) used modal analysis technique to detect damage in tubular joints of fixed offshore structures. They compared modal amplitude responses of intact and damaged structures. They concluded that modal analysis could be used to detect damage in tubular joints of fixed offshore structure.

Chen and Swamidas (1993) developed a procedure for modal testing using global sensors and local sensors. They used an accelerometer and a linear variable displacement transducer (LVDT) as global sensors and strain gauges as local sensors. In addition to experimental investigation, they also carried out finite element analysis to confirm the accuracy of experimental results. They concluded that global sensors could determine changes of natural frequencies due to small cracks existing in the structure. In the

following section a brief description is given detailing how each indicator is influenced by the defect.

Defect Indicators

Natural frequencies: Natural frequencies are global properties of a structure. It can be measured at any location of the structure and will remain unchanged. If any fault is developed in the structure, it will change the various natural frequencies of that structure. This change can be significant for a small structure but it will not be significant for a large structure; the influence depends on how much the presence of the crack affects the overall stiffness of the structure. If the overall reduction in stiffness is very small, then the change in frequency will also be very small. In large structures the changes are usually so small that crack detection by using this concept is almost unreliable and sometimes researchers are confused in determining whether it comes from the removal of the non-structural mass or some actual defect. To find out the location and size of a crack by using this concept alone is rather difficult, since similar cracks at different locations can produce the same changes in natural frequencies. Farrar et al (1994) demonstrated in a Report published by Los Alamos National Laboratory Report that the changes in natural frequencies were not sensitive enough for detecting defects in large structures. They conducted tests on an Interstate 40 highway bridge. They reduced the cross-sectional stiffness at the center of the main plate girder by 96.4% (by cutting it) and the bending stiffness of the overall bridge cross-section by 21%, but they didn't get any significant reduction in modal frequencies.

Mode Shapes: Since changes in physical properties produce changes in modal parameters (natural frequencies, mode shapes and modal damping factors), mode shapes can also be considered as indicators for the detection of damage, in conjunction with natural frequencies. Mode shape is a local as well as global characteristic of the structure. This indicator can give local responses by providing the local changes in mode shapes if any defects occur in a local region and also can give global responses due to a defect occurring in a local region. Changes in global mode shapes are usually very small and will become dominant only when defect in a local region is quite large. Normally higher frequency modes capture the local responses whereas lower frequency modes tend to capture global responses of the structure and are less sensitive to local damage in a structure. The measurement of responses from higher modes is very difficult. From an experimental point of view, it is seen that to produce measurable responses in the higher frequency ranges of a large scale test structure would require much larger amounts of energy than that required for exciting lower frequencies of the test structure. As indicators for crack detection, different types of mode shapes are used; among them, displacement, curvature and strain mode shapes are used widely. In recent years, researchers have stated that curvature and strain mode shapes can detect faults clearly than displacement mode shapes. Swamidas and Chen (1992) detected damage in a $1/50^{th}$ acrylic scale model of a Tripod Tower Platform (TTP) using modal analysis. They monitored natural frequencies and strain frequency response functions using strain gauges, accelerometers and a linear variable displacement transducer (LVDT). Cracks were made by making a saw cut on the platform; measurements of strains, accelerations and displacements were made for each size of saw cut, which simulated a fixed width and depth of crack. They did not get any

significant changes between acceleration and displacement transfer functions in the uncracked and cracked structure, but got significant changes in the strain transfer function, viz., by around 60% when crack grew through the thickness and around the tubular joint.

Curvature mode shape method in time domain was developed Pandey et al (1991). They used curvature mode shapes and natural frequencies to detect damages in a cantilever beam and a simply supported beam models. By plotting the absolute changes in displacement mode shapes and the curvature mode shapes over the length of the beam in cracked and uncracked conditions, damages were detected. From their analysis, they found that maximum absolute difference occurred for curvature mode shapes between undamaged and damaged beams in the damaged region, but no significant difference occurred in displacement mode shapes in the damaged region; maximum absolute difference increased when damages increased. They used the following bending moment-curvature relationship in their analysis:

$$v'' = M / (EI) \tag{2.12}$$

where v'' was the curvature at a section, M the bending moment at a section, E the modulus of elasticity and I the moment of inertia of the cross section.

Some values that are derived from these mode shapes such as Modal Assurance Criteria (MAC) and Coordinate MAC were also used to identify damage. But these methods are not so sensitive to detect cracks in the structure.

Fox (1992) showed that MAC is not relatively sensitive to damage in a beam with a saw cut. But he found out another parameter "Node line MAC," which proved to be a more sensitive indicator of changes in the mode shapes caused by damage. The "Node line MAC," is a MAC when measurement points are considered close to a node point for a particular mode. He stated that graphical comparisons of relative changes in mode shapes would be the best way of detecting the damage location when only resonant frequencies and mode shapes are examined. He also showed a simple correlation between node points and resonant frequencies to find out the location of damage.

Other Indicators: Modal damping, Anti-Resonance Frequency, Transmissibility, Random Decrement signature (RDD signatures), unexpected resonance frequencies, sub-/super- harmonic peaks in the spectral and probability density functions are also used by many researchers to detect faults in structures.

Yang et al (1980) used random decrement technique to detect induced cracks on an offshore platform model. They tested a welded steel space frame with four primary legs, and braced with horizontal and diagonal members. They induced a thin saw cut at a position near the welded joints of the structure and measured responses at various positions of the structure corresponding to a random excitation input. In order to confirm the accuracy of the experimental results, FE analysis of the structure was also carried out. After examining the random decrement signature in damaged and undamaged situations, they showed that this technique could be used to detect cracks in complex offshore structures.

Damage Detection using Neural Network-based Methods

A neural network is a dynamic system that has one-way interconnections (Harvey 1990). In this method, output responses are received by processing input data. The processing units are called nodes or neurons and nodes are connected by links. Actually this method was motivated by the functional relationships that existed between the human brain and nerve cells. It was developed to mimic the pattern recognition capabilities of the human brain. This method is also capable of self-organization and knowledge acquisition. Training is performed by providing a set of known input-output (pairs) patterns to the networks. To obtain a desired output within a required level of accuracy, the weights of each node are adjusted iteratively by the network. By measuring the difference between the computed pattern and the expected output pattern, errors are identified.

Neural networks are non-parametric identification approaches for detecting cracks in the structures related to civil, mechanical and aerospace engineering. This is a new identification methodology that is being used by many researchers (in diverse fields) to find out any unsolved complexity. There are many types of models that can be developed by changing the network topology, node characteristics and learning procedures. Among them, one of the most popular models is a multi-layer perception (MLP) or a back-propagation neural network (BPNN). The BPNN consists of an input layer, hidden layers, and an output layer. The input layer contains the measured properties and the output layer consists of the damage severity to be identified. A schematic view of a MLP neural network architecture is shown in Figure 2.4.

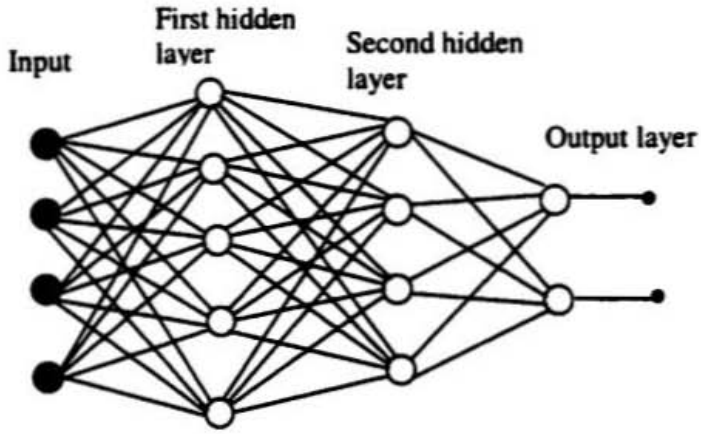

Figure 2.4: Multi-layer perception neural network architecture

Kudva et al (1991) used BPNN method to identify damage in a stiffened panel bay. They modeled the crack by cutting holes, of various diameters, in the plate at the center of bays. They predicted the location of these cracks without an error by using this method, but 50 % or more error was observed while predicting hole size.

Zubaydi (2001) used this method to identify the structural damage in ship structures, that are likely to occur at the locations of high stress concentration such as at the connection of longitudinal to heavy transverse members of the side shell. Yun and Bahng (2000) developed a method for estimating the stiffness parameters of a complex structural system using a MLP. They used natural frequencies and mode shapes as input patterns to the neural network for effective element-level identification. They adapted the Latin hypercube sampling and the component mode synthesis methods for efficient generation of the patterns for training the neural network and used noise injection technique during

the learning process to reduce the deterioration of the estimation accuracy due to measurement errors.

Wavelet theory

It is an improved version of Fourier analysis. Wavelet transform can clarify both spectral and temporal information within the signal, measured from a vibrating structure, simultaneously. And it also allows for the decomposition of the response signal while retaining temporal information. For this reason, global information as well as local specific feature in the signal are contained in wavelet transform. The time series obtained from a real observation are analyzed using a variety of wavelets at various resolution levels. In crack analysis, a mathematical model of the cracked structure is derived and wavelet expressions in the space/time domain are used for solution. The results obtained from this analysis are compared with those obtained from uncracked condition. The discrepancy in results will show the presence of crack. In order to reduce signal to noise ratio, wavelet filter bank is used. The application of this theory is now widespread and covers many fields of scientific research including medical science, geophysics, engineering, image analysis, fluid turbulence and financial analysis.

Laser-based Vibrometers

This is a new non-destructive damage estimation technique. In this method a Laser Doppler Vibrometer is used to measure the structural velocities and a single piezocermic actuator is bonded to the structure to excite the system over a high-frequency bandwidth. The non-contacting laser can be automated to scan large areas quickly and accurately and

it can operate at frequencies up to 100 kHz, which allows the technique to detect smaller defects. This method has some advantages; (i) it is a non-contacting procedure to detect cracks in structures; (ii) it can be used to detect cracks over large areas; and (iii) also it can be operated over a large-frequency bandwidth.

2.8 Finite Element Analysis

One of the best numerical methods to solve the variables that govern the design, analysis and assessment of structural integrity of any engineering problem is finite element method. This method was first introduced in the 1950s and since then it has been continually developed and improved for solving complex structural problems. Now it is an extremely sophisticated method and many researchers are using this method for different purposes.

The basic principle of this method is, "a piecewise approximation of the solution domain in which the approximating function ϕ is formed by connecting a number of simple functions, each defined over a small region" (Cook et al 1989). Each small region is called a finite element; a finite element is defined as "a region in space in which the function ϕ is interpolated from nodal values of ϕ on the boundary of the region" (Cook et al 1989). The whole structure is composed by assembling these elements and analysis is carried out for the entire structure. The main features of this method are, discretization of the whole domain and approximation of the solution using the solution of the nodal values on the element boundary. The nodes are defined as points in the structure over which elements are assumed to be interconnected.

This method gives an approximate solution. Its accuracy depends not only on the interpolation function but also on the reliable implementation of the algorithms in the computer software such as correct treatment of the prescribed loading and boundary conditions, the choice of proper element type and fineness of the meshes of the structure. More than one hundred different finite elements are available for the solution of different kinds of problems. The choice of element type depends on what kinds of problems are to be analyzed and how much of accuracy is needed. The engineer tries to predict the dimensionality (one, two or three dimensions) required for the model for proper analysis. The choice of proper dimensionality reduces the effort needed in solving the problem. In order to achieve a very good solution with accuracy, the engineer should choose the best combination of the element and mesh refinement.

2.9 Crack Analysis in Offshore Structures using Finite Element Method

Offshore steel structures are fabricated by connecting one tubular member to other tubular using welding procedures. Due to severe stress concentration and local triaxial stresses, crack normally develops at the weld toe of the chord. For an accurate analysis of stress and deformation fields near the weld toe, finite element method is utilized as the most powerful numerical method. Many engineers have used this method for the detection of cracks in a structure. Lie et al (2000) used this method for modelling an arbitrary through-thickness crack in a tubular T-joint based on detailed geometrical modelling and analysis. They defined the crack surface through which crack grows as well as the crack mouth

parameters and carried out their geometric analyses. In order to determine the accuracy of the model and the convergence of results, they used finite element results.

Wang et al (1997) carried out a non-linear finite element analysis on T, K, and TK tubular joints, subjected to axial brace loads by using the ABAQUS general purpose FE package. They proposed a damage criteria in the paper to predict the macrocrack initiation for tubular joints. They obtained the triaxial stress distributions and equivalent plastic strains near weld toes in the chord around the brace from finite element analysis results. Bowness and Lee (1994) employed the finite element method to make numerical investigations into crack curvature influence. They used three-dimensional solid finite elements to prepare the model of the doubly curved semi-elliptical weld toe crack in a tubular joint.

Modelling of a crack using efficient elements is an important part of the analysis of a cracked structure. Many researchers have used different kinds of elements in finite element analysis of a cracked body. Some of these elements are: (i) 3D solid; (ii) shell/plate; (iii) line spring and (iv) quarter point crack tip elements. A short description of these elements are given below:

3-D element: Tetrahedral and hexahedral families of elements are considered as 3-D elements. Tetrahedral elements can be 4-noded, 6-noded, 10-noded and 15-noded and hexahedral elements can be 8-noded, 20-noded, and 32-noded. In case of isoparametric formulation, 15-noded tetrahedral elements (wedge) and 20-noded hexahedral elements (brick) are used. Three-dimensional quadratic solid isoparametric elements (20-noded

brick) are normally used along with 15-noded wedge elements to model the cracked tubular joint. This element gives more accurate results of stress and displacement fields near the crack region. In steel tubular joints, the local stress concentration affects only the stresses near the surface of the tubes where stresses deviate from the thin shell theory by about 20% of the plate value (Burdekin 1985). Stress information can be predicted accurately along the thickness of the shell by using this element. Bowness and Lee (1994) used this element to model a doubly-curved semi-elliptical weld toe crack in a tubular joint. They used twenty-noded brick elements and fifteen-noded wedge elements (at geometrically complex regions) for the modelling of the crack. The advantages of these elements are that the results can also be acquired along the thickness direction. But uses of these elements, in structural modelling, are too expensive; in addition they also need more computational time and also more memory space in the computer.

Line Spring Element: The basic concept of the line spring element was first proposed by Rice and Levy (1972). This element is actually a series of one-dimensional finite elements (ABAQUS 1999). It is used only for the analysis of part-through cracks in plates and shells. When line spring elements are placed along the part-through crack, it will allow the local flexibility of one side of the flaw to be computed with respect to the other. Many engineers used the line spring elements for preparing model of a surface crack in the structure. Parks et al (1981) used this model to determine the J-integral and crack tip opening displacement of some surface cracks in plates and shells. Wang and Hu (2000) used line spring elements in conjunction with the Sih and Hagendorf shell theory (Sih and

Hagendorf 1977) to derive the governing equations of the spherical shell with semi-elliptical internal or external surface crack.

The objective of the line spring element is, to develop an alternate method of modelling the crack in a two-dimensional body with part through cracks instead of the complete 3-D analysis of a surface cracked component. It is a computationally very inexpensive tool for the analysis of a part through crack in plates and shells.

Quarter point crack tip element: Henshell and Shaw (1975) first introduced "quarter point" crack tip elements. This element is actually an 8-noded quadrilateral isoparametric shell element. In order to obtain $\frac{1}{\sqrt{r}}$ singularity required for elastic fracture mechanics analysis, the mid-nodes of these elements are moved to the quarter point near the crack tip. Mathematically the crack opening displacement is a function of the square root of the distance to the tip and this element successfully simulates this behavior. Till date this element has been used as the standard element for the analysis of through cracks in structures using finite element and boundary element procedures. In linear elastic fracture mechanics applications stress singularity (infinite stress) is quantified by the stress intensity factor which is a mathematical measure of the rate at which the stress goes to infinity. But this type element has some disadvantages. This element only produces reasonably accuracy for opening mode (K_I) stress intensity factors but its use for predicting mode two (K_{II}- sliding mode) and mode three (K_{III}- twisting mode) have been rather unsuccessful.

2.10 Substructuring

Most real structures such as offshore towers, various kinds of bridges, high rise buildings, etc, have a very large number of degrees of freedom. In order to design and analyze these types of structures more computational effort and resources are required. During recent years, enormous developments in finite element analysis and computer techniques have taken place and researchers have been able to overcome these difficulties. Finite element analysis of large structures need a very fast computer with a very large memory storage. When a structure is very large, an economical and almost accurate analysis, using finite element method, can be achieved only if it is broken down into parts; each part is analyzed separately and the results combined in a way that it satisfies the equilibrium, compatibility, and boundary conditions. This is done by using the substructuring technique (Przemieniecki 1968). In this technique, the entire structure is divided into a number of small parts, and each subdivided part is called a substructure; the approach of partitioning of the whole structure into smaller substructures is called the method of substructure, and process of analyzing a large finite element model as a collection of component finite element models is called substructuring. The substructures are connected to each other by the connectivity nodes on their common interfaces and the deformation/stress of each substructure can be expressed in terms of those values of their boundary nodes. A complete structure with three major substructures P, N, and Q are shown in Figure 2.5. If the stiffness matrix of each substructure is determined, the substructure can be treated as a complex element. The global matrix for the entire

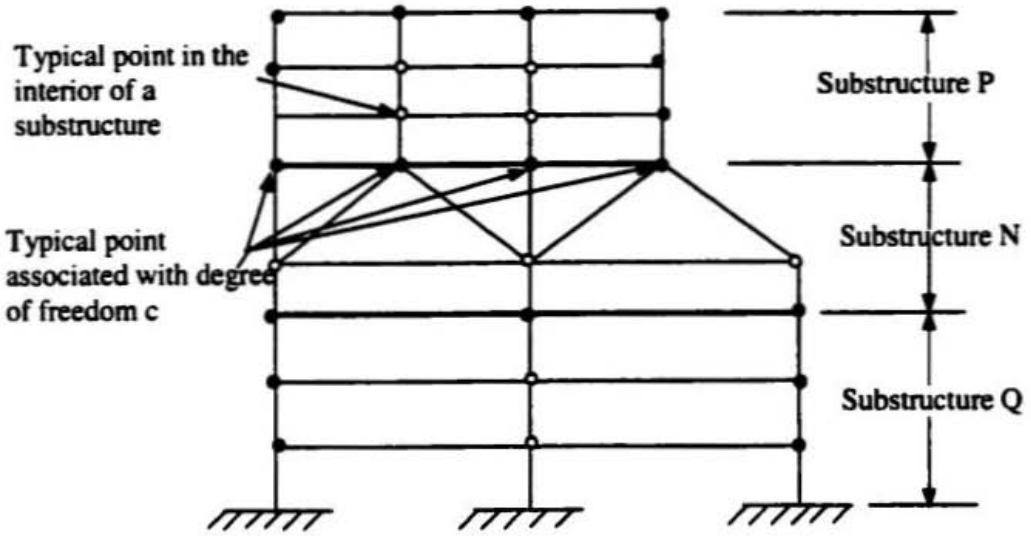

(a) Entire structure

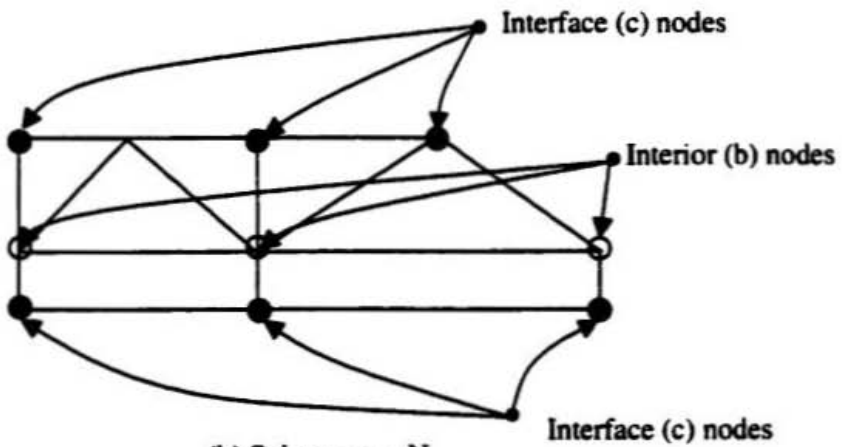

(b) Substructure N

Figure 2.5 (a) Entire structure and substructures; and (b) Typical interior and interface nodes of substructure N (McGuire and Gallagher 1979).

structure is determined by using substructure boundary degrees of freedom. Once the displacements of substructure boundary nodes are known, the displacements of the interior nodes of each substructure can be determined using the known displacements of

the substructure-boundary nodes. In substructuring technique, global level responses are only available at the substructure-boundaries. But each substructure can show detailed local responses either at the element level (stress, strain, etc.) or nodal level (displacement, velocity, acceleration, etc.). One important term essential to explain substructuring technique clearly is called as superelement. Superelement is a collection of standard elements which is used to represent a part or substructure of a large complex structure. The superelement is defined by the behavior of the boundary nodes and it can be used in the structure/substructure like any other finite element. In essence, the superelement represents a substructure and a number of superelements will be used in modelling a large structure. Substructuring technique can be used to solve both static and dynamic problems.

Static substructuring: The static responses of a superelement due to any static load are determined using the following equilibrium equation,

$$[K]\{u\} = \{P\} \tag{2.13}$$

where [K] is the stiffness matrix, {u} is the degrees of freedom vector for the superelement and {P} is the force vector. To perform static condensation, degrees of freedom {u} are divided into two parts such as retained degrees of freedom (u_r) and eliminated degrees of freedom (u_e); partitions are made on the stiffness matrix and force vector. Finally equilibrium equation for the retained degrees of freedom are written as,

$$[K_r]\{u_r\}=\{P_r\} \tag{2.14}$$

where $[K_r]$ is the reduced or condensed stiffness matrix and $[P_r]$ is the reduced force vector, are exactly equivalent to [K] and [P] but the dimension of $[K_r]$ matrix is much much smaller than [K]; it depends on the retained degrees of freedom of the assemblage of superelements. The advantages of static condensation are that the inversion of the stiffness matrix is easy to perform due to the lower order condensed matrix. Actually in the finite element analysis, large memory space (in CPU) is required for the inversion of stiffness matrices; in addition it also requires more CPU time. In the substructuring technique, global stiffness matrix (of retained degrees-of-freedom) and substructure stiffness matrices (of retained degrees-of-freedom) will be small due to the division of the structure into smaller parts; it also consumes less time to carry out matrix analysis of structure. In this case, response of a superelement is entirely linear. The complete theory related to static substructuring is given in the next chapter.

Dynamic Substructuring: The dynamic behavior of large complex structures is not easy to analyze using conventional finite element methods and are costly. Many researchers have tried to overcome this difficulty by using substructuring techniques. This method will give efficient and accurate results for the nodal quantities such as displacements or accelerations without excessively taxing the resources of the computer system. But there are some drawbacks to this method. It can give information easily at the boundary nodes. Sometimes some information is required based on element stresses or element forces located on the interior of the substructure (or superelement). In that case, all nodal data for the full, unreduced structure at each time interval are saved; then a second analysis is

carried out to recover the element level information in the interior of the substructure. In some cases it will be very difficult or impossible to store all the information in the host computer; to solve a large problem one may require few days of CPU time. During recent years, researchers have developed new methods to overcome this problem. Johal (2000) has developed an efficient method for transient data recovery from large degrees-of-freedom (DOF) FE models. In his method to recover the displacements of the internal points of the substructure, for each time step, from the transient analysis, one needs to use only the acceleration and velocity of the boundary degrees of freedom with respect to generalized modal coordinates. Then element forces and stresses can be calculated by using the available transformation matrix (between them). He developed his method based on UAI/Nastran computer package and Craig-Bampton methodology and compared the time saving achieved.

If the boundary degrees of freedom are large, then the application of substructuring technique in dynamic problem is also complicated. To overcome this difficulty, Brahmi et al (1995) suggested a method to reduce the junction degrees of freedom before assembly in dynamic substructuring. They used a modal projection procedure, on the basis of correctly chosen Ritz vectors, which reduced the boundary degrees of freedom. They were able to reduce 3744 DOF (degrees-of-freedom) of a finite element model to 100 DOF, while calculating the first 20 eigenmodes of the complete structure with good precision.

By reducing mass matrices with the same transformation that are used in stiffness matrices, dynamic representation of the superelement is carried out. In this case, it is assumed that the responses between the eliminated and retained degrees of freedom are correctly represented by the static modes only. It may not be correct if any inertia effects are important within the superelement. In that case, static modes are not enough to allow for this inertia response. To improve the dynamic representation of the superelement accurately, most of the software (ABAQUS, ANSYS, etc.) using finite element procedures have used Guyan reduction and restrained mode addition method. In Guyan reduction method, some additional degrees of freedom, which are not required to connect the superelement, are moved to the retained degrees of freedom. These additional degrees of freedom are some of the eliminated degrees of freedom. Guyan reduction can give accurate results if inertial effects within the superelement are small. Restrained mode addition method has overcome this restriction of the Guyan reduction method. In Restrained mode addition method, dynamic representation of the superelement is improved by adding some generalized degrees of freedom associated with the natural modes of the substructure. The simplest approach to do this is to extract some eigenmodes from the substructure with all of the physical retained degrees of freedom constrained.

Substructuring technique is used in this thesis while analyzing a large framed structure. Some of the advantages of this technique are: (i) System matries such as stiffness matrices, mass matrices and damping matrices are small due to the division of the entire

structure into small components; (ii) When a part of the entire structure is required to be remodelled, the matrices of other parts are retained as before; (iii) Same substructure can be used several times within a large structure to develop an efficient design; (iv) If any kinds of nonlinearities are present within the model, the iterations to solve these nonlinearities can be easily achieved due to the reduced number of degrees of freedom; and (v) A large problem can be analyzed by several groups of engineers with each group handling only one part or component of the whole structure.

2.11 Summary

In carrying out the literature survey related to the stress analysis of cracked structures the following topics have been considered viz., (i) Methods available to detect and identify cracks in steel jacket offshore platforms; (ii) Linear elastic fracture mechanics principles; (iii) Developments in finite element modelling of a crack; (iv) Application of finite element analysis; and (v) Substructuring technique and its application to analysis of large structures. Despite the numerous developments in crack detection and identification for offshore structures, very few studies have reported (in public domain) on the identification of cracked regions from the measurements and subsequent analysis of data obtained from a few points over the whole structure. Consequently an investigation concerning the stress-strain condition of the entire structure due to a crack, present at a critical region of welded joints, is carried out in this study. The following chapters will give an outline of the studies that were carried out in this direction and the results obtained in the process.

Chapter 3

Theoretical Background

3.1 General

Generally offshore steel jacket structures use hollow tubular members for fabricating the structural frame. Stress analysis of these types of structures are carried out through finite element procedures using shell and beam elements since it can account for any arbitrary geometry, loading and variation in material properties.

The basic concept of finite element procedures is that the entire body is divided into smaller elements of finite dimensions called 'finite element'; the original body is then considered as an assemblage of these elements, which are connected by a finite number of joints called 'nodes' so that continuity can be maintained between adjacent elements. To ensure the continuity of displacement at each node, the equations of equilibrium for the entire body are obtained by combining the equilibrium equations obtained for each element. The most widely used formulation technique is the displacement method. In this method, variation of displacements within the elements is considered as a simple power series (polynomial functions) for computing the element stiffness matrix and the corresponding loads for each node in local co-ordinate system. The individual element stiffness matrix and load vector are then transformed from their respective local co-ordinate systems to global co-ordinate systems through transformation matrices. Global stiffness matrix for the entire structure is assembled by superposing the individual

element stiffness matrices. After solving the equilibrium equation for displacements of the entire structure, one can obtain the structural displacements and member forces.

Shell elements used in the analysis are normally classified either as thin shell or thick shell elements. If the thickness of the shell is small, compared to the radius of curvature of the mid surface, then the shell is considered to be a geometrically thin shell and if the transverse shear forces per unit length are so small that their contributions are insignificant, then the shell is considered as a structurally thin shell. Most of the theories related to thin shell are based on Kirchhoff-Love assumption. According to this assumption, "When a shell deforms, its mid surface stretches and bends, and 'normal' to the mid surface remains perpendicular after deformation and also stress component normal to the shell mid-surface is disregarded". Some shell elements are formulated based on Reissner-Mindlin theory. In Reissner-Mindlin theory, shear flexibility is considered and in this case normal at the bottom surface and top surface of the shell may not lie in a straight line after deformation (Hinton and Owen 1984).

The degenerate isoparametric shell elements, originally introduced by Ahmad et al (1970), are the generally accepted formulation used for characterizing shell elements. Basically these elements are derived from three-dimensional elements by the degeneration concept and three dimensional stress and strain conditions are degenerated to give shell behavior. Ahmed et al (1970) avoided the Kirchhoff-Love assumption and incorporated the effect of shear deformation for the linear analysis of moderately thick shell elements by employing independent rotational and displacement degrees of

freedom. In these elements, five degrees of freedom (three displacements and two rotational degrees of freedom) are specified at each nodal point; rotations at the node are not tied to the slope of mid-surface. After developing these elements researchers were able to analyze any arbitrary shape of shell structures. But some difficulties were encountered when thickness of the element was reduced. These difficulties arose due to the presence of the shear-locking phenomenon. Investigators found out that the assumed displacement functions imposed large amounts of shear strain in the development of simple bending deformation. This phenomenon has been referred by many researchers as 'shear locking' (Doherty et al 1969 and Zienkiewicz et al 1971). They found out that by assessing the shear strain energy in the element considering a reduced integration technique (lower order integration procedure - 2×2), element performance could be greatly improved. This concept was observed to be acceptable up to moderately thin or thick shells. However, for very thin shells these results once again exhibited shear-locking phenomena and produced the problem of rank deficiency of the stiffness matrix. To overcome these difficulties, Hughes et al (1978) developed the selective integration technique. In this technique, reduced integration rule is used to evaluate the stiffness matrix associated with the shear strain energy and full integration is used for the remaining terms in an attempt to retain the required rank of the overall stiffness matrix.

Since the joint geometry of offshore steel structures is quite complex in comparison to other structures, the development of degenerate isoparametric elements and different types of integration techniques have reduced the complexity involved in the solution of

such types of structures. Figures 3.1 and 3.2 give some details of elements used in such investigation.

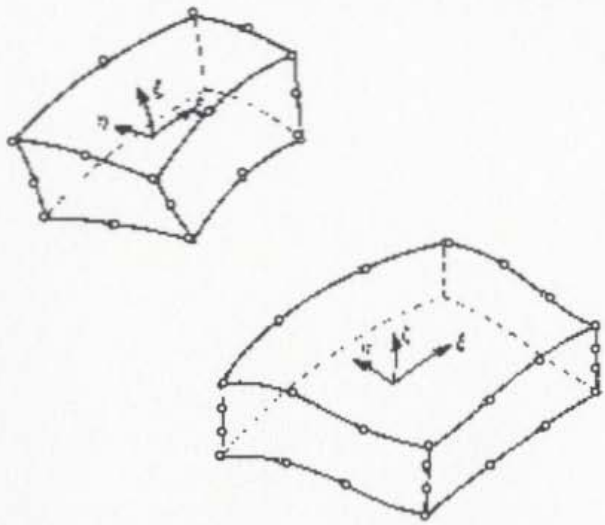

Figure 3.1: Three dimensional hexahedral elements of parabolic and cubic types (Ahmad et al 1970).

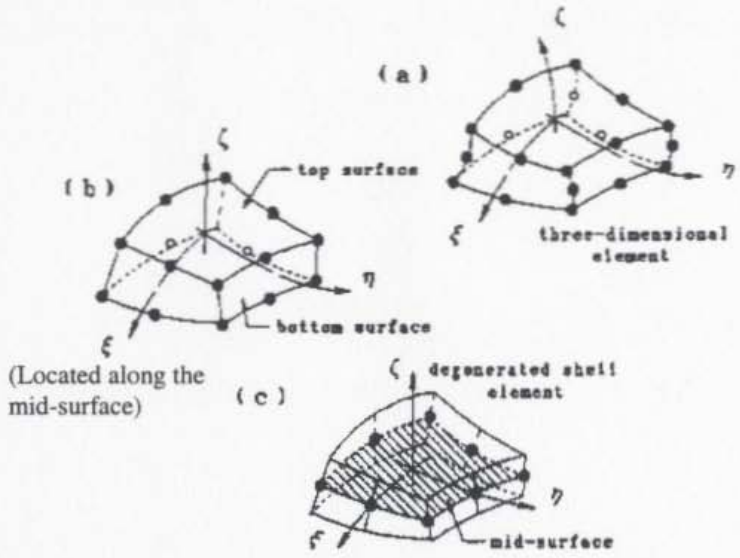

Figure 3.2: (a) and (b) Quadratic solid three-dimensional elements; and (c) The corresponding eight-noded degenerate shell elements (Nwosu 1993).

3.2 Co-ordinate Systems for Degenerate Isoparametric Shell Element

The following co-ordinate systems have been used to describe the general characteristics of the degenerate curved shell elements used in the present study.

1. Global co-ordinate system.
2. Nodal co-ordinate system.
3. Curvilinear co-ordinate system.
4. Local co-ordinate system.

Global coordinate system: This is the reference Cartesian co-ordinate system for individual elements, and the complete model, to which all other co-ordinate systems are referred. It can be chosen freely, in relation to which the geometry of the structure is defined in space. Nodal co-ordinates and displacements, as well as global stiffness matrix and applied force vector, are referred to this system. This co-ordinate system can be represented either by x_i (x_1, x_2, x_3) or x, y, z, where $x = x_1$, $y = y_1$ and $z = z_1$.

Nodal Co-ordinate System: Each nodal point at the reference surface (mid surface of the shell element) is defined by this co-ordinate system. It is a right-handed Cartesian co-ordinate system and the origin of this system is located at the i^{th} node on the mid surface. It is convenient to construct this co-ordinate system by vector representation. The vector $\mathbf{V}_{3i}$ at nodal point 'i' represents the direction at that node which is not necessarily perpendicular to the mid surface at i. It is constructed from the nodal co-ordinates of the top and bottom surfaces at node i, $\mathbf{V}_{3i} = \mathbf{x}_i^{top} - \mathbf{x}_i^{bot}$, where $\mathbf{x}_i = [x_i\ y_i\ z_i]^T$. The vector $\mathbf{V}_{1i}$ is

related to the vector $\mathbf{V}_{3i}$ and global co-ordinate system. It is perpendicular to $\mathbf{V}_{3i}$ and parallel to global xz-plane and is written as, $\mathbf{V}_{1i} = \mathbf{i} \otimes \mathbf{V}_{3i}$, where $\mathbf{i}$ is the unit vector along the global x-direction. The vector $\mathbf{V}_{2i}$ is perpendicular to both vectors $\mathbf{V}_{3i}$ and $\mathbf{V}_{1i}$ i.e., the plane defined by these vectors and is written as, $\mathbf{V}_{2i} = \mathbf{V}_{3i} \otimes \mathbf{V}_{1i}$. The advantage of considering this definition for $\mathbf{V}_{3i}$ vector (not perpendicular to the shell mid surface) is that, no gaps are formed along the element boundaries.

Curvilinear co-ordinate system: A local non-orthogonal coordinate system is used to define the curved shell element. The notations used in this co-ordinate system, are usually ξ, η, and ζ. The notation ξ and η are the two curvilinear co-ordinates in the mid plane of the shell and ζ is a linear co-ordinate in the thickness direction and assumed approximately perpendicular to the shell mid surface. In these co-ordinates, element sides are defined by $\xi = \pm 1$, $\eta = \pm 1$ and $\zeta = \pm 1$ on their respective faces of the element.

Local co-ordinate system: This is a Cartesian co-ordinate system defined at the sampling points of each individual element of the complete structure wherein stress and strain are to be calculated. Since the elements are in general differently oriented within the structure, this co-ordinate system will usually be differently oriented from one element to next. In this co-ordinate system, $\mathbf{x}'_3$ is considered as perpendicular to the surface ζ = constant and $\mathbf{x}'_1$ is chosen tangential to the ξ-direction at the sampling points. In ABAQUS finite element software, the default local $\mathbf{x}'_1$ direction is the projection of the global x-axis onto the surface. The $\mathbf{x}'_2$ co-ordinate is represented by the cross product of the direction $\mathbf{x}'_3$ and $\mathbf{x}'_1$.

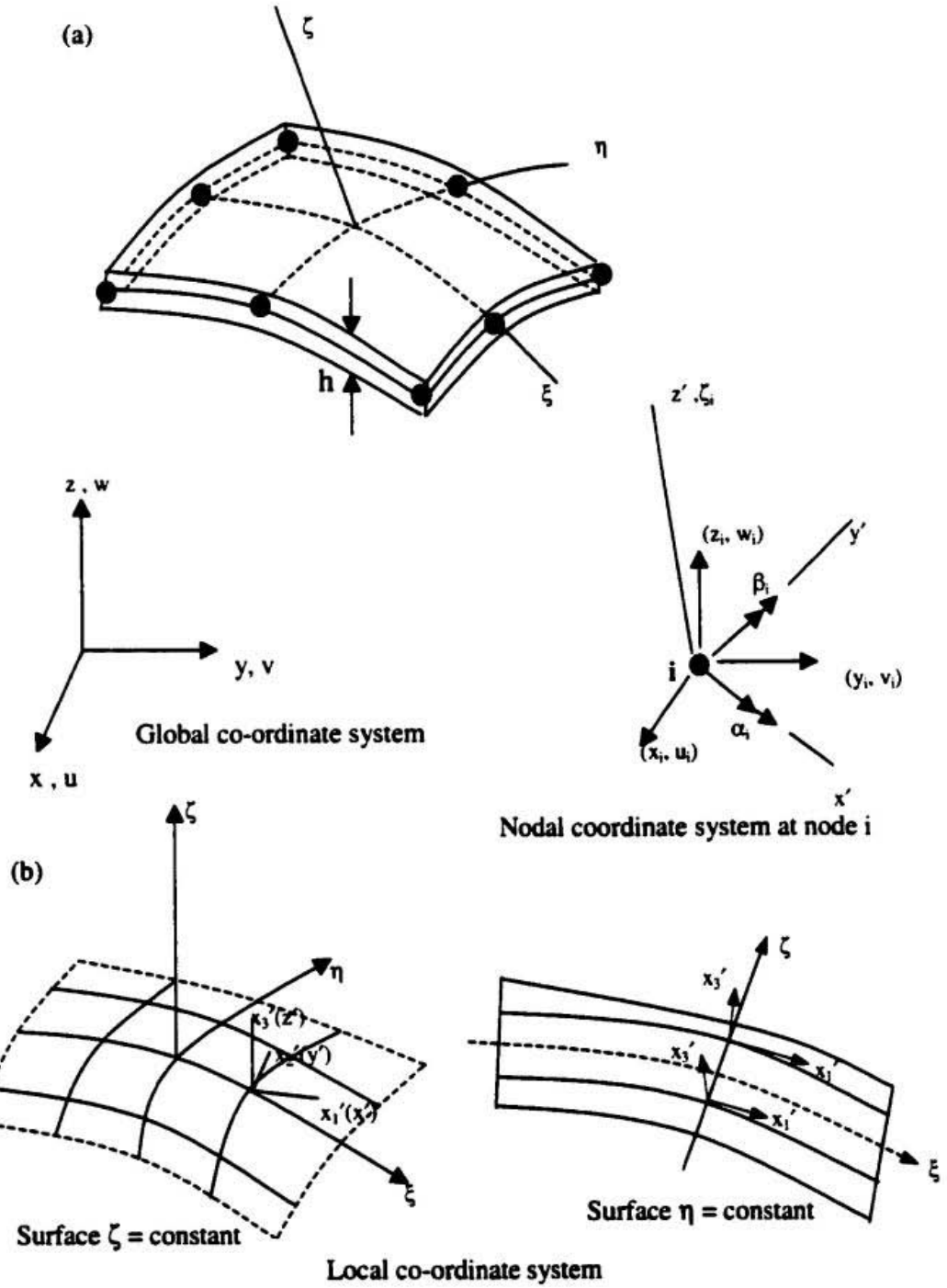

Figure 3.3: Co-ordinate system: (a) Nodal and curvilinear systems; and (b) Local system of axes.

If the shell curvature and thickness varies within the element, this co-ordinate system also varies along the thickness for any normal with this variation. Global co-ordinate system is obtained from this co-ordinate system by providing directional cosine matrix of transformation system. Directional cosine matrix is defined by, $[\theta] = [v_1, v_2, v_3]$, where v_1, v_2 and v_3 are the unit vectors in the x_1', x_2' and x_3' directions, respectively. The graphical representation of these four co-ordinate systems is given in Figure 3.3.

3.3 Element Geometry Definition

In finite element analysis, the element geometry is usually defined by the global co-ordinates, using the pairs of points on the top and bottom surface at each node. It can also be defined in other ways by considering mid surface of the element. In this case, mid surface nodal co-ordinates and corresponding direction of thickness are required to define the geometry of element. For the isoparametric formulation, to obtain the co-ordinate of a point within the element, the element shape functions are applied to the nodal co-ordinates. The global co-ordinates of any point within the element are written as,

$$\begin{Bmatrix} x \\ y \\ z \end{Bmatrix} = \sum_{i=1}^{n} N_i(\xi,\eta)\frac{(1+\zeta)}{2}\begin{Bmatrix} x_i \\ y_i \\ z_i \end{Bmatrix}_{top} + \sum_{i=1}^{n} N_i(\xi,\eta)\frac{(1-\zeta)}{2}\begin{Bmatrix} x_i \\ y_i \\ z_i \end{Bmatrix}_{bottom} \tag{3.3.1}$$

or alternatively, considering the nodal co-ordinate of the mid surface and the directional thickness h_i,

$$\begin{Bmatrix} x \\ y \\ z \end{Bmatrix} = \sum_{i=1}^{n} N_i(\xi,\eta)\begin{Bmatrix} x_i \\ y_i \\ z_i \end{Bmatrix}_{mid} + \sum_{i=1}^{n} N_i(\xi,\eta)\zeta\frac{h_i}{2}\begin{Bmatrix} l_{3i} \\ m_{3i} \\ n_{3i} \end{Bmatrix} \tag{3.3.2}$$

where ξ, η, ζ are the curvilinear co-ordinates of the point under consideration, 'n' is the number of nodes per element and N_i (i=1,n) are the element shape functions of the surface ζ = constant (given in Appendix) . The term l_{3i}, m_{3i} and n_{3i} represent the directional cosines of the vector V_{3i} normal to the mid-surface and of length equal to the thickness of the shell, and are calculated by the following expression, viz.,

$$V_{3i} = \begin{Bmatrix} x_{top} - x_{bottom} \\ y_{top} - y_{bottom} \\ z_{top} - z_{bottom} \end{Bmatrix} = \begin{Bmatrix} l_{3i} \\ m_{3i} \\ n_{3i} \end{Bmatrix} h_i \qquad (3.3.3)$$

The subscripts top and bottom in equation (3.3.3) represent the top and bottom surfaces of the shell element, respectively.

Eight-noded isoparametric shell elements were used in the present study for the whole finite element formulation. To use these elements, advantages of using geometric interpolation functions to be similar to the displacement shape functions, were taken into consideration. The eight-noded (serendipity) rectangular parent element and its isoparametric counterpart are shown in Figure 3.4.

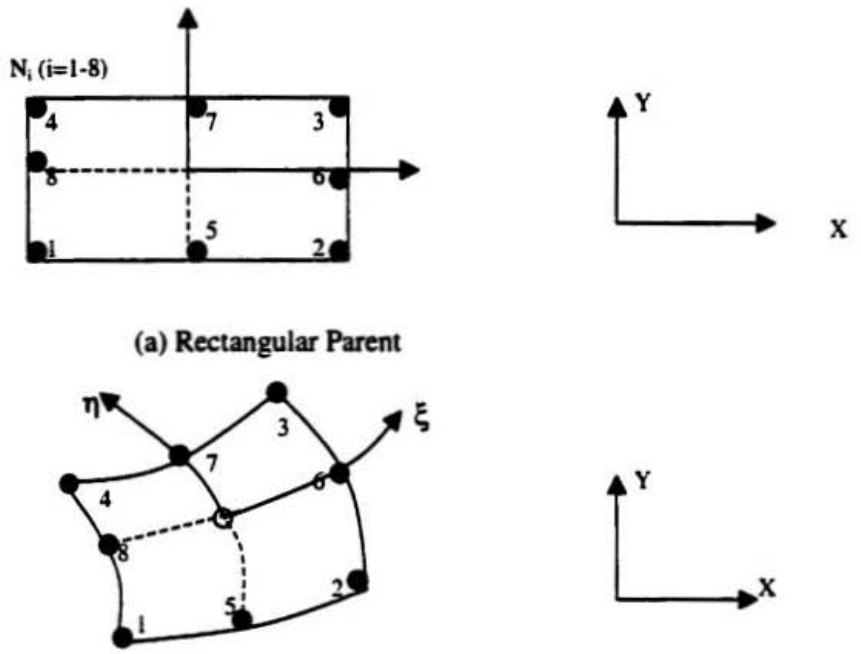

Figure 3.4: Nodal configuration of the quadratic shell elements: (a) rectangular parent; and (b) isoparametric counterpart.

3.4 Displacement Field

By applying the two shell assumptions mentioned in section 3.1 in the degeneration process, the displacement field within the element is described by using five degrees of freedom. In these five degrees of freedom, three degrees of freedom are related to the displacement of the mid-point of the 'normal' and the other two degrees of freedom are related to the two rotations of the nodal vector V_{3i} about orthogonal directions normal to it. In this case, rotational degrees of freedom are completely independent. For small

rotations, linear relationship are developed between the angle of rotation and shell thickness and can be related as shown in Figure 3.5.

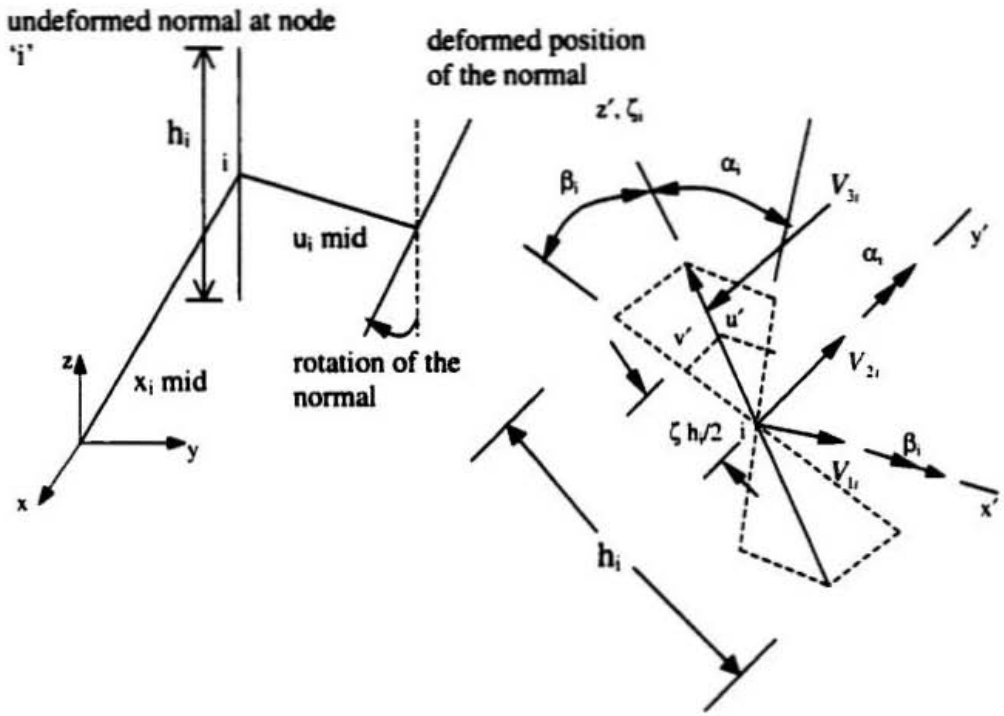

Figure 3.5: Displacement of a point on the "normal" at node i.

$$u' = \zeta(h_i/2)\,\alpha_i \qquad (3.3.4)$$

$$v' = \zeta(h_i/2)\,\beta_i \qquad (3.3.5)$$

where u′ is a displacement in the vector $\hat{v}_{1i}$ direction and v′ is a displacement in the negative $\hat{v}_{2i}$ direction. Here $\hat{v}_{1i}$, $\hat{v}_{2i}$ and $\hat{v}_{3i}$ are considered as unit vectors in the direction of V_{1i}, V_{2i} and V_{3i}. The corresponding displacement components are written as,

$$\left.\begin{aligned} u_i &= \zeta \frac{h_i}{2} \hat{v}_{1i} \alpha_i \\ v_i &= -\zeta \frac{h_i}{2} \hat{v}_{2i} \beta_i \end{aligned}\right\} \tag{3.3.6}$$

If the vector $\hat{v}_{1i}$ and vector $\hat{v}_{2i}$ (of unit magnitude) represent the two such orthogonal direction with corresponding (scalar) rotations α_i and β_i, then displacement field can be written as,

$$\begin{Bmatrix} u \\ v \\ w \end{Bmatrix} = \sum_{i=1}^{n} N_i(\xi,\eta) \begin{Bmatrix} u_i \\ v_i \\ w_i \end{Bmatrix} + \sum_{i=1}^{n} N_i(\xi,\eta) \zeta \frac{h_i}{2} [\hat{v}_{1i} \quad -\hat{v}_{2i}] \begin{Bmatrix} \alpha_i \\ \beta_i \end{Bmatrix} \tag{3.3.7}$$

where unit vector matrix can be written in terms of directional cosines as,

$$[\hat{v}_{1i} \quad -\hat{v}_{2i}] = \begin{bmatrix} l_{1i} & -l_{2i} \\ m_{1i} & -m_{2i} \\ n_{1i} & -n_{2i} \end{bmatrix} \tag{3.3.8}$$

The equation (3.3.7) can be written more explicitly as,

$$\begin{Bmatrix} u \\ v \\ w \end{Bmatrix} = \sum_{i=1}^{n} N_i(\xi,\eta) \begin{Bmatrix} u_i \\ v_i \\ w_i \end{Bmatrix} + \sum_{i=1}^{n} N_i(\xi,\eta) \zeta \frac{h_i}{2} \begin{bmatrix} l_{1i} & -l_{2i} \\ m_{1i} & -m_{2i} \\ n_{1i} & -n_{2i} \end{bmatrix} \begin{Bmatrix} \alpha_i \\ \beta_i \end{Bmatrix} \tag{3.3.9}$$

where u, v and w are the general displacements at any point within the shell element in the direction of global axes, u_i, v_i and w_i are the three Cartesian components of the nodal displacements and α_i and β_i are the two rotations of the nodal vector V_{3i}.

The equation (3.3.9) can be expressed as

$$\begin{Bmatrix} u \\ v \\ w \end{Bmatrix} = \begin{bmatrix} N_i & 0 & 0 & N_i\zeta\frac{h_i}{2}l_{1i} & -N_i\zeta\frac{h_i}{2}l_{2i} \\ 0 & N_i & 0 & N_i\zeta\frac{h_i}{2}m_{1i} & -N_i\zeta\frac{h_i}{2}m_{2i} \\ 0 & 0 & N_i & N_i\zeta\frac{h_i}{2}n_{1i} & -N_i\zeta\frac{h_i}{2}n_{2i} \end{bmatrix} \begin{Bmatrix} u_i \\ v_i \\ w_i \\ \alpha_i \\ \beta_i \end{Bmatrix} \qquad (3.3.10)$$

or, $$\{u_i\} = [N_i]\{\delta_i\} \qquad (3.3.11)$$

For the complete element it is defined as,

$$\{u\} = [N]\{\delta\} \qquad (3.3.12)$$

where $\{u\} = \{u, v, w\}^T$, $N = [N_1,....N_i,....N_n]$ is the shape function matrix of the degenerate element, and $\{\delta\}=\{\delta_1,.....\delta_i,.....\delta_n\}^T$ is the vector of the element nodal variables.

3.5 Definition of Strains and Stresses

According to the second assumption of the shell theory, normal stress along the z′ direction is considered as zero. This assumption has created a scope to define stress-strain relationships in terms of the local system of axes x'_i where $x'_3 = z'$ is perpendicular to the ξη-plane. In order to help in the analysis and design of a shell, the local system of axes is also the most convenient system for expressing the stress components and their resultants. In this case, five significant strain components are expressed in terms of the local axes x′, y′ and z′ as,

$$\varepsilon = \begin{bmatrix} \varepsilon_{x'} \\ \varepsilon_{y'} \\ \gamma_{x'y'} \\ \gamma_{x'z'} \\ \gamma_{y'z'} \end{bmatrix} = \begin{bmatrix} \dfrac{\partial u'}{\partial x'} \\ \dfrac{\partial v'}{\partial y'} \\ \dfrac{\partial u'}{\partial y'} + \dfrac{\partial v'}{\partial x'} \\ \dfrac{\partial u'}{\partial z'} + \dfrac{\partial w'}{\partial x'} \\ \dfrac{\partial v'}{\partial z'} + \dfrac{\partial w'}{\partial y'} \end{bmatrix} \tag{3.4.1}$$

where u′, v′ and w′ are the displacement components in the local x′, y′and z′ axes, respectively. The strain in the z′ direction is neglected to maintain the consistency with the shell assumption. These local derivatives are related to the global derivatives in the following manner, viz.,

$$\begin{bmatrix} \frac{\partial u'}{\partial x'} & \frac{\partial v'}{\partial x'} & \frac{\partial w'}{\partial x'} \\ \frac{\partial u'}{\partial y'} & \frac{\partial v'}{\partial y'} & \frac{\partial w'}{\partial y'} \\ \frac{\partial u'}{\partial z'} & \frac{\partial v'}{\partial z'} & \frac{\partial w'}{\partial z'} \end{bmatrix} = [\theta]^T \begin{bmatrix} \frac{\partial u}{\partial x} & \frac{\partial v}{\partial x} & \frac{\partial w}{\partial x} \\ \frac{\partial u}{\partial y} & \frac{\partial v}{\partial y} & \frac{\partial w}{\partial y} \\ \frac{\partial u}{\partial z} & \frac{\partial v}{\partial z} & \frac{\partial w}{\partial z} \end{bmatrix} [\theta] \tag{3.4.2}$$

where u, v and w are the displacement components of a point in the global system of axes and [θ] is the directional cosine matrix. The derivatives of displacements with respect to the global co-ordinates are related to the derivatives of displacement with respect to the curvilinear co-ordinates by the following relationship,

$$\begin{bmatrix} \frac{\partial u}{\partial x} & \frac{\partial v}{\partial x} & \frac{\partial w}{\partial x} \\ \frac{\partial u}{\partial y} & \frac{\partial v}{\partial y} & \frac{\partial w}{\partial y} \\ \frac{\partial u}{\partial z} & \frac{\partial v}{\partial z} & \frac{\partial w}{\partial z} \end{bmatrix} = [J]^{-1} \begin{bmatrix} \frac{\partial u}{\partial \xi} & \frac{\partial v}{\partial \xi} & \frac{\partial w}{\partial \xi} \\ \frac{\partial u}{\partial \eta} & \frac{\partial v}{\partial \eta} & \frac{\partial w}{\partial \eta} \\ \frac{\partial u}{\partial \zeta} & \frac{\partial v}{\partial \zeta} & \frac{\partial w}{\partial \zeta} \end{bmatrix} \tag{3.4.3}$$

where [J] is the Jacobian matrix and it is expressed as,

$$[J] = \begin{bmatrix} \frac{\partial x}{\partial \xi} & \frac{\partial y}{\partial \xi} & \frac{\partial z}{\partial \xi} \\ \frac{\partial x}{\partial \eta} & \frac{\partial y}{\partial \eta} & \frac{\partial z}{\partial \eta} \\ \frac{\partial x}{\partial \zeta} & \frac{\partial y}{\partial \zeta} & \frac{\partial z}{\partial \zeta} \end{bmatrix} \tag{3.4.4}$$

The strain matrix [B′] relating the strain components in the local system to the element nodal variables, are constructed as,

$$\{\varepsilon'\} = [B']\{\delta\} \tag{3.4.5}$$

where [B′] is a matrix with five rows and number of column equal to the number of element nodal variables.

Substitution of equation (3.4.3) into equation (3.4.2) leads to,

$$\begin{bmatrix} \frac{\partial u'}{\partial x'} & \frac{\partial v'}{\partial x'} & \frac{\partial w'}{\partial x'} \\ \frac{\partial u'}{\partial y'} & \frac{\partial v'}{\partial y'} & \frac{\partial w'}{\partial y'} \\ \frac{\partial u'}{\partial z'} & \frac{\partial v'}{\partial z'} & \frac{\partial w'}{\partial z'} \end{bmatrix} = [\theta]^T [J]^{-1} \begin{bmatrix} \frac{\partial u}{\partial \xi} & \frac{\partial v}{\partial \xi} & \frac{\partial w}{\partial \xi} \\ \frac{\partial u}{\partial \eta} & \frac{\partial v}{\partial \eta} & \frac{\partial w}{\partial \eta} \\ \frac{\partial u}{\partial \zeta} & \frac{\partial v}{\partial \zeta} & \frac{\partial w}{\partial \xi} \end{bmatrix} [\theta] \tag{3.4.6}$$

To determine the inverse of the Jacobian matrix, some mathematical operations are required. The Jacobian matrix can be expressed in terms of three vectors as (Nwosu 1993),

$$[J] = \begin{bmatrix} \vec{P} \\ \vec{Q} \\ \vec{V}_3 \end{bmatrix} \tag{3.4.7}$$

Then, the inverse of the Jacobian matrix can be written as,

$$[J]^{-1} = \frac{\left[\vec{Q}\times\vec{V}_3,\ \ \vec{V}_3\times\vec{P},\ \ \vec{P}\times\vec{Q}\right]}{\|J\|} \tag{3.4.8}$$

where $\|J\|$ represents the determinant of the Jacobian matrix $[J]$.

From equation (3.4.6), considering

$$[A] = [\theta]^T [J]^{-1}$$

one can express [A] by

$$[A] = \begin{bmatrix} \hat{v}_1 \\ \hat{v}_2 \\ \hat{v}_3 \end{bmatrix} \left[\vec{Q}\times\vec{V}_3,\ \ \vec{V}_3\times\vec{P},\ \ \vec{P}\times\vec{Q}\right] \div \|J\| \tag{3.4.9}$$

Equation (3.4.9) can be expressed in the special form of A as

$$[\mathrm{A}] = \begin{bmatrix} A_{11} & A_{12} & 0 \\ A_{21} & A_{22} & 0 \\ 0 & 0 & A_{33} \end{bmatrix} \tag{3.4.10}$$

where all components of [A] matrix depend on the vectors and the determinant of the Jacobian matrix of equation (3.4.9). The stresses corresponding to these strains are defined as,

$$\{\sigma'\} = \begin{bmatrix} \sigma_{x'} \\ \sigma_{y'} \\ \tau_{x'y'} \\ \tau_{x'z'} \\ \tau_{y'z'} \end{bmatrix} = [D'] \left(\varepsilon' - \varepsilon_0{}' \right) \tag{3.4.11}$$

where $\{\sigma'\}$ is the local stress component vector and [D'] is the elasticity matrix (5×5). The [D'] matrix depends on the material properties such as Young's modulus of elasticity (E) and Poisson's ratio (ν). Sometimes shear deformation correction factor (κ) is also included in addition to the above parameters. This correction factor is considered for the analysis of thick shell section. Most of the offshore tubular joints are constructed with members whose thickness to diameter ratio is very small and consequently shear deformation is small in comparison to deformation due to bending. But some structures such as pressure vessel, boiler, etc., require greater thickness to diameter ratio and analysis is performed considering thick shell structures. In that case shear deformations have to be considered. During the formulation of displacements of the nodal variables it is considered that the shear distribution through the thickness is approximately constant. But actually its distribution through the thickness is approximately parabolic. For this reason this correction factor (κ) is taken as 1.2, to improve the shear deformation approximation.

The [D'] matrix is defined considering all of the above parameters as,

$$[D'] = \frac{E}{1-\nu^2}\begin{bmatrix} 1 & \nu & 0 & 0 & 0 \\ \nu & 1 & 0 & 0 & 0 \\ 0 & 0 & \frac{1-\nu}{2} & 0 & 0 \\ 0 & 0 & 0 & \frac{1-\nu}{2\kappa} & 0 \\ 0 & 0 & 0 & 0 & \frac{1-\nu}{2\kappa} \end{bmatrix} \qquad (3.4.12)$$

3.6 Element Properties and Transformations

In order to calculate the element property matrices such as stiffness matrix, the integrals over the volume of the element are necessary. The form of this type is generally written as,

$$\int_{vol} [S] dx dy dz \tag{3.5.1}$$

where the matrix [S] is a function of the co-ordinates. It is equal to,

$$[S] = [B]^T [D][B] \tag{3.5.2}$$

where [D] is the elasticity matrix and [B] matrix relates strains to the nodal parameters in the form $\{\varepsilon\}=[B]\{\delta\}^e$.

The numerical integration of equation (3.5.1) would be straightforward if the matrix [S] and the infinitesimal volume *dxdydz* are expressed in terms of the curvilinear co-ordinates system. In order to do this one needs some transformation operations. In the previous section all transformations related to curvilinear to global and then global to local are shown. The infinitesimal volume is written in terms of curvilinear co-ordinates as,

$$dx\, dy\, dz = \|J\|\, d\xi\, d\eta\, d\zeta \tag{3.5.3}$$

The strain vector equation (3.4.5) or (3.4.11) can also be written as,

$$\{\varepsilon'\} = \begin{bmatrix} \frac{\partial}{\partial x'} & 0 & 0 \\ 0 & \frac{\partial}{\partial y'} & 0 \\ \frac{\partial}{\partial y'} & \frac{\partial}{\partial x'} & 0 \\ \frac{\partial}{\partial z'} & 0 & \frac{\partial}{\partial x'} \\ 0 & \frac{\partial}{\partial z'} & \frac{\partial}{\partial y'} \end{bmatrix} \begin{Bmatrix} u' \\ v' \\ w' \end{Bmatrix} = [G] \begin{Bmatrix} u' \\ v' \\ w' \end{Bmatrix} \tag{3.5.4}$$

The local displacement vectors are transferred to the global displacement vectors by the following expression, viz.,

$$\{\varepsilon'\} = [G][\theta^T] \begin{Bmatrix} u \\ v \\ w \end{Bmatrix} \tag{3.5.5}$$

Expanding this equation using equations (3.3.7) and (3.4.10),

$$\{\varepsilon'\} = [B_i][\theta^T] \begin{Bmatrix} u_i \\ v_i \\ w_i \end{Bmatrix} + \frac{h_i}{2}[\zeta[B_i] + [C_i]][\theta]^T [\hat{v}_{1i}, -\hat{v}_{2i}] \begin{Bmatrix} \alpha_i \\ \beta_i \end{Bmatrix} \tag{3.5.6}$$

where i denotes the nodal number of an element, and $[B_i]$ and $[C_i]$ matrices are represented as,

$$[B_i]=\begin{bmatrix} B_1 & 0 & 0 \\ 0 & B_2 & 0 \\ B_2 & B_1 & 0 \\ 0 & 0 & B_1 \\ 0 & 0 & B_2 \end{bmatrix};\quad [C_i]=\begin{bmatrix} 0 & 0 & 0 \\ 0 & 0 & 0 \\ 0 & 0 & 0 \\ C_1 & 0 & 0 \\ 0 & C_1 & 0 \end{bmatrix} \tag{3.5.7}$$

where

$$\left.\begin{aligned} B_1 &= A_{11}\frac{\partial N_i}{\partial \xi}+A_{12}\frac{\partial N_i}{\partial \eta} \\ B_2 &= A_{21}\frac{\partial N_i}{\partial \xi}+A_{22}\frac{\partial N_i}{\partial \eta} \\ C_1 &= A_{33}N_i \end{aligned}\right\} \tag{3.5.8}$$

After minimizing the strain energy of the element domain with respect to nodal displacement parameters, the stiffness matrix is obtained as,

$$[K]^e=\int_{-1}^{+1}\int_{-1}^{+1}\int_{-1}^{+1}[B']^T[D'][B']|J|d\xi\,d\eta\,d\zeta \tag{3.5.9}$$

By superposing these local stiffness matrices of the elements, global stiffness matrix is assembled for the entire structure.

3.7 Crack Analysis using Eight-Noded Quadrilateral Shell Elements with Mid-Side Node of Two Sides containing the crack shifted to the Quarter Point

3.7.1 General

The critical point in the design of any structure is dependent on the ability to predict the failure of its most critical component. Numerous incidences have occurred where failures took place at stresses lower than design stresses. For this reason, the precise evaluation of safety and strength of the structure are important tasks for researchers. When a crack is developed in the structure, stresses are concentrated near the crack tip region. To predict this stress concentration precisely, special care should be taken. Many researchers have used different methods to analyze stress-strain characteristics near the crack tip accurately and to predict the variation of stresses and strains. Williams (1961) showed that the stresses display singularities as inverse square root of the distance from the crack tip, for a cracked plate in bending. Barsoum (1976) used a quarter point node on two sides of the crack tip elements to achieve the stress-strain singularity in the quadratic isoparametric elements. He also used the same concept to attain $1/\sqrt{r}$ singularity in the degenerate 20–noded solid elements. In this study it was observed that the substructure concept of modelling the structure was not compatible with the line spring elements (discussed earlier in section 2.9) to model the growth of surface cracks through the thickness of the structure. Hence the crack had to be modelled as a through-thickness crack. Consequently, Barsoum's concept was used to discretize the model of the crack at the junction of the brace and chord member. The theory related to $1/\sqrt{r}$ singularity in stresses

and strains within the element is given in the next section.

3.7.2 Investigation of the Type of Stress-Strain Singularity in Quadrilateral Isoparametric Shell Element Formulation

The element stiffness matrix formulation for the quadrilateral isoparametric shell elements has been shown in the previous section 3.4; in addition it also shows the strain-displacement and stress-strain relationships. From equation (3.4.5) of section 3.4 it is seen that local strains are related to local nodal displacements by [B′] matrix. The strain singularity is achieved by making [B′] matrix to be singular. In the same section 3.4 it has also been shown that derivatives of global displacements are transformed to the derivatives of local displacements by using the transformation matrix [θ]. But this transformation matrix is a non-singular matrix. However, the derivatives of the global displacement matrix can be made singular by requiring that the Jacobian matrix [J] be singular at the crack tip or by making the determinant of the Jacobian to vanish at the crack tip. For clarity, calculation is shown for an 8-noded plate element. According to section 3.4, the strain matrix for a plate element is written as

$$\{\varepsilon\} = [J]^{-1}[B']\begin{Bmatrix} u_i \\ v_i \\ w_i \\ \alpha_i \\ \beta_i \end{Bmatrix} \tag{3.6.1}$$

$$\text{where } \det|J| = \frac{\partial(x, y, z)}{\partial(\xi, \eta, \zeta)} \tag{3.6.2}$$

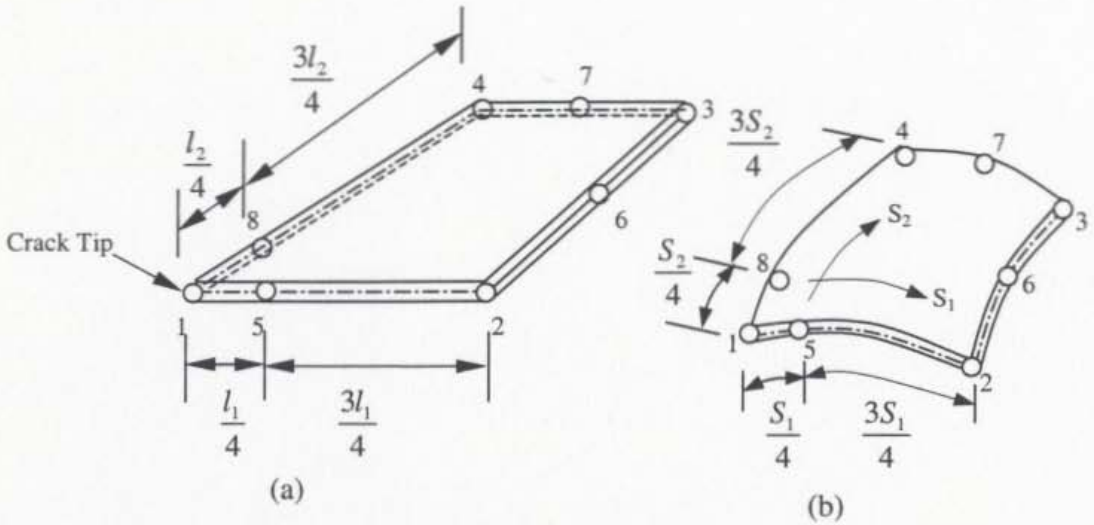

Figure 3.6: (a) Crack tip plate bending element; and (b) Crack tip quadrilateral general shell element (Barsoum 1976).

The following transformation is used to map the geometry of an 8-noded isoparametric element into the normalized space (ξ,η,ζ) $(-1\geq \xi \leq 1, -1\geq \eta \leq 1, -1\geq \zeta \leq 1)$ (Barsoum 1976),

$$\begin{Bmatrix} x \\ y \\ z \end{Bmatrix} = \sum_{i=1}^{8} N_i(\xi,\eta) \begin{Bmatrix} x_i \\ y_i \\ z_i \end{Bmatrix} + \sum_{i=1}^{8} N_i(\xi,\eta) \frac{\zeta}{2} V_{3i} \tag{3.6.3}$$

And the displacements are interpolated by

$$\begin{Bmatrix} u \\ v \\ w \end{Bmatrix} = \sum_{i=1}^{8} N_i(\xi,\eta) \begin{Bmatrix} u_i \\ v_i \\ w_i \end{Bmatrix} + \sum_{i=1}^{8} N_i(\xi,\eta) \zeta \frac{h_i}{2} [\hat{v}_{1i}, \hat{v}_{2i}] \begin{Bmatrix} \alpha_i \\ \beta_i \end{Bmatrix} \tag{3.6.3 a}$$

where,

$$N_i = \left[(1+\xi\xi_i)(1+\eta\eta_i) - (1-\xi^2)(1+\eta\eta_i) - (1-\eta^2)(1+\xi\xi_i)\right] \xi_i^2\eta_i^2/4 + (1-\xi^2)(1+\eta\eta_i)(1-\xi_i^2)\eta_i^2/2 + (1-\eta^2)(1+\xi\xi_i)(1-\eta_i^2)\xi_i^2/2 \quad \text{(3.6.3 b)}$$

The shape functions are written along line 1-2 in Figure 3.6 (a) as (Barsoum 1976),

$$\left.\begin{aligned} N_1 &= -\frac{1}{2}\xi(1-\xi) \\ N_2 &= \frac{1}{2}\xi(1+\xi) \\ N_5 &= (1-\xi^2) \end{aligned}\right\} \quad (3.6.4)$$

Therefore, from equation (3.6.3) and (3.6.4) we can write,

$$x = -\frac{1}{2}\xi(1-\xi)x_1 + \frac{1}{2}\xi(1+\xi)x_2 + (1-\xi^2)x_5 \quad (3.6.5)$$

Assuming $x_1 = 0$, $x_2 = L_1$, $x_5 = L_1/4$, then

$$x = \frac{1}{2}\xi(1+\xi)L_1 + (1-\xi^2)\frac{L_1}{4} \quad (3.6.6)$$

Therefore,

$$\xi = (-1 + 2\sqrt{\frac{x}{L_1}}) \quad (3.6.7)$$

In the Jacobian the term $\partial x / \partial \xi$ is given by

$$\frac{\partial x}{\partial \xi} = \frac{L_1}{2}(1+\xi) = L_1\sqrt{\frac{x}{L_1}} \quad (3.6.8)$$

which makes the singularity of the Jacobian at (x = 0, ξ = -1). Assuming only the displacements of the points 1, 2, and 5, the displacement function is written along the line 1-2 as,

$$u = N_1 u_1 + N_2 u_2 + N_5 u_5 + N_1 \frac{h_1}{2} \zeta B_1 + N_2 \frac{h_2}{2} \zeta B_2 + N_5 \frac{h_5}{2} \zeta B_5 \qquad (3.6.9)$$

where ζ varies from -1 for bottom surface to +1 for top surface, h_1, h_2, and h_5 are the thicknesses of the shell element at points 1, 2, and 5 and B_1, B_2, and B_5 are function of $\hat{v}_{1i}$, $\hat{v}_{2i}$, and α_i. Substituting equation (3.6.4) into equation (3.6.9) one obtains,

$$u = -\frac{1}{2}\xi(1-\xi)u_1 + \frac{1}{2}\xi(1+\xi)u_2 + (1-\xi^2)u_5 + (-\frac{1}{2})\xi(1-\xi)\frac{h_1}{2}\zeta B_1 + \frac{1}{2}\xi(1+\xi)\frac{h_2}{2}\zeta B_2 + (1-\xi^2)\frac{h_5}{2}\zeta B_5 \qquad (3.6.10)$$

Putting the value of ξ in equation (3.6.10) and rearranging the terms, equation (3.6.10) can be written as,

$$u = -\frac{1}{2}\left(-1+2\sqrt{\frac{x}{L_1}}\right)\left[2-2\sqrt{\frac{x}{L_1}}\right]\left[u_1 + \frac{h_1}{2}\zeta B_1\right] + \frac{1}{2}\left(-1+2\sqrt{\frac{x}{L_1}}\right)\left[2\sqrt{\frac{x}{L_1}}\right]\left[u_2 + \frac{h_2}{2}\zeta B_2\right] + \left(4\sqrt{\frac{x}{L_1}} - 4\frac{x}{L_1}\right)\left[u_5 + \frac{h_5}{2}\zeta B_5\right] \qquad (3.6.11)$$

where L_1 is the length of the side 1-2.

The strain in the x-direction is written as,

$$\varepsilon_x = \frac{\partial u}{\partial x} = J^{-1}\frac{\partial u}{\partial \xi} = \frac{\partial \xi}{\partial x}\frac{\partial u}{\partial \xi} = -\frac{1}{2}\left[\frac{3}{\sqrt{(xL_1)}} - \frac{4}{L_1}\right]\left[u_1 + \frac{h_1}{2}\zeta B_1\right] + \frac{1}{2}\left[-\frac{1}{\sqrt{xL_1}} + \frac{4}{L_1}\right]$$
$$\left[u_2 + \frac{h_2}{2}\zeta B_2\right] + \left[\frac{2}{\sqrt{(xL_1)}} - \frac{4}{L_1}\right]\left[u_5 + \frac{h_5}{2}\zeta B_5\right] \qquad (3.6.12)$$

The strain singularity is therefore $1/\sqrt{(r)}$ along the line 1-2, where $r = (xL_1)$. In case of a curved shell, the strain along the co-ordinate S_1, could be shown to have a variation of $1/\sqrt{(r)}$ where r is measured along the shell surface from the crack tip. By using elasticity matrix in addition to strain singularity, it is shown that stresses have the $1/\sqrt{(r)}$ singularity for plates and shells.

Therefore, the singularity (of stresses and strains around the crack tip singular) is achieved by providing the mid-side node at the quarter points of the sides, facing the crack tip.

3.8 Static Substructuring

3.8.1 General

The detailed analysis of an offshore steel structure with a plane frame configuration is very difficult, using conventional finite element analysis. The development of substructuring techniques in finite element analysis has reduced such difficulties. This technique follows basically the static condensation method in which any unwanted degrees of freedom are condensed out from the substructure global matrices. Numerous programs using finite element analysis use this technique to solve very large problems. In the present study ABAQUS finite element software (1999) was used to obtain the results of static analysis of the offshore structural plane frame by static substructuring technique. In the following section, the theory related to the static condensation and substructure matrix formulation is given for the better understanding of the analysis carried out in this study.

3.8.2 Static Condensation

The term condensation means to contract the size of a system of equations by eliminating certain degrees of freedom. In this process the total original set of degrees of freedom are divided into retained quantities and eliminated quantities. The condensed equations are expressed in terms of the eliminated degrees of freedom and retained degrees of freedom. Mathematically, the matrix equilibrium equation in the finite element analysis is written as (Mcguire and Gallagher 1979),

$$[K]\{\Delta\}=\{P\} \qquad (3.7.1)$$

and

$$\{\Delta\} = \begin{Bmatrix} \Delta_b \\ \Delta_i \end{Bmatrix} \tag{3.7.2}$$

where [K] is the stiffness matrix, $\{\Delta\}$ is the nodal variable vectors, $\{P\}$ is the nodal load vectors, $\{\Delta_b\}$ is the eliminated degrees of freedom and $\{\Delta_i\}$ is the retained degrees of freedom.

In the partitioned form the equilibrium equation is written as,

$$\left[\begin{array}{c|c} K_{bb} & K_{bi} \\ \hline K_{ib} & K_{ii} \end{array}\right] \left\{\begin{array}{c} \Delta_b \\ \hline \Delta_i \end{array}\right\} = \left\{\begin{array}{c} P_b \\ \hline P_i \end{array}\right\} \tag{3.7.3}$$

By solving the first set of equations, one obtains

$$\{\Delta_b\} = -[K_{bb}]^{-1}[K_{bi}]\{\Delta_i\} + [K_{bb}]^{-1}\{P_b\} \tag{3.7.4}$$

Substituting equation (3.7.4) into the second set obtained from equation (3.7.3),

$$\left[-[K_{ib}][K_{bb}]^{-1}[K_{bi}] + [K_{ii}]\right]\{\Delta_i\} = \{P_i\} - [K_{ib}][K_{bb}]^{-1}\{P_b\} \tag{3.7.5}$$

In an abbreviated form, it can be written as,

$$[\hat{K}_{ii}]\{\Delta_i\} = \{\hat{P}_i\} \tag{3.7.6}$$

where

$$[\hat{K}_{ii}] = [[K_{ii}] - [K_{ib}][K_{bb}]^{-1}[K_{bi}]] \tag{3.7.7}$$

$$\{\hat{P}_i\} = \{P_i\} - [K_{ib}][K_{bb}]^{-1}\{P_b\} \tag{3.7.8}$$

and

Then Δ_i is calculated according to equation (3.7.6) as,

$$\{\Delta_i\} = [\hat{K}_{ii}]^{-1}\{\hat{P}_i\} \tag{3.7.9}$$

By substituting the value of 'Δ_i' in equation (3.7.4),

$$\{\Delta_b\} = [K_{bb}]^{-1}\{P_b\} - [K_{bb}]^{-1}[K_{bi}][\hat{K}_{ii}]^{-1}\{\hat{P}_i\} \tag{3.7.10}$$

The advantage of this method is that the original matrix (without partition) is divided into a number of small matrices, so that the inversion operation is done easily and this can be important in treating problems of very large size or in using limited computer in-core memory storage.

3.8.3 Matrix Formulation for Static Substructuring

In static substructuring method, major components of the structure, called substructures, are first analyzed independently and the results are then combined for the entire structure. The equations of condensation are directly followed by the mathematics of substructuring. The stiffness equation for a specified substructure 'N' can be written in the partitioned form as,

$$\begin{Bmatrix} P_b^N \\ --- \\ P_i^N \end{Bmatrix} = \begin{bmatrix} K_{bb}^N & | & K_{bi}^N \\ --- & --- & --- \\ K_{ib}^N & | & K_{ii}^N \end{bmatrix} \begin{Bmatrix} \Delta_b^N \\ --- \\ \Delta_i^N \end{Bmatrix} \tag{3.7.11}$$

The subscript 'b' and 'i', respectively denote the degrees of freedom internal to the substructure, viz., not associated with any other substructure and degrees of freedom located on the interface between two substructures.

By applying the same concept that has been applied to the static condensation, the retained nodal displacements are obtained as,

$$\{\Delta_i^N\} = [\hat{K}_{ii}^N]^{-1}\{\hat{P}_i^N\} \tag{3.7.12}$$

where,

$$[\hat{K}_{ii}^N] = [[K_{ii}^N] - [K_{ib}^N][K_{bb}^N]^{-1}[K_{bi}^N] \quad \textit{and}$$

$$\{\hat{P}_i^N\} = \{P_i^N\} - [K_{ib}^N][K_{bb}^N]^{-1}\{P_b^N\} \tag{3.7.13}$$

Assuming $[K_{ib}^N][K_{bb}^N]^{-1}\{P_b^N\}=\{R_i^N\}$ equation (3.7.12) can be written as,

$$[\hat{K}_{ii}^N]\{\Delta_i^N\} = \{P_i^N\} - \{R_i^N\} \tag{3.7.14}$$

In this equation, it is seen that condensed stiffness matrix $[\hat{K}_{ii}^N]$ relates the interface degrees of freedom $\{\Delta_i^N\}$ and the force acting at the interface nodes, $\{P_i^N\}$, plus fictitious

nodal loads, $(-\{R_i^N\})$, which are equivalent to the effect of real forces acting at the interior nodes. According to equation (3.7.14) it is clear that the entire substructure N can be treated as a single element having substructure stiffness matrix $[\hat{K}_{ii}^N]$. Then the stiffness equations for all the interface degrees of freedom for the complete structure are obtained and assembled to form substructure stiffness matrices, interface nodal forces, and equivalent nodal loads. It is written in the following form,

$$[\hat{K}_{ii}]\{\Delta_i\} = \{P_i\} - \{R_i\} \tag{3.7.15}$$

where $[\hat{K}_{ii}]$ is the stiffness matrix for the interface degrees of freedom for the complete structure, $\{\Delta_i\}$ is all the interface nodal degrees of freedom, and $\{P_i\}$ and $\{R_i\}$ are the interface nodal forces and equivalent nodal loads, respectively. The rules of assembly of substructure equations are the same as the conventional finite element analysis. The displacements of all the interface nodes are calculated after solving equation (3.7.15). The displacement of interior nodes within the substructure are then calculated by using the displacement of the interface nodes of the substructure. The equation for this case is written as,

$$\{\Delta_b^N\} = -[K_{bb}^N]^{-1}[K_{bi}^N]\{\Delta_i^N\} + [K_{bb}^N]^{-1}\{P_b^N\} \tag{3.7.16}$$

By calculating all of the nodal-point displacements, element outputs such as stresses, strains, forces and support reactions are obtained in the usual manner.

3.9 Summary

In this chapter the theory associated with the formulation of stiffness matrices of 8-noded isoparametric quadrilateral thin shell elements, and elements having stress-strain singularity (around the crack-tip nodes) are discussed along with the substructuring technique. The results presented and discussed in the subsequent chapters are based on these theoretical developments.

Chapter 4

Stress Analysis of Uncracked and Cracked Joints of an Offshore Plane Frame

4.1 General

Stress analysis at critical regions (junctions or joints) of an offshore jacket structure fabricated from tubular members is required to predict the fatigue life of the structure and to understand the behaviour of such joints under severe environmental loading. In order to do these, several attempts have been made in the past to determine stresses in tubular joints (with or without stiffeners) of various geometrical shapes by means of experimental and analytical methods. In order to determine the location of hotspot regions and the amount of stress concentration present at these locations, static analysis of the entire structure is essential. Approximate localized loading of the brace cylinder has been made using analytical solutions obtained on the basis of classical thin shell theories. However, these theories have not assisted in the analysis of complex tubular joints. In recent years, due to the development of finite element method, the most realistic and accurate stress analysis of tubular joints has become possible without taking recourse to any drastic approximations. Reliable values of stress concentration factors (SCF is the ratio of hot spot stress to nominal stress in the brace) for the joints are required to predict accurately the fatigue lives of various joints of these jacket structures. Any reduction in stress

concentration factor will lead to an increase in the estimate of overall fatigue life of the structure. In the present study, interest is focused on the evaluation of local stress-strain variations at different joints of the offshore plane frame due to the development of cracks at the complex tubular YT intersection. For the cracked structure, the crack was introduced at the highest stress location called the hot spot. In order to determine this location, prior analysis for stress and strain distribution around the intersection of tubular members in a joint without a crack, is required.

Two types of arbitrary through-thickness crack models were considered for use in the present study. In the first case, crack was modeled considering regular elements (in the finite element analysis) and in the second case, it was modeled by special elements having their mid side nodes (facing the crack tip) shifted to quarter points of the 8-noded quadrilateral isoparametric shell elements, with a reduced integration of 2×2 Gaussian quadrature. However, in both cases, the magnitude and distribution of stresses near the crack tip were necessary to determine the crack tip stress intensity factor and corresponding crack growth rate. It will be shown that the second type of element gives the proper representation of stress concentration at the joint.

In order to carry out the studies mentioned above, an extensive stress analysis using finite element method was carried out for the offshore plane frame with YT, Y, LY and L joints. The plane frame was taken as one side panel of a three-dimensional offshore jacket structure and is shown in Figure 4.1. The reduction become necessary due to the very

large matrix size required for modelling the whole prototype structure. This study was carried out only for an in-plane bending load that was applied at the top of the framed structure.

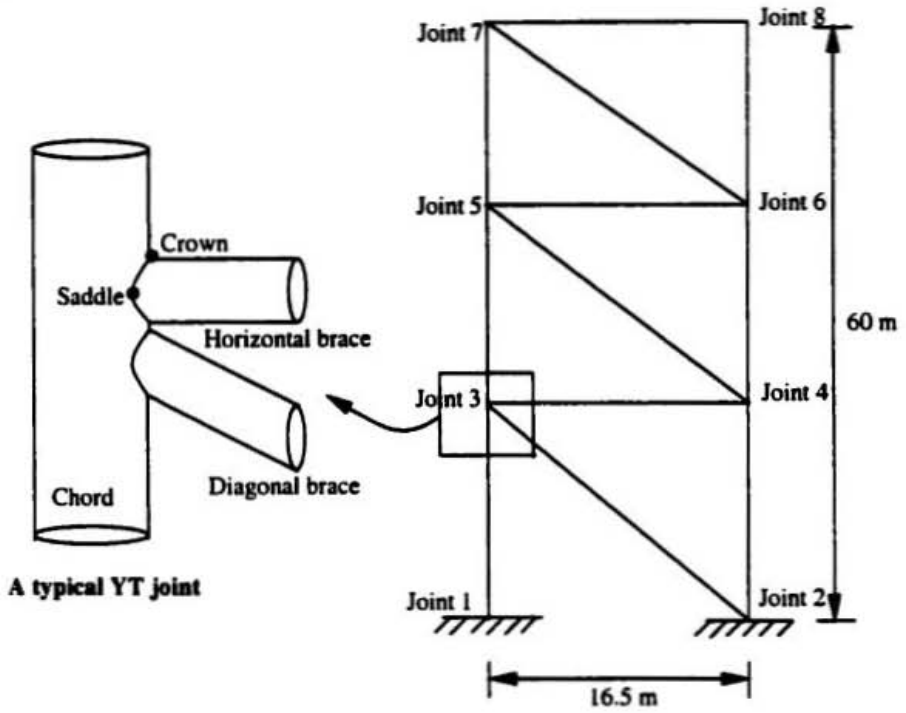

Figure 4.1: One side panel of a three-dimensional offshore jacket structure.

4. 2 Stresses in Tubular Joints

It is well known that axial stiffness of a tubular member is quite large, and it is more compliant to forces that cause ovalisation of the member. The geometry of the tubular-jointed structure is such that brace is compliant in directions where chord is stiff, and vice versa. Complex patterns of displacements occur at these joints due to the large differences that exist between relative stiffnesses in orthogonal directions and the consequent deformation stresses that are developed (which maintain the continuity at the intersection)

(Nwosu 1993). In order to have a clear idea about the deformation stresses that are developed, graphical plots of deformations that occur in a tubular T-joint, under brace tension loading, are shown in Figure 4.2.

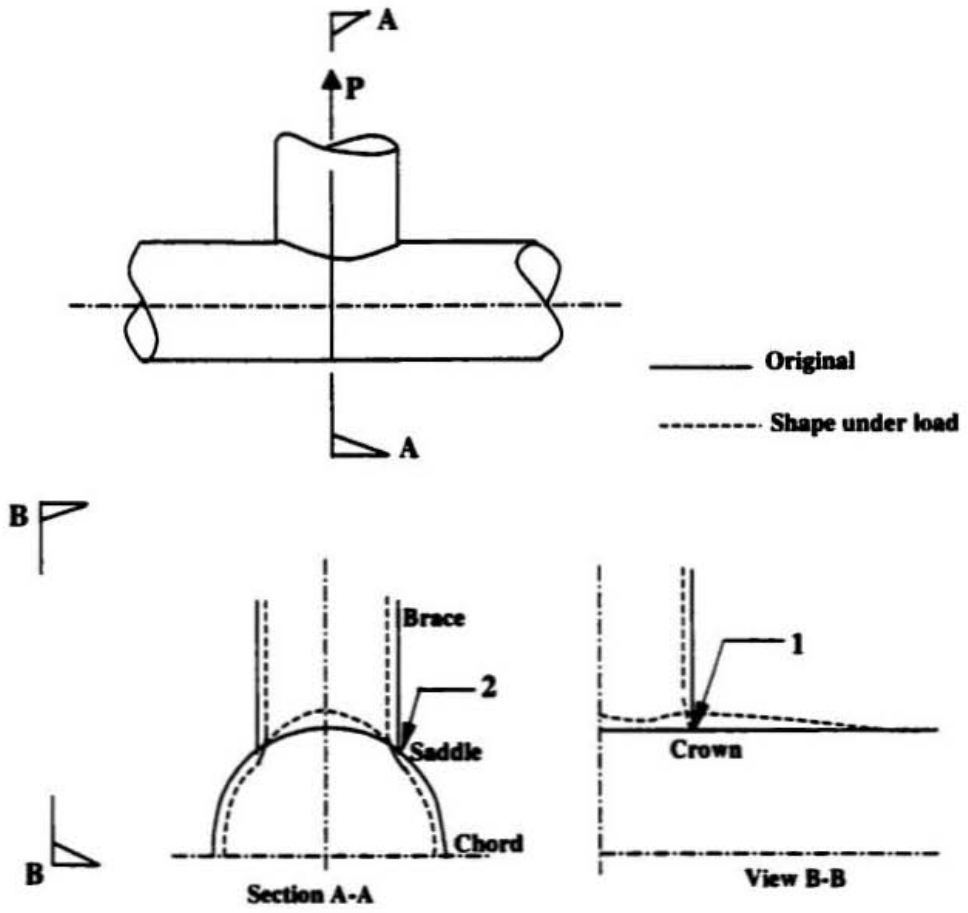

Figure 4.2: Deformation stresses at a T joint under brace tension load (Nwosu 1993)

If the tension load was to be applied to the brace alone, then due to the constant stiffness of the brace, saddle point (2) and crown point (1) should displace by similar amounts. In order to maintain compatibility at the joint intersection, chord wall deforms, thereby

developing bending and membrane stresses in the chord wall. In case of axial loading and out-of-plane bending loads, a large force is required at the saddle than at the crown to develop the same amount of deformation (as the brace) due to greater chord stiffness present at the saddle than that at the crown. On the other hand, for in-plane bending a large force is required at the crown than at the saddle. As a consequence a nonuniform stress distribution is developed near the intersection of the tubular joints. This phenomenon is shown in Figure 4.3.

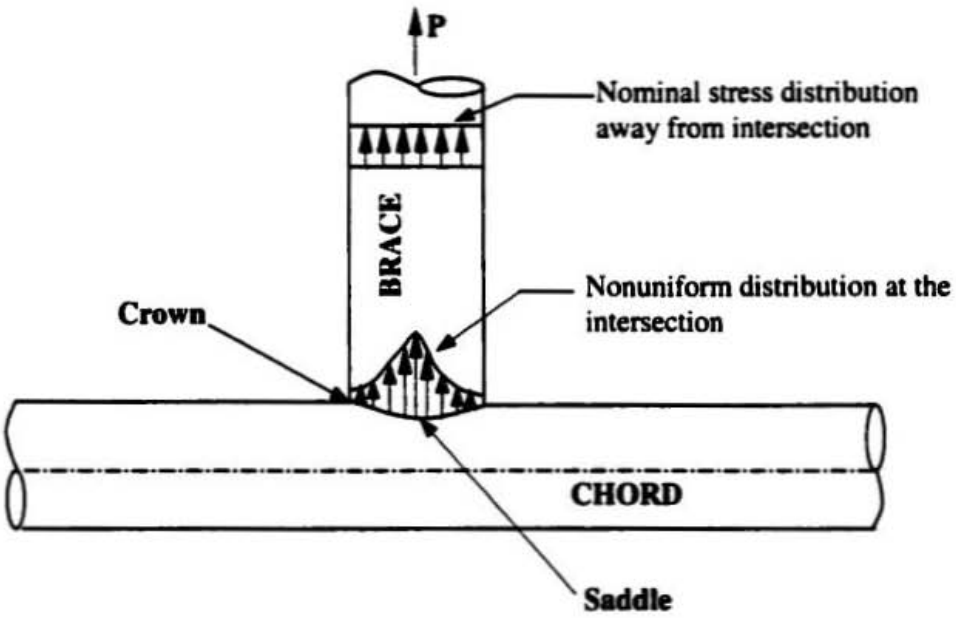

Figure 4.3: Nonuniform distribution of stresses at the intersection under axial tensile loading (Nwosu 1993)

The deformation stresses indicated in Figure 4.3 arise at the intersection due to the development of non-uniform distribution of stresses that cause the various bending and membrane (in-plane) deformations at the joint. Other factors that contribute to the

development of high stresses in the tubular joints are the constraints that are exercised around the intersection and the geometric discontinuity that is present due to the presence of weld. Traditionally nominal stresses at the joints of offshore jacket structures are determined using a space frame analysis. Uncertainties due to nonlinear behavior of foundations (due to soil-structure interaction), load transfer between jacket legs and main piles, joint eccentricities, and joint flexibilities that arise due to improper welding at joints will modify the stresses/strains obtained from a deterministic analysis. Usually for the analysis of these types of structures, rigid connections at the base are assumed, eliminating the influence of soil foundation. In case of fatigue analysis, axial and bending stresses obtained from frame analysis (considering beam elements and rigid connection at joints) are considered as nominal stresses. Moreover, bending stresses caused by the local secondary moment that develops due to the deformations occuring in the joint area (due to brace stresses) are also significant compared to total stresses. This secondary bending effect can be included in the analysis of total stresses if the model of the joint is prepared properly using shell or solid elements instead of beam elements; consequently the joint flexibility (or stiffness) is determined with much greater accuracy.

4.3 Finite Element Mesh Generation

The mesh for the entire plane frame was generated using the finite element software ABAQUS and FORTRAN programming. Ahmad et al's (1970) finite element development using three-dimensional 20-noded brick element, degenerated to two-dimensional 8-noded isoparametric shell elements with reduced integration (S8R5), was

used to discretize the cylindrical surface of brace and chord members. This element has the advantage that extra degrees of freedom in the thickness direction can be reduced and it has the inherent feature of modeling any curved geometry. At each node of the shell element five degrees of freedom are considered (three displacements and two rotations). Common joint intersection approach was used to identify the coordinates of the nodes along the brace and chord member intersections and FORTRAN programming was used to generate the coordinates of these nodes and elements. The mesh for other regions of the chord and brace were generated using automatic mesh generation facilities available in 'ABAQUS'. In order to avoid excessive element distortion within the model proper aspect ratios (using BIAS formulation available in ABAQUS) were used. However, it was not possible to provide similar aspect ratios in some regions of the frame due to the introduction of coarse mesh sizes, specially in the middle portion of the brace and chord members. For this reason some warning messages were observed during the running of the program. Special care was taken during the generation of mesh sizes near the intersection of members. Relatively fine meshes were used near the intersection of the cylindrical members to account for the inherent effects of stress concentrations around the joints (0.75<aspect ratio<1.5). The transition from a fine mesh to a coarse one was made in a gradual manner. At the intersection of horizontal brace and chord (where the crack was to be located), three rows of elements were used with 48-elements in each row around the intersection; thereafter the next 5 rows contained 24 elements in each row and the rest of the chord had 12 and 6 elements in each row (maximum aspect ratio = 2.875). However, at the intersection of all the other joints, two rows of elements were used consisting of 24 elements in each row and the remaining part was discretized using

reductions similar to the above procedure. In order to reduce the elements from 48 to 24 to 12 to 6, multi-point constraints (MPCs) were used along the line of transition elements. These constraints enforce boundary conditions at the element boundary. For this reason, these MPCs were not used in the region with high stress and deformation gradients and near positions where details of local stresses/strains and deformations were of primary interest. Each YT joint itself consisted of four different components, namely, the plug, chord, diagonal brace and horizontal brace. The components of a tubular YT joint are shown in Figure 4.4.

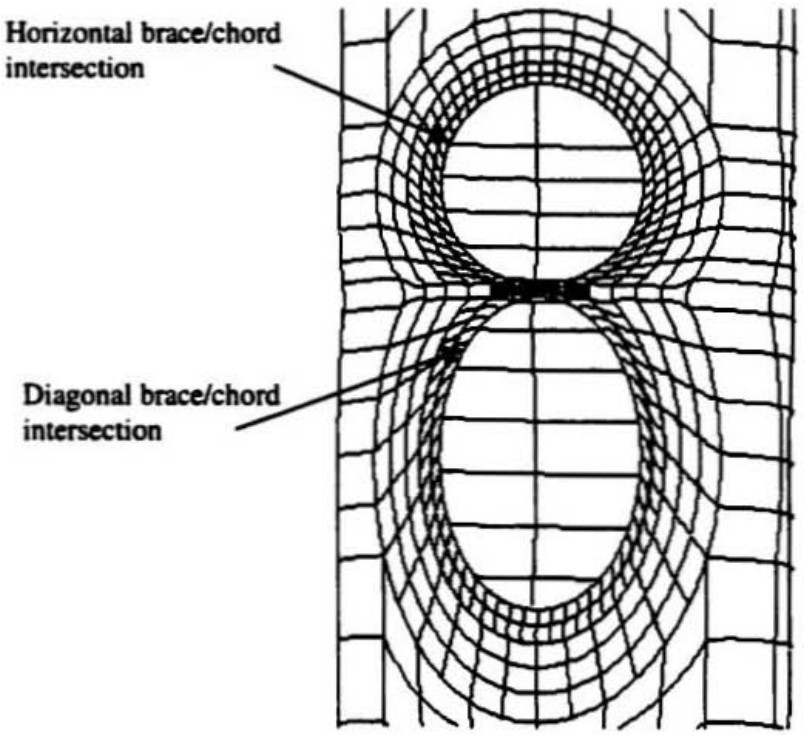

(a)

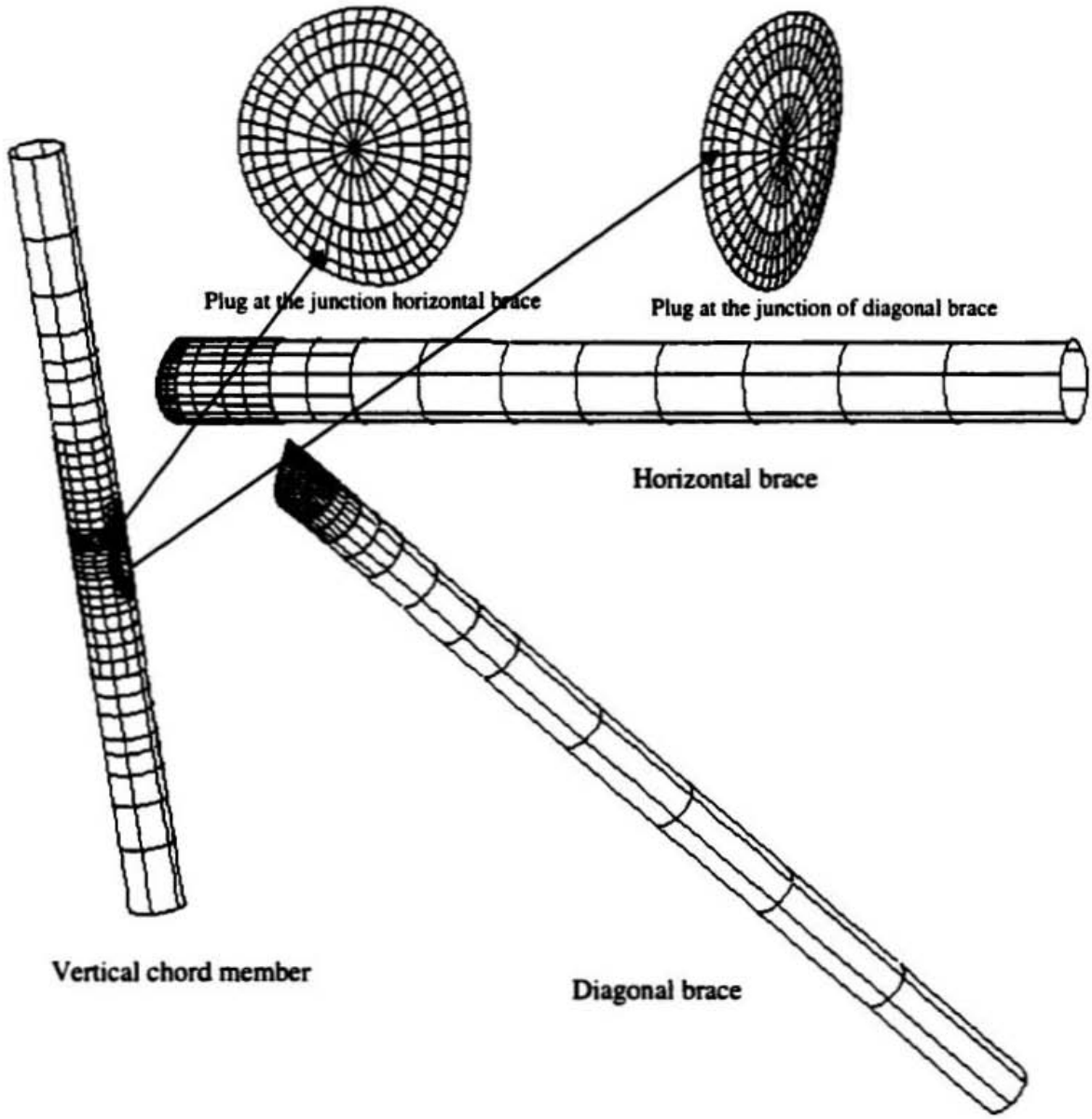
Plug at the junction horizontal brace
Plug at the junction of diagonal brace
Horizontal brace
Vertical chord member
Diagonal brace

(b)

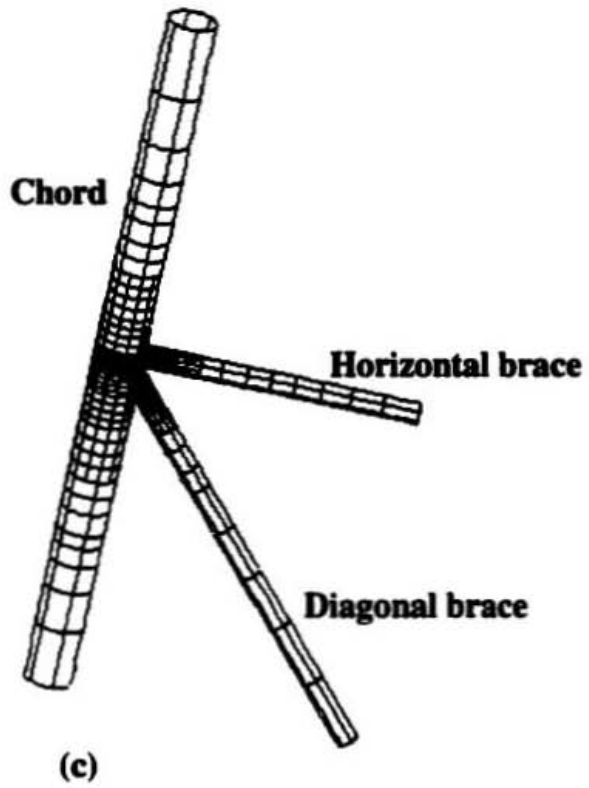

Figure 4.4: Typical computer mesh generation for YT joints; (a) At the intersection of brace and chord member; (b) Details showing the brace, chord and plug; and (c) Full joint configuration.

Substructuring finite element technique was utilized to analyze the entire structure. The entire structure was divided into eight substructures as shown in Figure 4.5. Multilevel application of substructuring technique reduced the mesh generation effort for the whole frame enormously. Mesh generation of substructures 3 and 4 was used in substructures 5 and 6 due to their identical geometry within the structure. In this case different node numbers were used only at the substructure boundary to connect each substructure to the other one. Within the substructure, changes were made for the nodal co-ordinates.

Substructures 1, 2, 7, and 8 were considered as independent substructures. The partitions that were considered for the sub-structuring are shown in the Figure 4.5.

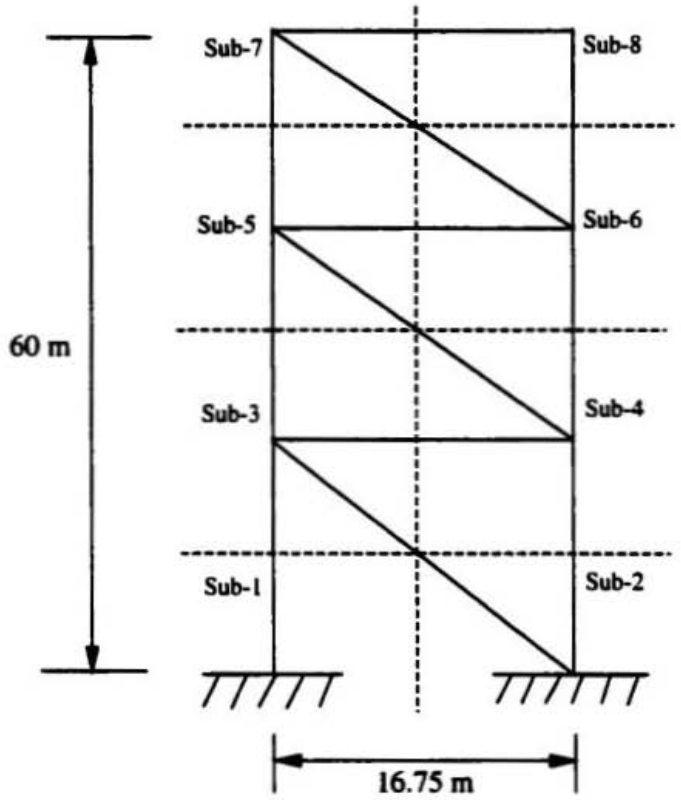

Figure 4.5: Substructures of the plane frame structure

Because of geometrical compatibility at the intersection of the brace, chord and plug, the mesh generation of the plug region was performed in such a manner that from the intersection to a substantial distance away from it, quadrilateral elements were used; and the remaining part of the plug was filled with triangular elements (see Figure 4.4 (b)). For the whole structure, eight substructures were considered and the total degrees of freedom

for the entire structure were obtained as 211,270. Substructure 3 alone had 36,670 DOFs. When substructuring approach was applied it reduced the DOFs to 1180.

4.4 Finite Element Model of the Cracked Joint

After completing the stress analysis of the intact structure, the critical region (hot spot) was found out in order to introduce the through-thickness crack. In the present study load was applied at the top of the frame and the shape of the joint configuration, where critical stress developed, was a YT joint. Due to the nature of the joint, non symmetric stress distributions were developed around the intersection; the maximum local stresses were not developed exactly at the saddle point or at the crown point. In order to exactly determine the stress field clearly near the crack tip, the analysis would require the use of solid 3-D elements, which also incorporated the stress singularity at the crack tip. However, mesh generation using this element would be quite expensive and cumbersome; also it would need a very large computer facility with a very large in-core memory. Depending on the present computer facilities available to the author, a crack analysis using 3D elements for the entire structure was not possible. Another possibility was to use the line-spring elements developed by Rice and Levy (1972) for the growth of surface crack through wall thickness; but the substructuring application of ABAQUS did not allow one to use the line spring elements that were available in ABAQUS.

In the present study, crack was considered to be a through-thickness crack, i.e., depth of the crack was equal to the entire thickness of the chord wall. It was located 3 cms away

from the line of intersection of the horizontal brace and chord, along the line of intersection of the first and second rows of elements in the chord, around the weld-toe (to facilitate the computer to understand that the crack was occurring in the chord wall; and in addition it also facilitated the inclusion of the effect of weld metal thickness, around the toe of the joint, to be made equal to one element width). For the consideration of the effect of crack lengths, the study considered one symmetrical half of crack to extend over one, two, three, four, five, six and seven elements, respectively, along the weld toe. One element length was equal to approximately 0.0405 m. Crack was introduced along the weld toe by applying different node numbers at the same co-ordinate as shown in Figure 4.6. ABAQUS has the capability to develop a cracked surface, if two different node numbers are used in the same coordinate. The finite element model of the crack was prepared using this facility. In order to obtain the stress singularity at the crack tip, the concept of the quarter point node in 8-noded isoparametric shell element, developed by Barsoum (1976), was used.

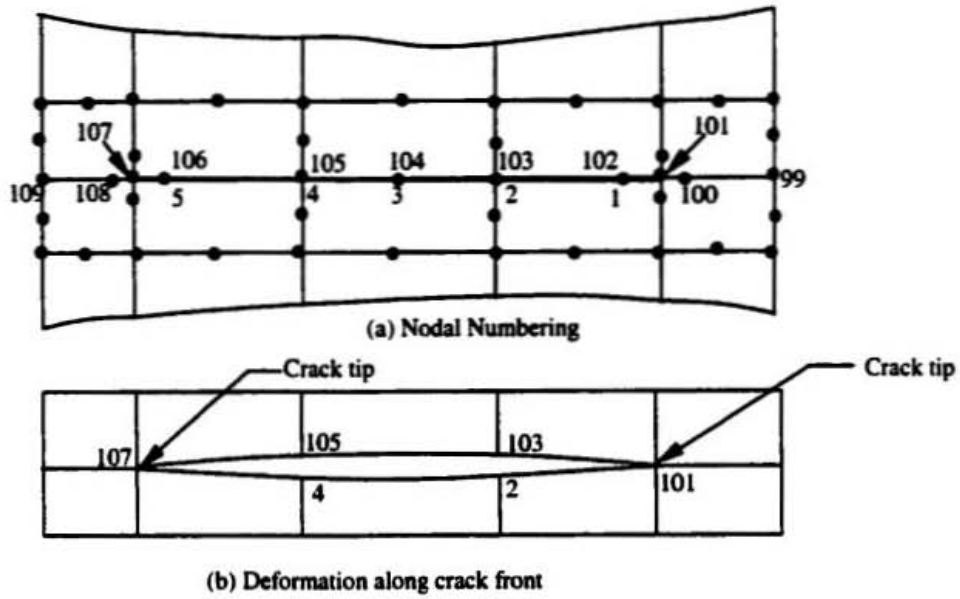

Figure 4.6: Implementation of crack in ABAQUS

4.5 Model Dimension

The use of a real three-dimensional frame structure would require a large amount of computational effort, computer resources and time. For this reason the structure considered in this study (as mentioned earlier) was an idealized two-dimensional version of three-dimensional framed offshore structure. The height and width of this plane frame was considered to be 60 m and 16.75 m, respectively. The chord and brace diameters were assumed as 135 cm and 60 cm, respectively, and the thickness of both members was assumed as 2.5 cm. However, along the intersection of the members at the joint, the thickness of two rows (one row of elements on the chord side and the second row of elements on the brace side) of elements was considered to be 3.5 cm, taking into account

the effect of weld thickness at the joint. The centre line diagram of this frame, with dimensions, was given earlier in Figure 4.5.

4.6 Boundary Conditions and Loading

Fixed boundary conditions, i.e., all displacement degrees of freedom and rotational degrees of freedom equal to zero, were considered at all nodes at the bottom of the frame. A static concentrated horizontal load was applied at the center of the top plug of the left chord in substructure 7. It acted on the structure in such a way as to impose an in-plane bending load on the entire structure. Loading direction was chosen perpendicular to the chord member and the magnitude was 200 kN.

4.7 Model Accuracy

In order to verify the correctness of the model, results obtained considering quadrilateral shell elements and substructuring technique were compared with those obtained with a frame structure, using two noded cubic beam elements. In this case the global displacements at different locations of the frame agreed to within 5 to 10% error. The stresses at the middle of all relevant elements also agreed to within the same limits. However, the stress values obtained around the intersection of various member of the structure were quite different from those obtained using beam elements. This difference is due to the fact that large stress concentrations occur at the intersection due to the geometric discontinuity of the braces and the effect of weld notch; these stresses cannot be determined properly using beam elements. When discretization of the entire frame was

made using beam elements, appropriate modeling of the joints was not possible due to its one-dimensional nature of element geometry. But modeling of the tubular member surface and intersection using 8-noded quadrilateral isoparametric elements with reduced integration points gives a better estimate of stress distribution. The displacement and stress results, for both cases, are given in Figures 4.7 and 4.8, respectively, for the sake of comparison; very good correlations are obtained for the global displacements and stresses.

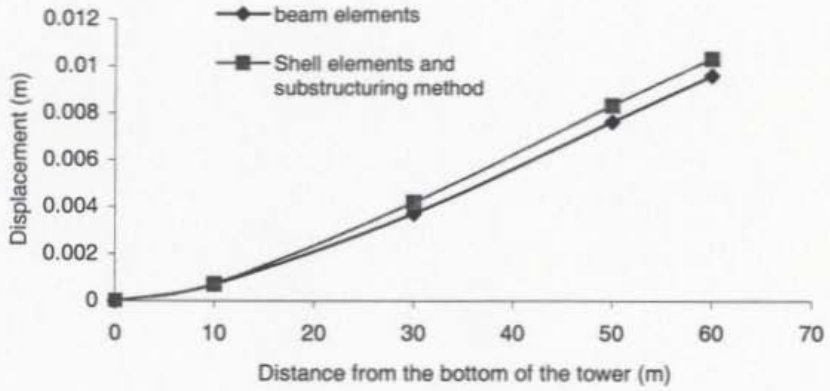

Figure 4.7 (a): Comparison of global x-displacements, along the frame height, using beam element and substructuring (with shell elements) - Displacements considered along the mid-plane of the left-side vertical chord member.

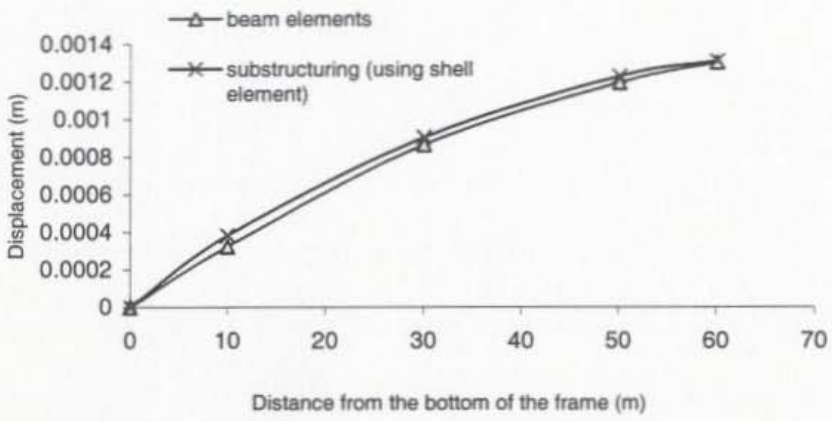

Figure 4.7 (b): Comparison of global y-displacement, along the frame height using beam elements and substructuring (with shell elements) - Displacements considered along the mid-plane of the left-side vertical chord member.

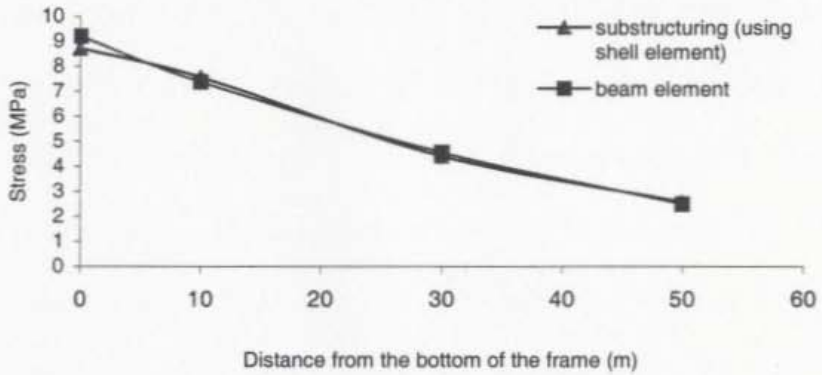

Figure 4.8: Comparison of stresses using beam elements and substructuring (with shell elements) (stress is considered along the middle plane of the left-side vertical chord members).

4.8 Stress Concentration Factors for Axial loading, In-Plane Bending and Out-of-Plane Bending Loads

Stress concentration factors were calculated for three types of loading situations in order to measure the accuracy inherent in the model. Figures 4.9 through 4.11 show the variation of stress concentration factors around the weld toe on the chord side under three loading conditions (axial tension, in-plane bending and out-of-plane bending). These results have shown very good agreement with the results obtained from other researchers. Nwosu (1993) has shown that the maximum stress concentration factor (calculated considering principal stresses) for the axial tension loading and out-of-plane bending develops at the saddle point, and for in-plane bending, it occurs at an angular distance of 37^0 from the crown (see Table 4.1). The model used for the finite element analysis has shown reasonably good agreement in results with those obtained from Nwosu's analysis at some critical points of the model, inspite of some model parameters not being the same. However, other points of the intersection have not shown good agreement. The probable reason might be due to the improper mesh generation at the intersecting region between two braces (horizontal and diagonal brace); in addition it could also be due to the two close-together thick elements (representing the weld thickness) at the adjacent crowns of horizontal and diagonal braces. The space between the two braces on the surface of chord was very small (0.03m). It was found very difficult to maintain the continuity of the mesh generation in this region. The varying thickness of adjacent weld toes at the neighboring crown will cause less load to be transferred to the thinner chord

section in between crowns. Moreover, the stiffness of the diagonal brace would also modify the state of stress at the crown.

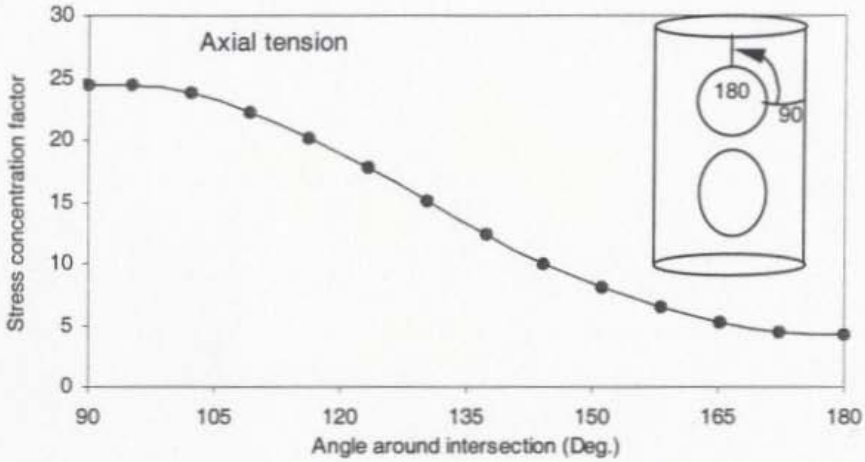

Figure 4.9: Stress concentration factors along the weld toe on the surface of chord at the intersection of horizontal brace and chord (for axial tension) - Angle measured from the bottom crown of horizontal brace/chord intersection at joint 3.

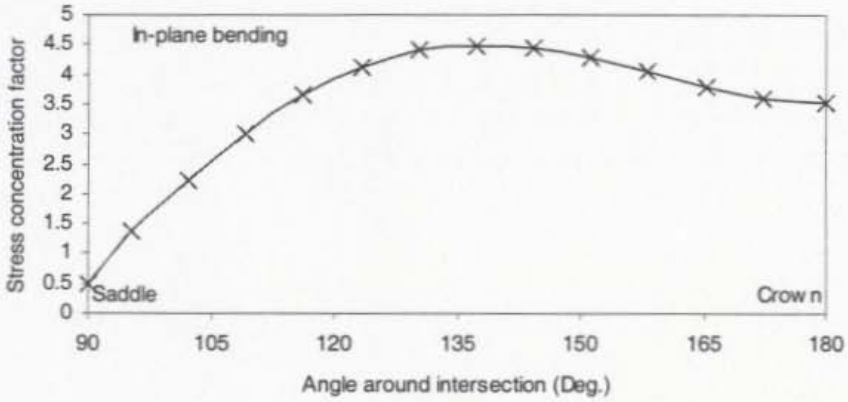

Figure 4.10: Stress concentration factors along the weld toe on the surface of chord at the intersection of horizontal brace and chord (for in-plane bending) - Angle measured from the bottom crown of horizontal brace/chord intersection at joint 3.

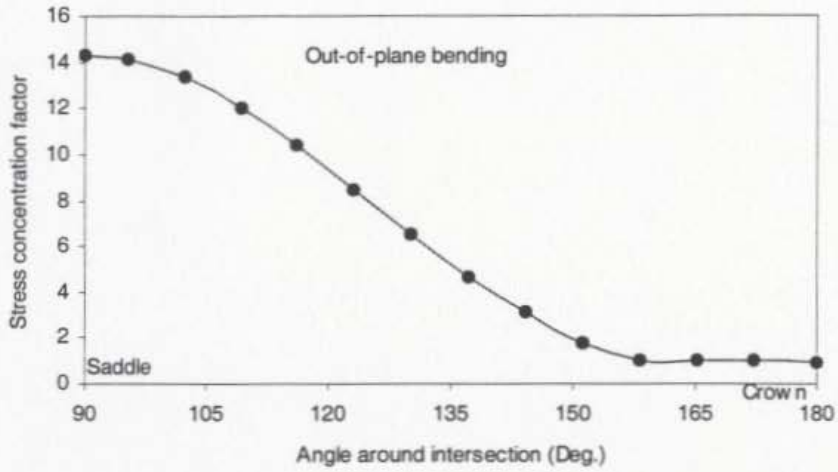

Figure 4.11: Stress concentration factors along the weld toe on the surface of chord at the intersection of horizontal brace and chord (for out-of-plane bending) - Angle measured from the bottom crown of horizontal brace/chord intersection at joint 3.

Table 4.1: Comparison of SCFs between Nwosu's (1993) analysis results and present study at different points along the weld toe; (a) Model Parameters for Nwosu's analysis and present study; and (b) Comparison of results.

(a) Model Parameters for Nwosu's analysis and present study

Model parameters	Nwosu - $\alpha = 2L/D = 7.02$, $\gamma = D/2T = 24$, $\tau = t/T = 1$, $\beta = d/D = 0.5$
	Present study - $\alpha = 29.63$, $\gamma = 27$, $\tau = 1$, $\beta = 0.444$

(b) Comparison of results

Angle around intersection (Deg.)	Axial tension		In-plane bending		Out-of-plane bending	
	Nwosu (1993) results	Present study	Nwosu (1993) results	Present study	Nwosu (1993) results	Present study
90	24.9	24.50	0	0.4766	21.1268	14.294
102.25	23.25	23.77	2.5	2.2352	19.7596	13.38
123.25	16.2	17.74	6.5	4.115	11.34	8.4662
144.25	9.0	10.04	7.5	4.4475	3.7732	3.1046
158.25	6.5	6.43	6.9	4.0601	1.9118	1.0532
180	6	4.23	6.7	3.5189	1.0452	0.9152

4.9 Processing of Results

The stress analysis performed in this study was carried out for an offshore plane frame with tubular Y, YT, LY and L joints. The results of the element stresses and strains at integration points in the local co-ordinate system were taken directly from the values given by 'ABAQUS'. ABAQUS post processor has built-in capability to read and write the stress-strain results from the finite element analysis, to an output file. The input file was prepared for the entire frame using ABAQUS/standard user's manual Vols.1 and II (1999). After preparing this input file, output file required for relating the nodal variables and element variables were developed using a post processing program. The stress output file from the analysis was read by the post processing program and it automatically plotted the local stress distribution for the substructure or for the entire structure. For the comparison study of the stress-strain values at different points of the joint between uncracked and cracked structures, the stress-strain results along the outer wall of the tubular member were taken into account. During the initial stage of the development of crack, high shear stresses are developed; consequently the initiated crack opens at an angle other than 90^0 to the tensile load (shown by the angle between the principal plane and the original direction at the saddle); however, very soon it tends to grow perpendicular to the radial direction along the weld toe.

The local stresses were the preferred stresses to work with, instead of the principal stresses, since in dealing with the principal stresses the orientation of these stresses are required. To define these stress components in a shell element, local directions are required on surfaces in space. The convention of the local co-ordinate system considered

in ABAQUS is that the local axis in 1-direction, at a given point is defined as the projection of the global x-axis onto the shell surface. If the global x-axis is within 0.10 of being normal to the surface, the local 1-direction is taken to be the projection of the global z-axis onto the shell surface. The local 2-direction is then at right angles to the local 1- direction, so that these two local co-ordinates and the positive normal to the surface form a right-handed orthogonal co-ordinate system. The positive normal direction is accounted in an element by the right-hand rotation rule going around the nodes of the element. The local co-ordinate system considered in ABAQUS finite element program is shown in Figure 4.12.

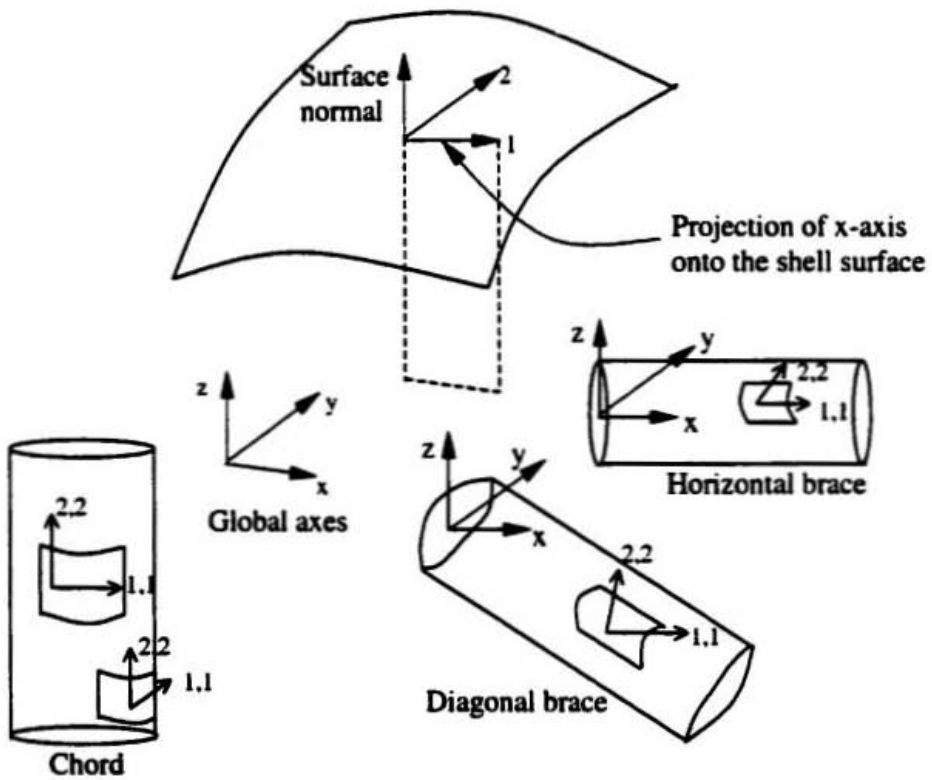

Figure 4.12: The orientation of the local 1-2-3 axes

For determining the deformations, stresses and strains of the uncracked structure, finite element analysis of the intact frame was carried out using the substructure and superelement analysis. Thereafter, an artificial through crack, at the intersection of the horizontal brace and chord of super element 3 (or substructure 3 shown in figure 4.5) was introduced and the analysis carried out for the cracked structure. The changes of local stresses in different elements around the crack region, due to crack development at the hot spot region, were compared with those of the uncracked structure to study the influence due to the presence of cracking at the joint.

4.10 Convergence Test

In order to verify the proper sizing of the elements of the model, a convergence test was carried out on substructure 3 by determining the stresses around the intersection with reasonable accuracy. The substructure 3 was separated from the frame to carry out this analysis. Out-of-plane motion was restrained for the end points of the horizontal brace. At first, 24 elements were used in each of the first three rows on both chord and horizontal brace near the intersection (and each of the first two rows on both chord and diagonal brace intersection also used 48 elements). Thereafter, element numbers were reduced from 24 elements to 12 elements and 12 elements to 6 elements in the remaining portion of the model by providing multi-point constraints along the element transition line. The diagonal brace end was allowed to deform unhindered without any load applied to it. Fixed boundary conditions were imposed at all nodes of both ends of the chord member (of substructure 3) and an axial tensile force (20 kN) was applied at all nodes (12 nodes)

at the end of the horizontal brace. Same procedure was applied in the case of 48 elements and 96 elements (in the first three rows of the chord and horizontal brace intersection). In this study the YT joint with different number of element discretization (24, 48 and 96) around the intersection of the horizontal brace and chord was considered for the comparison of results. The comparison studies of local stress in 1-direction along the weld toe on the chord surface (at a distance 0.0374 m away from the horizontal brace/chord intersection) and around the circumference of brace (at a distance of 0.0325 m away on the horizontal brace from the same intersection) are shown in Figures 4.13 and 4.14. It is observed that maximum differences of stresses in local 1-direction for axial tension loading obtained from 24 elements and 48 elements in each row mesh agree to within 1-5% at different locations on the chord along the weld toe and 25-30% on the brace surface. However, the results obtained with 96 elements in each row are 8-10% greater than the 24 and 48 elements meshes at the chord saddle, and 75% less than the 24 elements mesh and 50% less than the 48 elements meshes at the saddle of the brace. Since chord stresses are greater than the brace stresses (see Figure 4.13 and 4.14) and the difference in stresses between 24, 48 and 96 elements is less than 15% of the stresses along the weld toe on the chord surface, the analysis was carried out using 48 elements. In addition to the above reason it must also be said that the use of 96 elements around the vicinity of weld toe (for the whole structure) was not possible, since it takes a large amount of computer time and in-core memory.

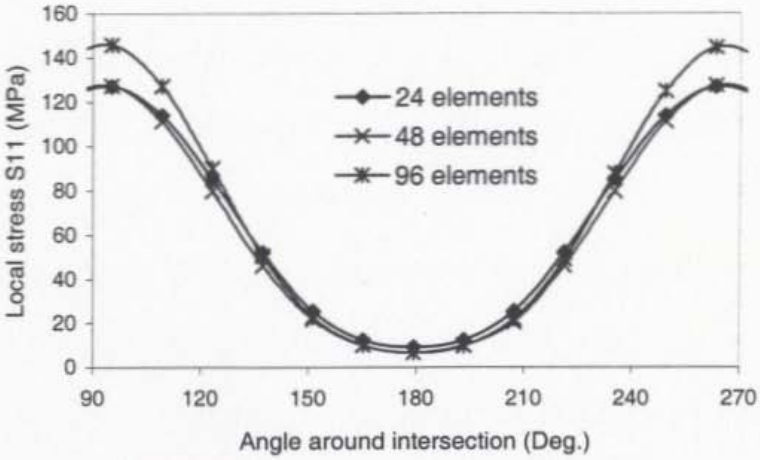

Figure 4.13: Comparison of stresses along the weld toe on the chord surface at a distance of 0.0374 m away from the horizontal brace/chord intersection between 24, 48 and 96 elements near the joints for axial tension loading.

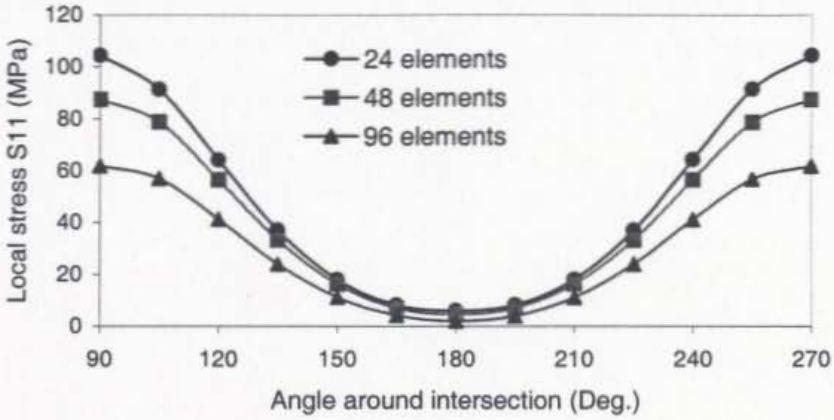

Figure 4.14: Comparison of stresses along the circumference of horizontal brace at a distance of 0.0325 m away from the horizontal brace/chord intersection between 24, 48 and 96 elements near the joints for axial tension loading.

4.11 Results and Discussion

For the given dimensions of chord and brace of the YT joint in substructure 3, under the loading condition prescribed in section 4.6, stresses along the weld toe at the intersection of horizontal brace and chord were observed to be greater than those for the corresponding diagonal brace. This comparison is shown in Figure 4.15 (b). The load on the horizontal brace is a tensile load, while the load on the diagonal brace is compressive. In case of horizontal brace/chord intersection, the chord side had the larger stress than the brace near the weld toe. As stated earlier the horizontal load applied in x-direction, for all the subsequent analysis, was 200 kN at the top of the tower.

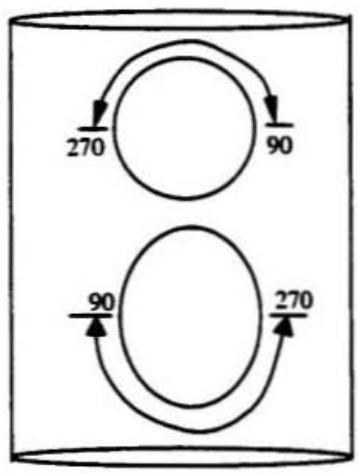

Figure 4.15 (a) Region on chord surface around horizontal brace/chord and diagonal brace/chord intersection to obtain data for comparison of results in Figure 4.15 (b).

For this reason crack was considered to occur at the weld toe of chord surface (along second row of elements at the intersection) and only the stresses at the chord end of the intersection were considered to be of interest. The comparison of local stresses S11 of uncracked structure between chord and brace near the intersection is shown in Figure 4.16.

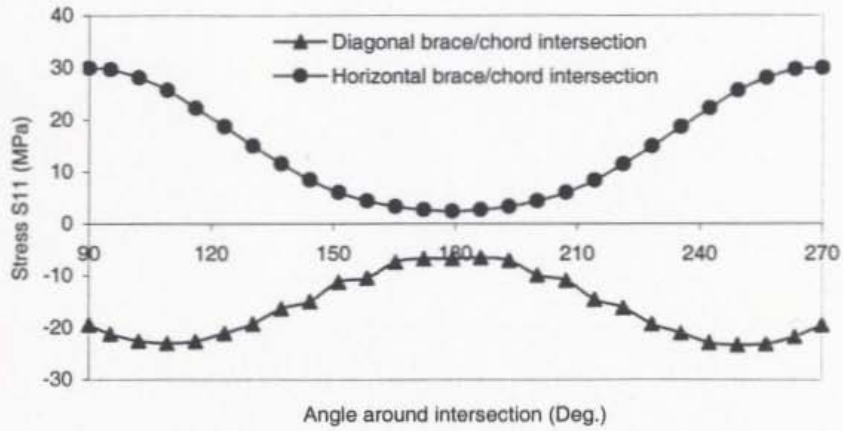

Figure 4.15 (b): Comparison of local stresses in 1-direction along the weld toe on the chord surface between horizontal brace/chord intersection and diagonal brace/chord intersection (at the third Gaussian points of the elements along the second row).

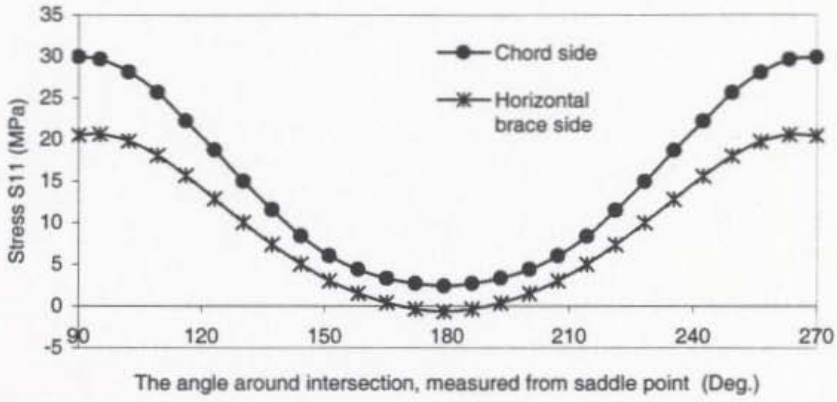

Figure 4.16: Local stresses S11 for uncracked chord and horizontal brace [at the third Gaussian points (on chord surface) and second Gaussian point (on brace surface) of the elements along the second row].

The local stresses in 1- (S11) and 2- directions (S22) as a function of the angle around the chord surface and distance along the horizontal brace surface from the intersection for the given loading condition are shown in Figure 4.17 to 4.19.

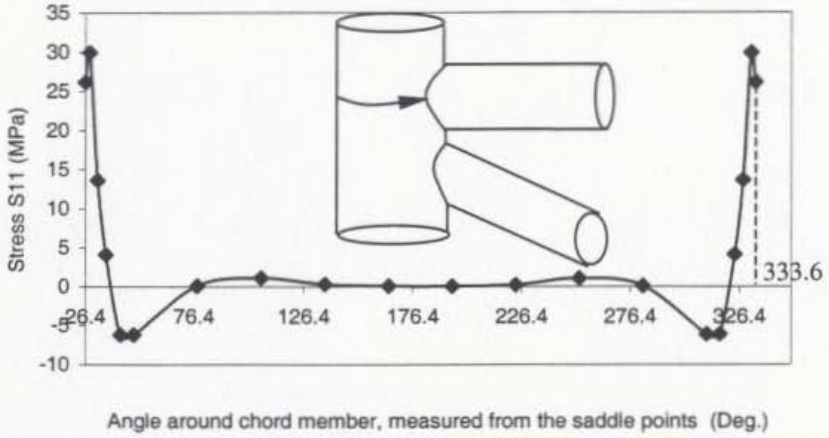

(a)

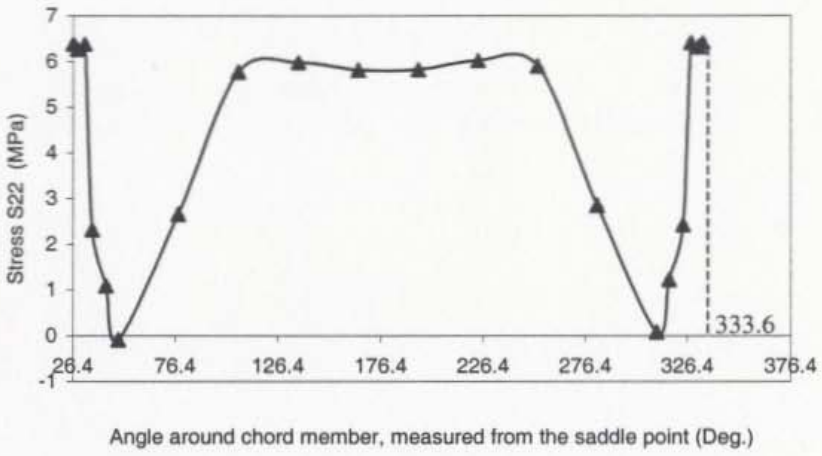

(b)

Figure 4.17: (a) and (b): Local stresses in 1- and 2- directions around the uncracked chord member (at the Gaussian points).

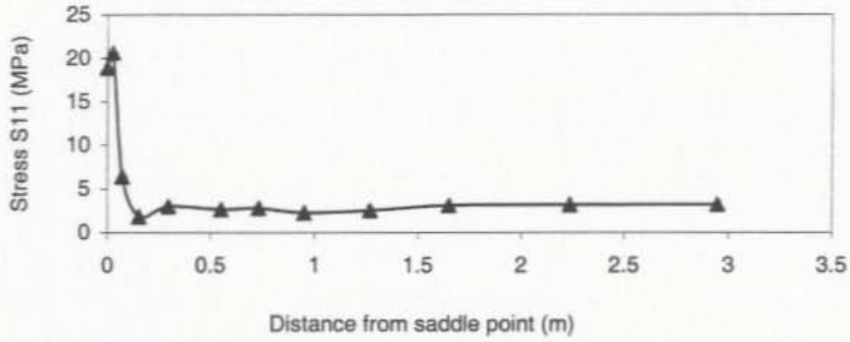

(a)

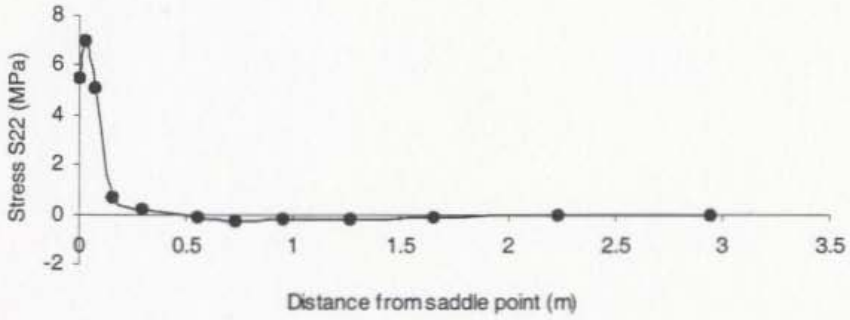

(b)

Figure 4.18: (a) and (b): Local stresses in 1- and 2- directions along the length of uncracked horizontal brace member (at the Gaussian points).

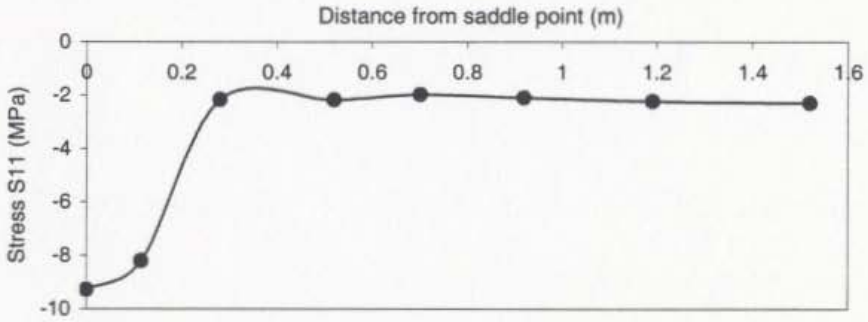

(a)

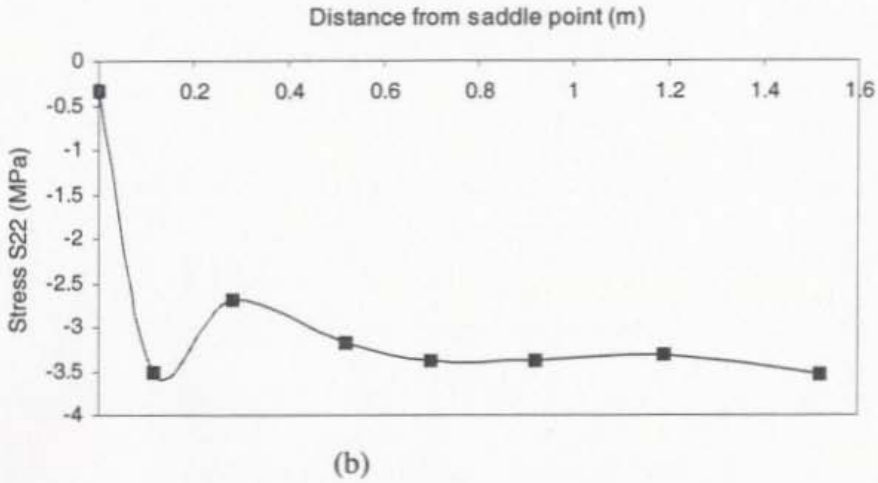

(b)

Figure 4.19: (a) and (b): Local stresses in 1- and 2- directions along the length of uncracked diagonal brace member (at the Gaussian points).

These stresses can be used to estimate the maximum stress at the weld toe by using extrapolation. Since the modelling of weld thickness is almost impossible using shell elements due to the varying thickness of the weld around the intersection, in the present study, it was considered to be have a constant thickness in the two rows of elements (one row in brace and one row in chord at the intersection); the effect of weld was considered to provide an additional 0.01m thickness. It is seen that stresses in the elements, very close to the weld toe (0.0374 m away on the chord surface from the intersection), are much larger on the chord side of horizontal brace/chord intersection than on the brace side surface (0.0325 m away on the brace surface from the intersection) (see Figure 4.17(a)). From Figures 4.18 (a) and (b) and Figures 4.19 (a) and (b) it is also observed that stresses beyond 0.3 m along the horizontal and diagonal brace members from the

intersection (saddle point) are almost constant, indicating that the horizontal brace is subjected to an axial tensile load while the diagonal brace is subjected to an axial compressive load.

The local stress distributions in 1- and 2- directions around the uncracked and cracked substructure 3 (crack length equal to 0.81 times brace radius) are shown in Figure 4.20 and Figure 4.21. From Figure 4.20 it is observed that high local stresses are developed near the saddle point (at 88.25^0 or 271.75^0 from the crown of horizontal brace/chord intersection) of the uncracked section; this occurs due to the location and nature of the applied loads around this weld toe region. The magnitude of stress beyond the hot spot region decreases gradually due to the load distribution on an increasing area. Figure 4.21 shows that the highest stresses in a cracked structure occur at its crack tip.

The variation of local stresses (i) along the weld toe; (ii) around the circumference of the chord; (iii) around the circumference of the horizontal brace near the intersection; and (iv) along the horizontal brace from saddle point between uncracked joint and the presence of crack at the hot region, are shown in Figures 4.22 to 4.25. These figures also show the comparison study of the variation of stresses between the uncracked and cracked structure, with the crack located in substructure 3. The crack lengths considered for presentation are 0.81 times and 1.35 times the radius of the brace member. From Figure 4.22 it is evident, that the maximum stresses are developed at the tip of crack and the magnitude increases as the crack length increases; it is seen from Figure 4.22 (a) that the S_{11} stress (at crack tip) gets amplified by 3.6 times the uncracked hot spot stress when the crack length is 1.35 times the brace radius. The reason for this high stress concentration is

the stress singularity present at the crack tip region. It is also important to note that the stresses in elements which are directly along the crack line at its tip, contain the largest of stresses; the local stress in 1-direction within the elements (other than the crack tip stresses) are also small (see Figure 4.21) and local stress in 2-direction is much larger. The S_{22} stresses increase gradually from a smaller crack to a larger one along the weld toe of the chord surface. This is due to the redistribution of loads that take place along the crack front, as the crack grows from a smaller to a larger crack.

In case of horizontal brace, of stress variations (shown in Figure 4.23) in the elements that are near the crack tip, due to the growth of crack at the critical region, are significant. It is observed that when crack length increases, the magnitude of local stresses in 1- and 2-directions (near the crack tip) decrease slightly; however, both stresses decrease significantly in the elements, which are near the crack. The probable reason for this reduction is the stress relief and load redistribution that occur in the region of the brace, close to the crack.

The stresses around the chord circumference and along the brace is considerably influenced by the development of crack at the hot spot region. Figures 4.24 and 4.25 show the comparison study of stresses around the circumference of chord and along the horizontal brace due to the crack development. In these figures it is observed that local stresses, in 1- and 2- directions near the crack region, are influenced significantly on the chord side. The formation of a through crack, along the weld toe, relieves considerably the S_{11} stress acting along the chord circumference (see Figure 4.24 (a)). However, along the brace this variation is almost negligible (see Figure 4.25 (a)).

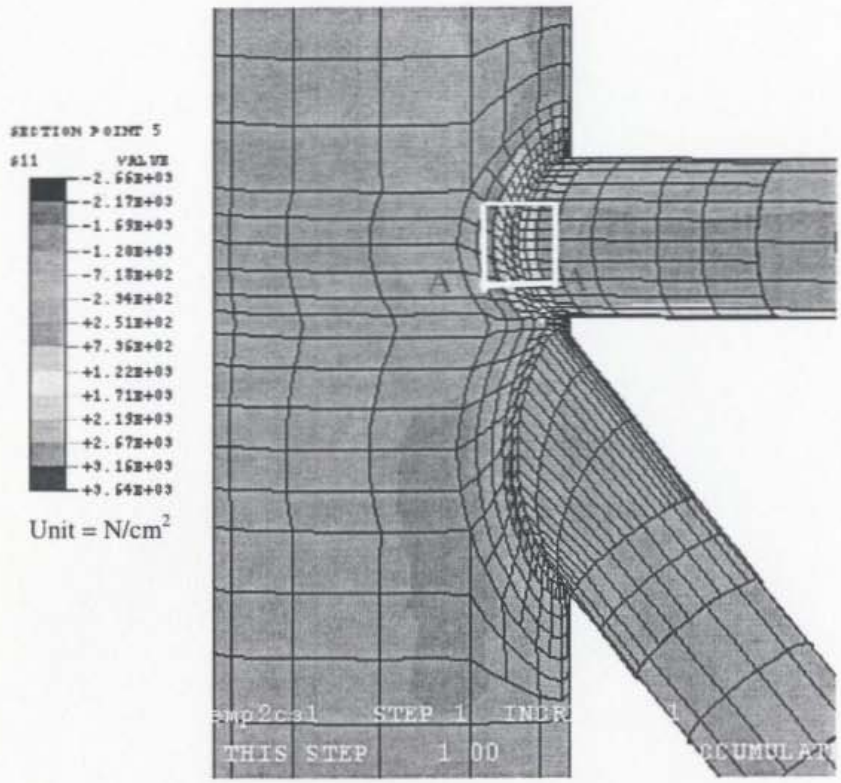

Joint-3 of the plane frame without crack

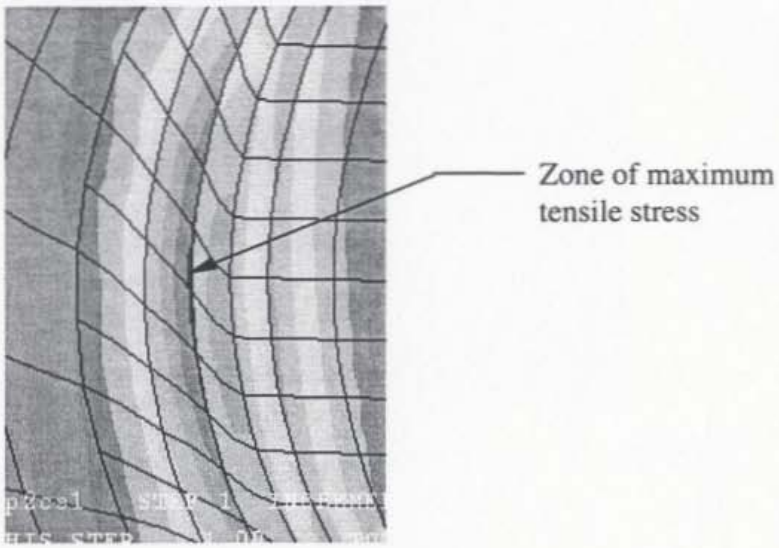

Zoomed picture of portion A-A

Figure 4.20: Local stress distribution in 1-direction around uncracked joint 3 of offshore plane frame.

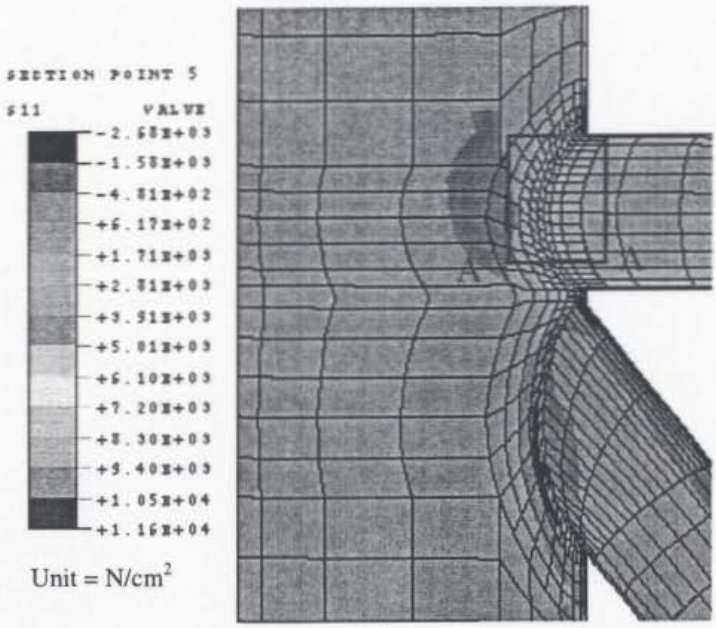

Joint-3 of the plane frame with crack

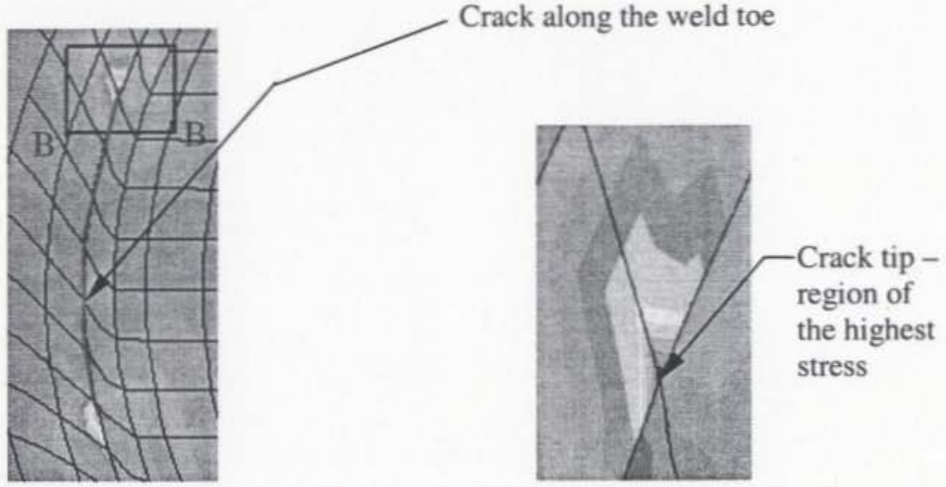

Zoomed picture of portion A-A

Zoomed picture of portion B-B

Figure 4.21: Local stress distribution in 1-direction around cracked joint 3 of offshore plane frame

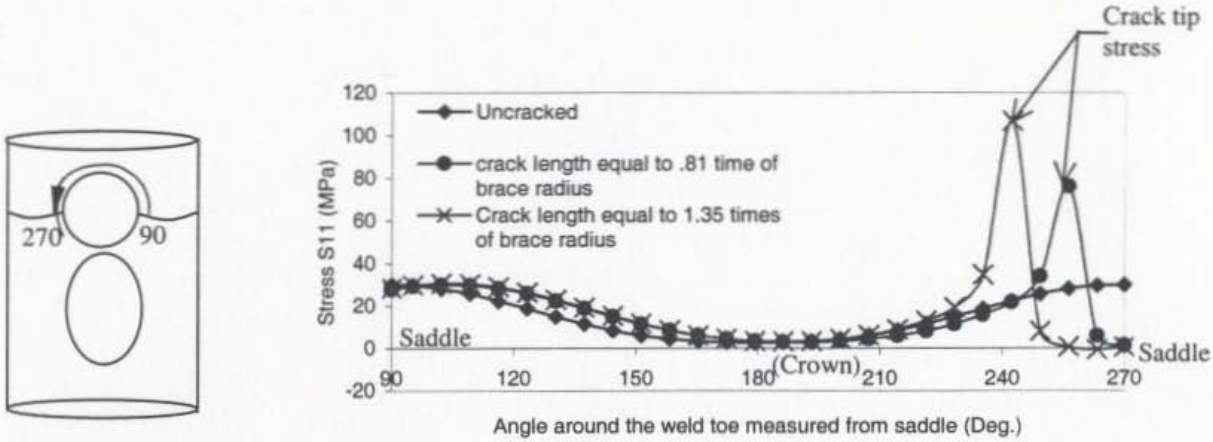

(a)

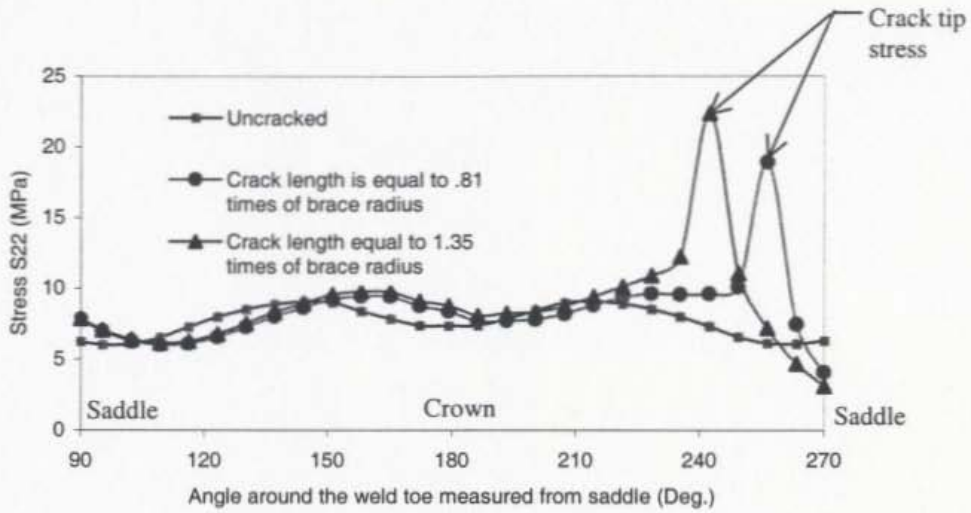

(b)

Figure 4.22: (a) and (b): Comparison of stresses between uncracked and cracked structures with a crack in substructure 3 - Stresses on chord surface.

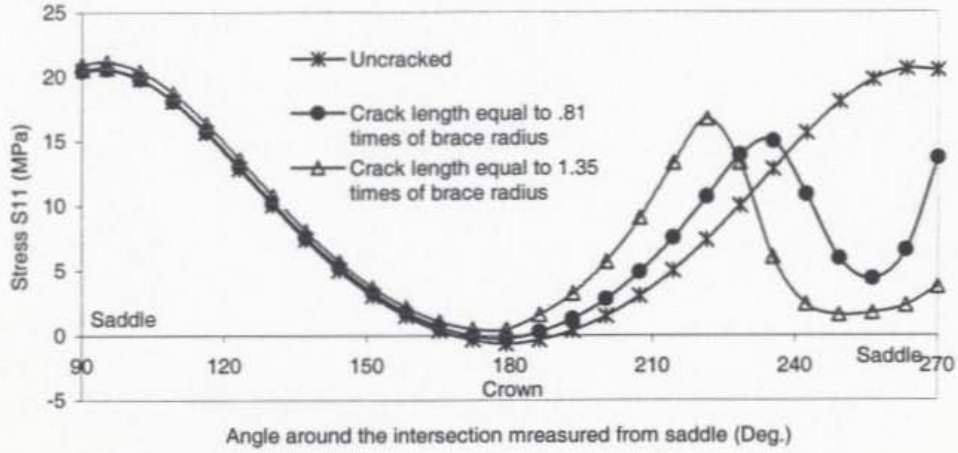

(a)

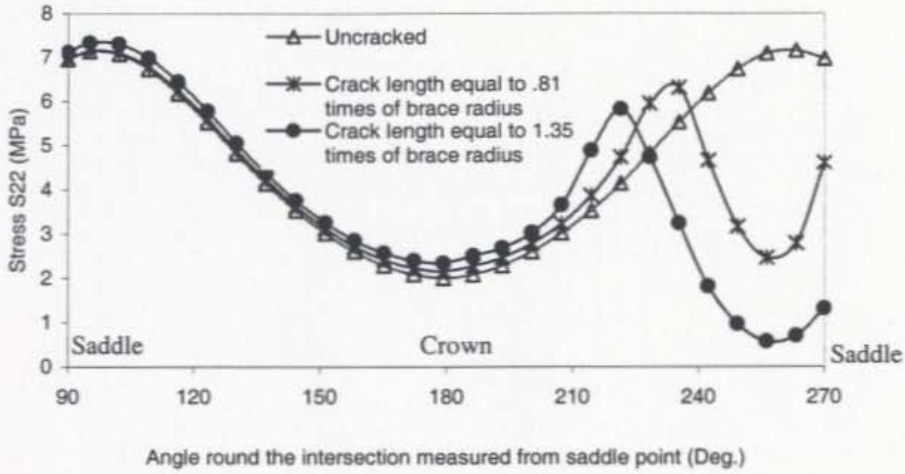

(b)

Figure 4.23: (a) and (b): Comparison of stresses in the horizontal brace between the uncracked and cracked structures having different lengths of cracks in substructure 3 – Stresses at a distance of 0.0325 m away from the intersection.

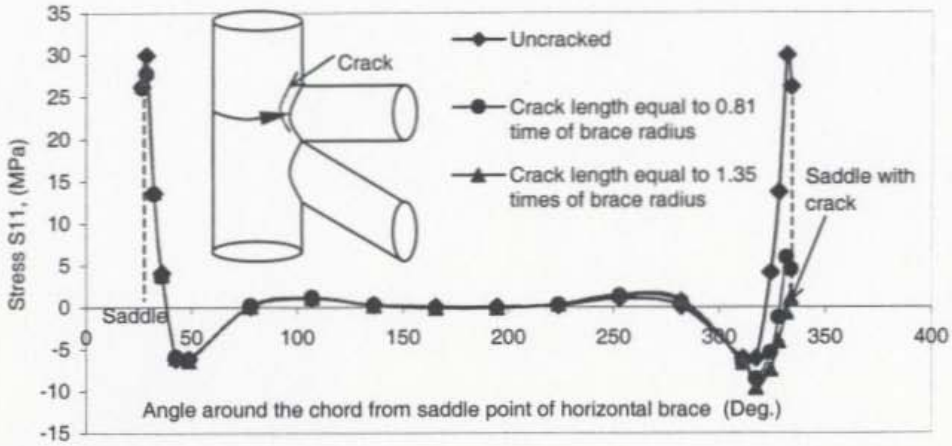

(a)

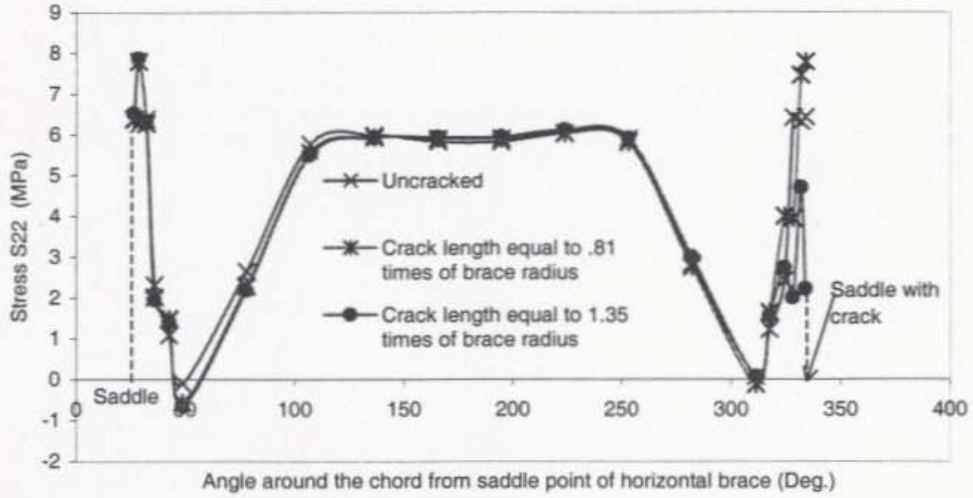

(b)

Figure 4.24: (a) and (b): Comparison of stresses (along chord circumference) between uncracked and cracked structures due to crack in substructure 3 – Stresses on chord surface.

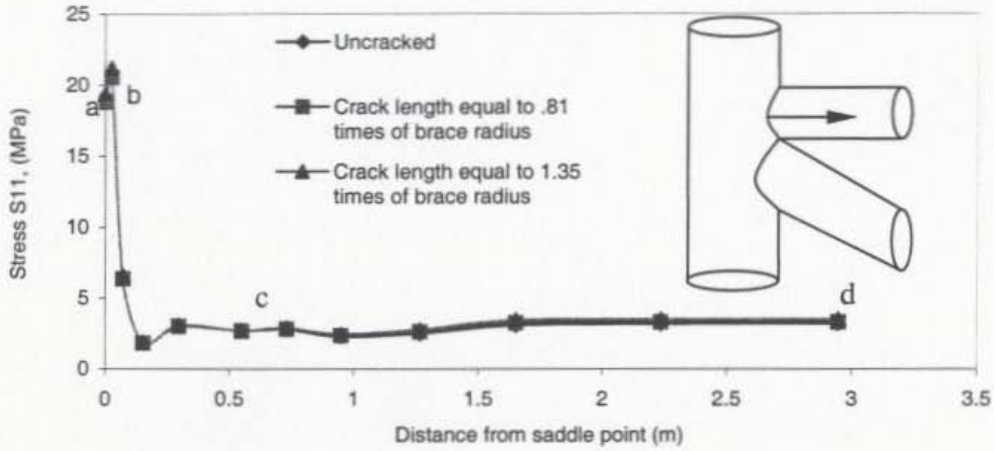

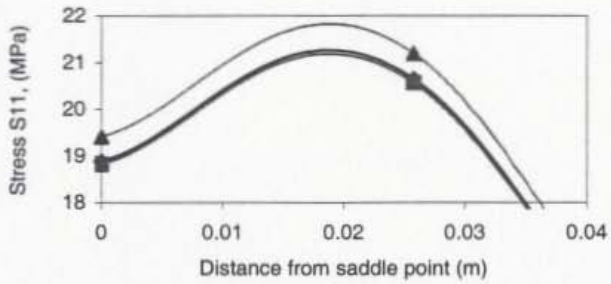

Zoom of the curve portion 'ab'

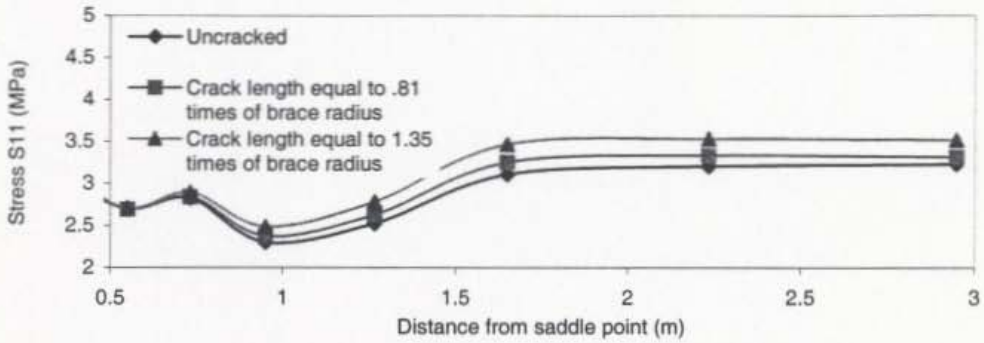

Zoom of the curve portion 'cd'

(a)

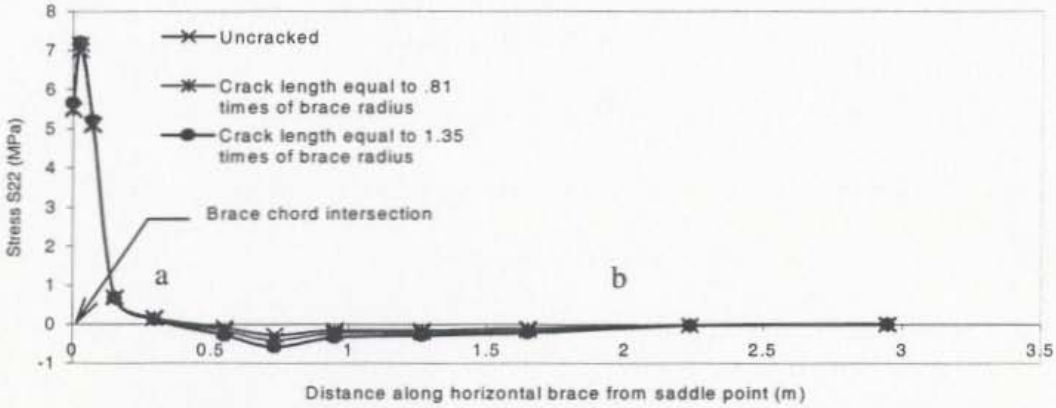

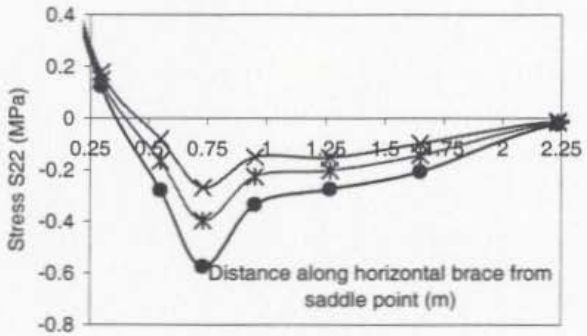

Zoom of the curve portion 'ab'

(b)

Figure 4.25: (a) and (b): Comparison of stresses between uncracked and cracked structure due to a crack in substructure 3 - Distances along the horizontal brace from saddle point of horizontal brace/chord intersection.

4.11.1 Comparison of Stresses With and Without Quarter Point Nodes in Crack Tip Elements

In a comparative study, finite element model was utilized using 8-noded quadrilateral isoparametric shell elements with and without quarter point nodes in the crack tip elements, to examine the nature and magnitude of the stress state around the crack tip. The results obtained from this study are shown in Figures 4.26 and 4.27. These stresses are at the Gaussian points and are at a distance of 0.0074 m from the crack tip.

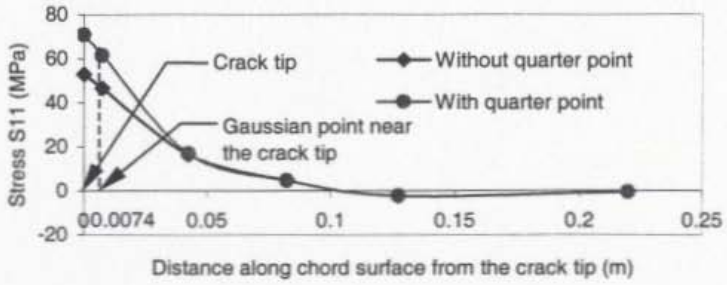

(a)

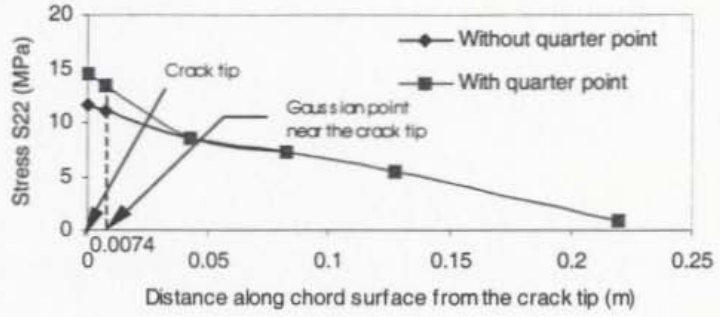

(b)

Figure 4.26: (a) and (b): Comparison of stresses without quarter point node and with quarter point node in crack tip elements (crack length equal to the length of 2 elements).

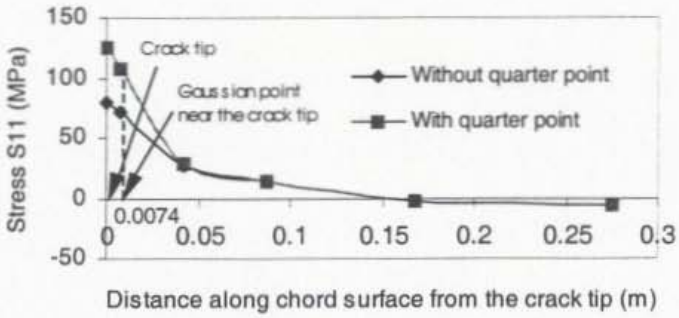

(a)

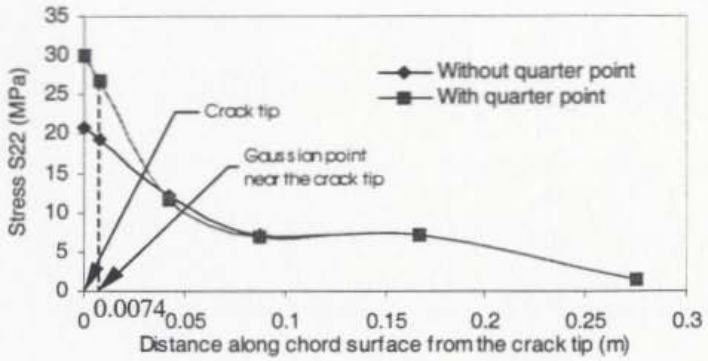

(b)

Figure 4.27: (a) and (b): Comparison of stresses without quarter point node and with quarter point node in the crack tip elements (crack length equal to the length of 10 elements).

Figures 4.26 and 4.27 show the variation of results obtained with a crack extending over 2 elements and a crack extending over 10 elements (each element length is 0.0405 m) with or without quarter points, respectively. Four points (Gaussian points) were chosen (along the circumference of chord from the Gaussian point of crack tip element) to compare the results of stress analysis. First Gaussian point is at 0.0074 m away from the crack tip. The

distances from crack (from the first Gaussian point) to these four points are 0.0325 m, 0.08 m, 0.135 m and 0.225 m, respectively along the chord surface. According to this comparison, it is seen that differences in stresses are maximum at the crack tip and it is almost negligible at other points, which are away from the crack tip element. From these figures it can be observed that the stress state around the crack tip could be defined clearly only by shifting the crack face middle node to quarter points, toward the crack tip.

4.11.2 Variation of Stresses in Elements far away from the Crack

In the elements, which are far away from the crack region, the stresses within the element was not significant between the uncracked and cracked section. In order to quantify the variation of stresses, element stresses from different positions of chord member were plotted and compared. The results obtained from this study are shown in Figure 4.28 and 4.29. It is seen that when crack length is equal to 1.9 times of the radius of brace, the stresses in the local 1-direction at two points on the chord surface, that were 0.225 m and 1.81 m away from the saddle point, change by 49.11% and 82.46% (very small stresses), respevtively, from that of the uncracked structure. However, the change of stresses in the local 2-direction (in the same element) is observed to be more than 92.56% (very small stresses only) at the first location that is 0.225 cm away from the intersection; but it is only 3.303% in the element which is 1.81 m away from the saddle point. If these small stresses can be measured accurately in the tubular-jointed member, then this can be used as an indicator of the crack presence. The load released due to development of crack is concentrated near the crack tip region. For this reason, variation of stresses in cracked and

uncracked condition is large near the crack tip region and less far away from the crack region; but the variation of stresses seem to be considerable all around the chord.

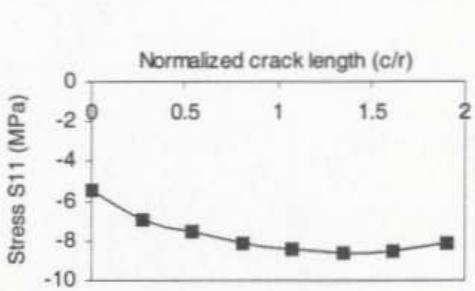

(a)

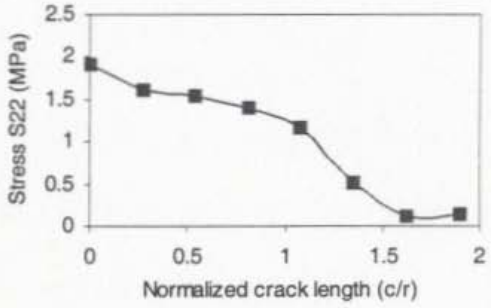

(b)

Figure 4.28 (a) and (b): Variation of stresses in the chord due to crack at a location that is 0.225 m away from the intersection (saddle point) of horizontal brace and chord.

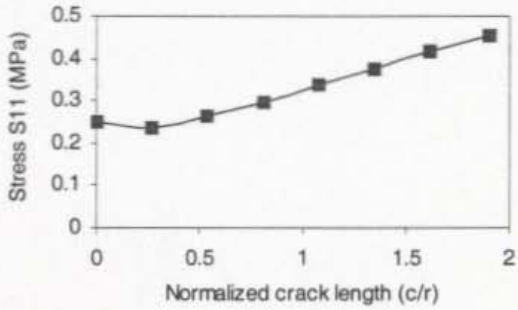

(a)

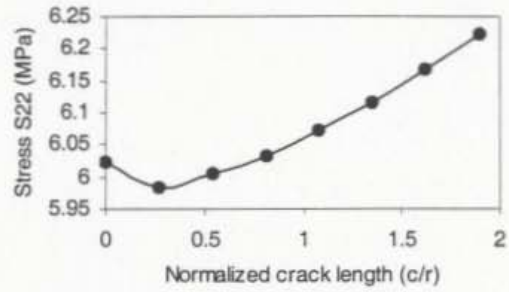

(b)

Figure 4.29 (a) and (b): Variation of stresses in the chord due to crack at a location that is 1.81 m away (farthest point from the two saddle points) from the intersection of horizontal brace and chord.

4.11.3 Effect on Principal Plane Angles at Different Locations on the Chord Surface due to the Presence of Crack in Substructure 3

In order to have a clear understanding about the behavior of cracks in tubular joints, the analysis of principal plane angles due to various crack lengths at the weld toe were also considered. Figure 4.30 shows the variation of the principal plane angle with respect to the normalized crack length. In this figure, it is seen that when a crack length equal to 0.27 times of radius of brace occurs, the change of principal plane angles at points (on the surface of chord, along the line normal to the intersection at saddle) that are 0.043 m, 0.225 m and 1.81 m away from the crack are 666.21%, 53.57% and 103.08%, respectively, from its uncracked condition. In this case it is observed that the change of principal plane angle at points that are close to the crack is very high. But, this change is small at points which are far away from the crack. However, when crack length is extended to more than 6 elements then these changes decrease and become very small. Hence this can be used as an indicator be detecting the initial crack growth

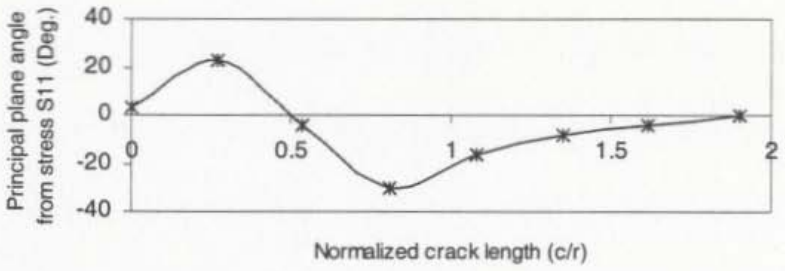

(a)

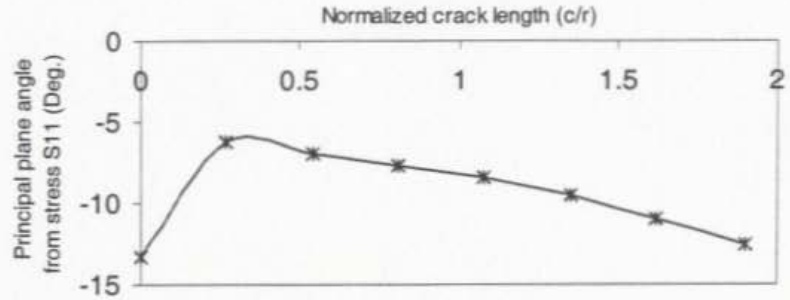

(b)

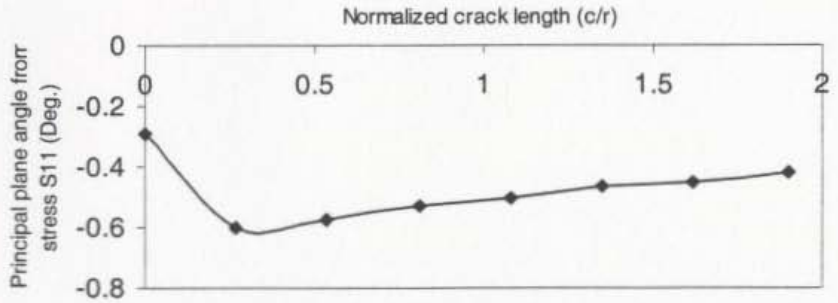

(c)

Figure 4.30: (a), (b) and (c): Variation of principal plane angles in the elements that are 0.043 m, 0.225 m and 1.81 m away from the crack line due to the extension of crack up to 14 elements (1.9 times of radius of the horizontal brace) around the weld toe.

4.11.4 Effect on Shear Stress at different Locations on the Chord Surface due to the Presence of Crack at Substructure 3

Values of the shear stress at different points on the chord surface, along the line normal to the intersection at saddle, are given in Figure 4.31. The maximum variation was found to occur near the crack region. The change of shear stress at a point 0.043 m away from the crack was found to increase up to a crack length equal to the length of 4 elements (each

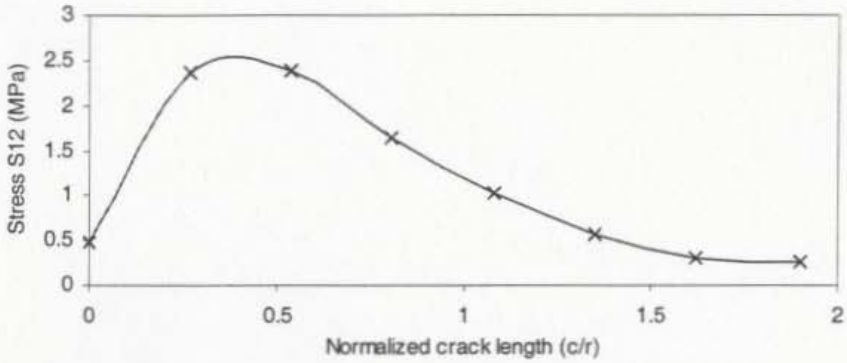
Stress S12 (MPa)
3
2.5
2
1.5
1
0.5
0
0
0.5
1
1.5
2
Normalized crack length (c/r)

(a)

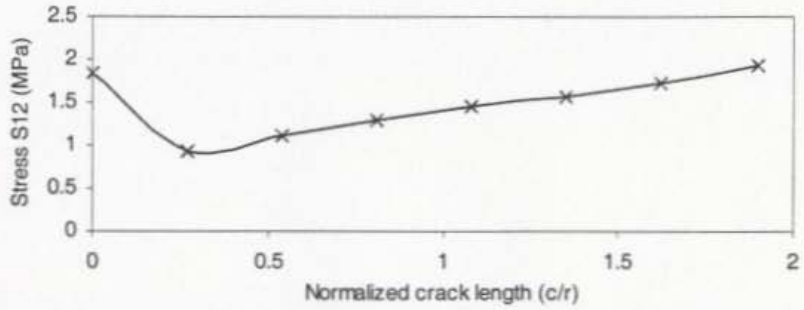
Stress S12 (MPa)
2.5
2
1.5
1
0.5
0
0
0.5
1
1.5
2
Normalized crack length (c/r)

(b)

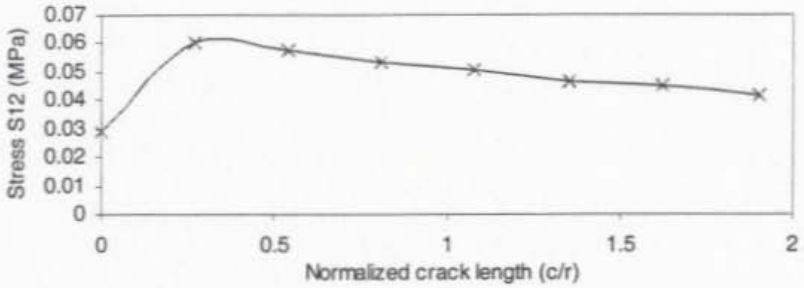

(c)

Figure 4.31: (a), (b) and (c): Variation of shear stresses at locations that are 0.043 m, 0.225 m. and 1.81 m away from the crack line due to the extension of crack up to 14 elements (1.9 times of radius) around the weld toe.

element length equal to 0.0405 m), i.e., 0.54 times of brace radius (diameter of brace is 0.6 m). Its value decreased when the crack length was increased gradually to extend across twelve and fourteen elements along the weld toe of the joint. However, at points which were far away from the crack, the magnitude of shear stresses was not significant. It is important to mention that when the crack length was higher than the length of 2 elements, shear stresses and principal plane angles nearer the crack region changed their directions.

4.11.5 Comparison of Stresses between "One Side" Crack and "Both Sides" Crack at the Critical Region of Substructure 3

The variation of stresses at different points on the chord surface from uncracked condition to crack at one side of the intersection (of chord and horizontal brace) and cracks at both sides of the same intersection are shown in Figures 4.32 to 4.34, respectively. These figures illustrate the possibility of the detection of crack by evaluating the stresses at

different points on the chord surface. It is seen that the variation of stresses in the case of "one side" crack is almost similar to the variation of stresses on "both sides" cracks at the intersection. From this analysis it is observed that "both sides" crack affects the far away element by showing greater changes at that location (viz., at 1.81m away from the intersection); these changes become significant when the crack length is large, i.e., equal to or more than 6 elements length. In both side cracks (symmetric), the load is released from the crack region, and is transferred to the crack tip region. The crack tip stress is very high due to the shifting of energy to the crack tip region.

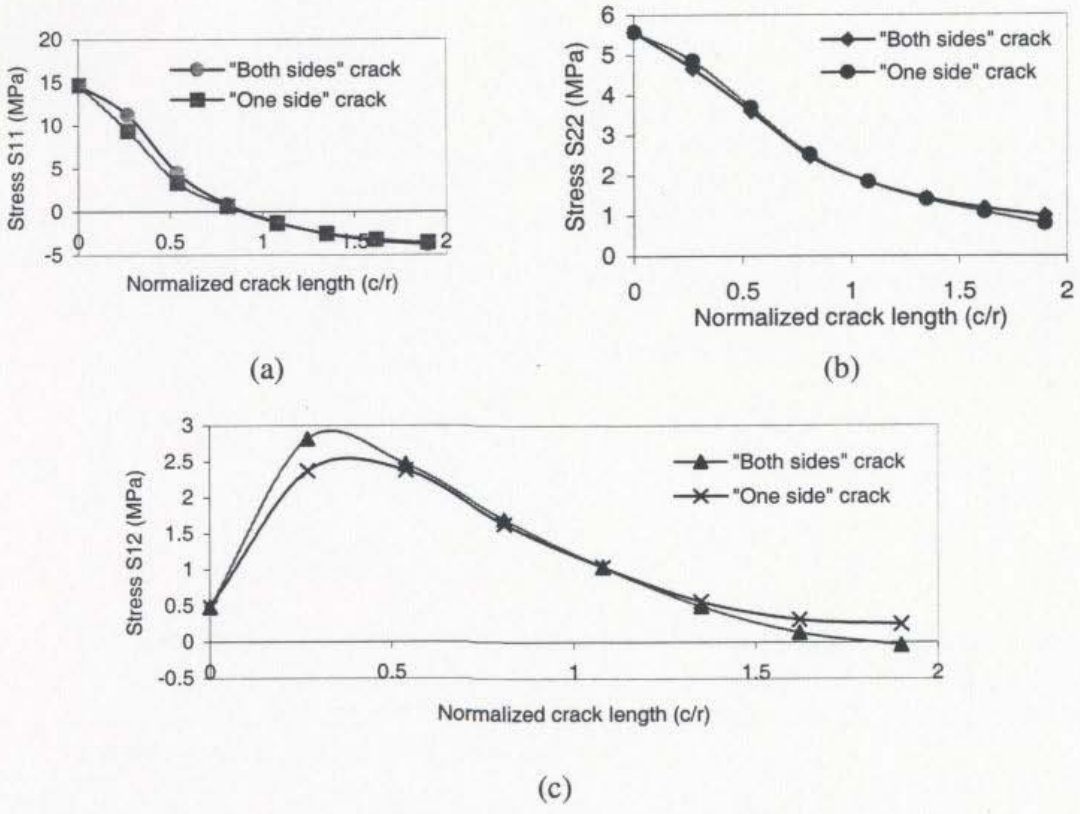

Figure 4.32: (a), (b) and (c): Comparison of local normal stresses (in 1- and 2-directions) and shear stress (at a point 0.043 m away from the crack) between crack on one side and crack on both sides of the intersection (of horizontal brace and chord member) in substructure 3.

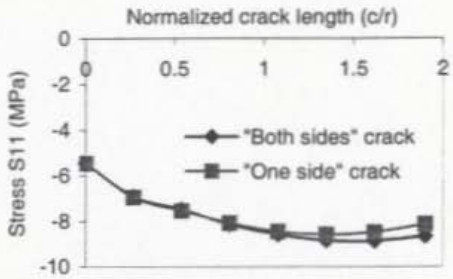

(a)

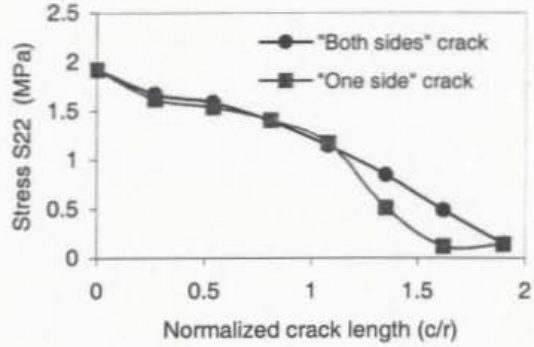

(b)

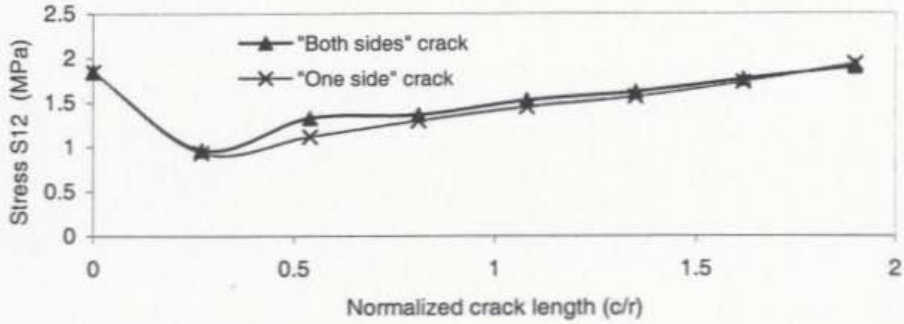

(c)

Figure 4.33: (a), (b) and (c): Comparison of local normal stresses (in 1- and 2-directions) and shear stress (at a point 0.225 m away from the crack) between crack on one side and crack on both sides of the intersection (of horizontal brace and chord member) in substructure 3.

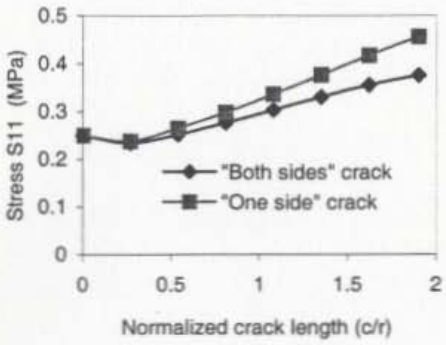

(a)

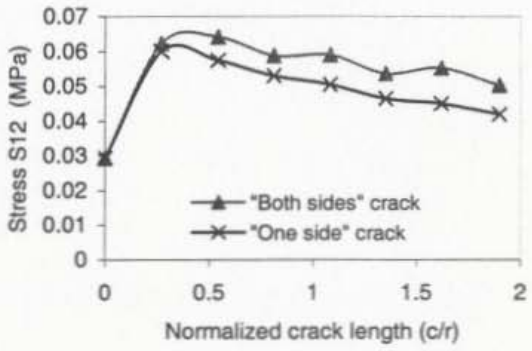

(b)

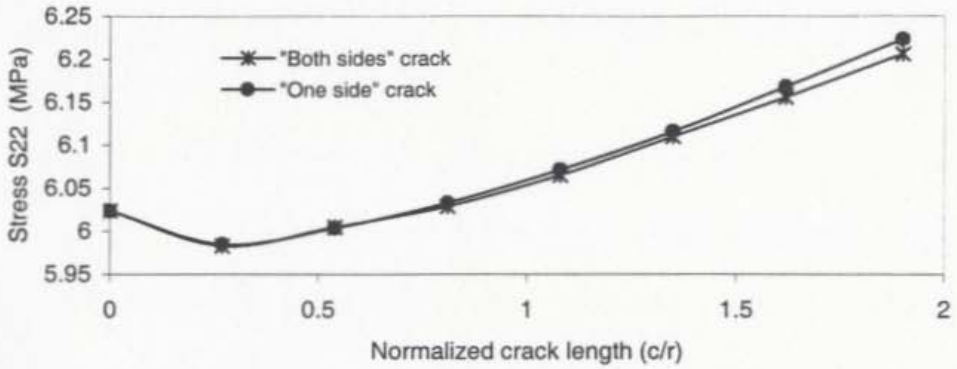

(c)

Figure 4.34: (a), (b) and (c): Comparison of local normal stresses (in 1- and 2- directions) and shear stress (at a point 1.81 m away from the crack) between crack on one side and crack on both sides of the intersection (of horizontal brace and chord member) in substructure 3.

4.12 Summary

The following studies have been carried out in this chapter to analyze the change of stresses that occurs explicitly around YT intersection in substructure 3 of the offshore plane frame, due to the growth of crack around the weld toe:

(i) Mesh generation procedures in uncracked and cracked structures for preparing the finite element model of the entire structure;

(ii) Model accuracy check by comparing of displacements and stresses using beam elements and substructuring (with shell elements) results;

(iii) Calculation of stress concentration factors for axial tension, in-plane bending and out-of-plane bending loads and comparison of these results with those extracted from Nwosu's (1993) analysis;

(iv) Proper sizing of the elements check using a convergence test corresponding to 24, 48 and 96 elements;

(v) In order to obtain hot spot region stresses at YT intersection of substructure 3, stresses in local 1- direction on the chord side of horizontal brace/chord and diagonal brace/chord intersection have been compared; in addition comparison of stresses between chord side and horizontal brace side, near the intersection, has also been made;

(vi) Local stresses in 1- and 2- directions, around the uncracked chord member and along the horizontal and diagonal braces from the saddle point of the intersection, have been examined to locate the hot spot region;

(vii) Comparison of stress distribution in local 1- direction around uncracked and cracked (crack length equal to 0.81 times of brace radius) structures with a crack in substructure 3 has been made for better understanding about the changes of stresses in crack region due to the development of crack at critical regions;

(viii) Comparison of local normal stresses, shear stresses and principal plane angles between uncracked and cracked structures with different lengths of crack, at a critical region of the on chord member;

(ix) Comparison of stresses at Gaussian point near the crack tip between quarter point node in crack tip elements and regular shell elements (without shifting midside node at quarter point); and

(x) Finally, a comparison of local stresses at different locations of substructure 3 between crack on one side and crack on both sides of the intersection to obtain the possible variations that can occur due to various crack lengths.

Chapter 5

Influence of Crack on an Offshore Framed Structure

5.1 General

During the service life of an offshore structure, defects or any other kinds of faults may be developed by environmental cyclic loading or by accidental damages caused by ship collision, dropped objects, etc. Due to this reason, the static strength of the in-service structure would be expected to be lower than the static strength of the intact structure. In order to ensure the reliability of the service life of structure it becomes essential to quantify the behavior of tubular joints containing defects. This can be done using different approaches such as fracture mechanics in conjunction with inspection schedules and the fitness-for-purpose assessment of structures, to detect assess and quantify fabrication or in-service defects. In another way, it can be said that static strength variation could be one method by which cracking in a structure during its service life could be detected and identified. Static strength variation can be identified by measuring stress (or strain) changes occurring around the joints.

The local stress and strain distribution around welded tubular joints depends on the geometric parameters (e.g., brace-to-chord diameter ratio, wall thickness ratio, angle of intersection, number of members mating at the joint, etc.), weld profile, radius of the weld toe, defect at the weld toe and load variation occurring around the joints. It is sometimes

impossible to describe the different forms of stress distribution that are present at tubular joint intersections by the basic method of mechanics. Different peak stresses developing at particular spots of the joint cause differences in the development and propagation of cracks. Many researchers have observed that the crack propagation pattern changes when applied loading is changed from constant amplitude to variable amplitude. The information regarding these stress distributions around the joints is required to identify any kind of cracking that is likely to occur in the structure and to locate possible problem sites around intersecting joints.

Most of the plots and identification procedures discussed in this chapter use the normalized displacement or strain ratios occurring at a location. Normalized ratio of any variable is defined as the ratio between that value of the variable under cracked condition to that value of the variable under intact condition. Consequently the initial normalized value at any location in the structure will be one. Moreover this procedure is utilized to compare the theoretical prediction and experimental observations. It has been observed from earlier experiments that the normalized values are almost the same for experimental and theoretical results of the same structure, having the same cracked state (Owolabi 2001). As a result, it was assumed that the virgin state calibration resorted to in all the inspection methodologies, was not necessary in this study. Moreover if there is a sensitive experimental device to measure the initial state of deformation than it will be easier to designate and characterize the changes that occur at that location by the variation of various parametric ratios.

5.2 Different Types of Failure Modes of Welded Tubular Joints

The failure of a welded tubular joint can occur on the chord side, the brace side, the overlapping position between the braces or anywhere on the joint, depending on the geometric and load parameters. Bucak et al (1994) showed four types of failure modes for a uniplanar truss, made of welded circular hollow section joints, based on geometric parameters. (i) They showed that, in joints with gap or small overlap and small wall thickness ratios (chord thickness / brace thickness), the crack developed in the transition zone of the fillet weld of the chord member (mode 1). In this case, since a large bend is developed near the weld toe due to the ovalization of the chord member for the effect of punching shear failure, the local stresses caused by the punching shear may exceed the yield stress under even a relatively small loading. Cracks usually start from these points. When the first cracks start around the critical hot spot regions, the high local stresses shift to the crack tip and become higher than the initial local stresses obtained in the uncracked condition at this point. This phenomenon increases the crack growth rate at this joint. (ii) For large overlaps and small thickness ratios, crack develops perpendicular to the longitudinal axis of the chord, around the crown (mode 2). (iii) When all dimensions except the wall thickness of the chord member and brace member remain unchanged [for wall thickness ratios (chord wall thickness/brace wall thickness) higher than 2], crack occurs on the tension bracing member and starts from the crown of the weld toe (mode 3). They stated that failure stress in the brace does not change for different thickness ratios. (vi) Finally, when the chord wall thickness is increased and brace dimensions are kept unchanged, the crack develops in the overlap area of the brace members (mode 4). These

four modes of failures have been observed to occur in welded tubular joints. However, it is also possible to have the occurrence of a combination of the above modes of failure. These four kinds of failure modes are shown in the figures given below (Figure 5.1).

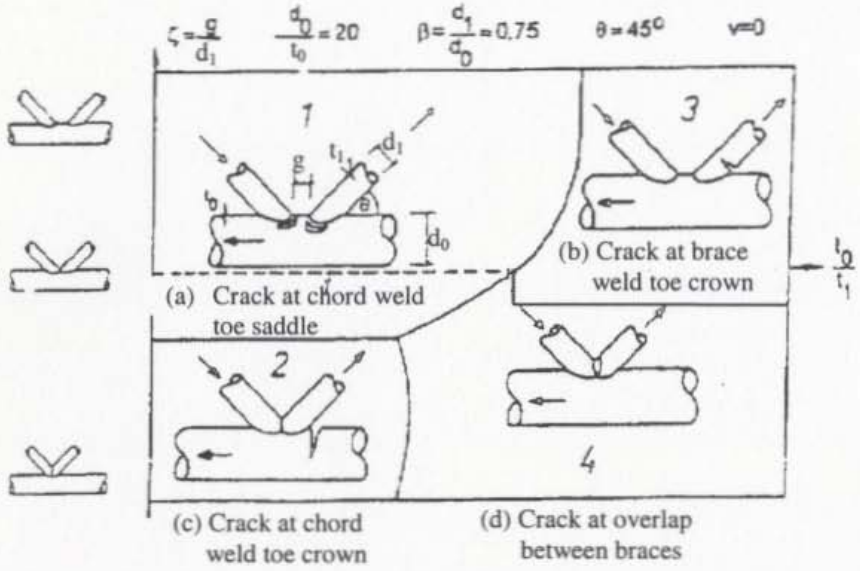

Figure 5.1: Failure modes for uniplanar truss joint of circular hollow sections (Bucak et al 1994).

The failure modes discussed above occur only when cracks start from the outside of the tube. But when the wall thickness ratio of chord and brace increases with a higher diameter ratio (brace diameter/chord diameter), then cracking tends to start from the inside of the tubular cross section.

5.3 Influence of Crack on the Local Strains and Stresses around the Joint

When any crack develops in the structural member, it changes the properties of that structure, both locally and globally. This concept is used in this study to detect cracks in the structure. In the present study, stress and strain changes that occur in the structure were taken into account while determining the changes that occur in the structure. Since stress measurement is not possible practically, the strain measurements are used for the detection of cracks in the structure. During recent years, different kinds of strain gauge sensors with high fidelity have been available at a reasonable price. These strain gauge sensors should be used to acquire data from the critical and other locations of the structure. In the previous chapter, it was observed that stresses at a point near the crack region change significantly as the crack length increases. In this chapter the changes that occur in strains at different locations of the plane frame structure, due to the existence of a crack, are examined to find a methodology for detecting the location of a crack and identifying its size.

5.4 Variation of Hot Spot Strain for Different Lengths of Crack

The variation of strains near the weld toe at a point, which is 0.043 m away from the saddle of the weld toe, is shown in Figures 5.2 (a) and (b). According to these results it is seen that around the crack location the strains decrease even from the beginning of the crack. This occurs due to the "strain-shadow" of the crack (shown in Figure 5.3), which develops between the measuring point and the crack tip region. As a consequence, it

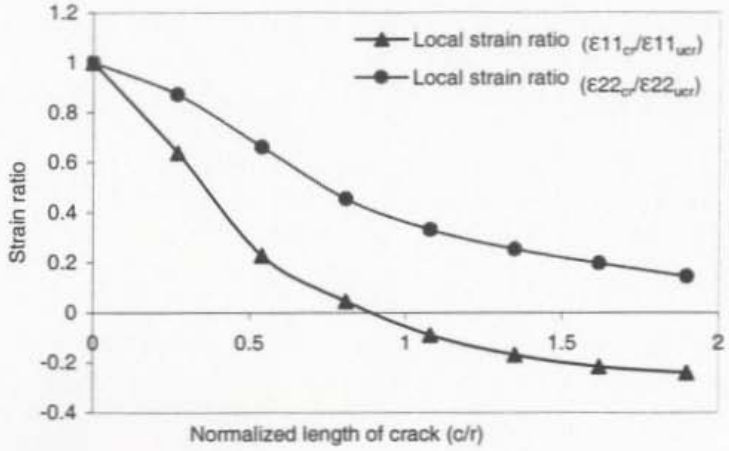

Figure 5.2 (a): Variation of strain ratios at a point 0.043 m away from the crack (saddle) on chord surface due to the extension of crack along the weld toe.

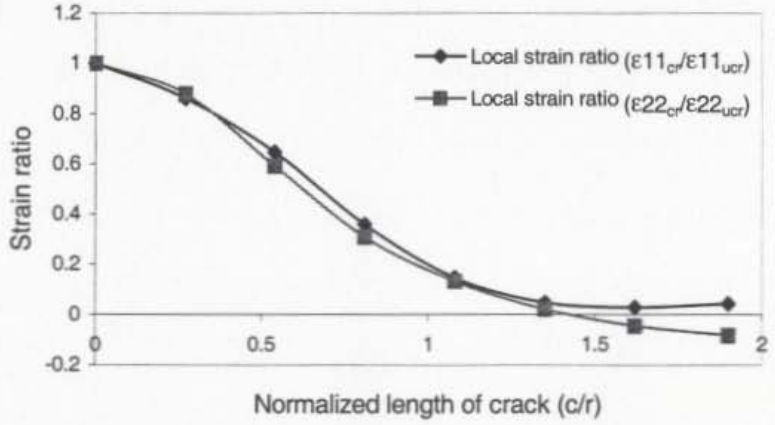

Figure 5.2 (b): Variation of strain ratios at a point 0.0325 m away from the joint intersection on the horizontal brace member due to the extension of the crack along the weld toe.

can be seen that the strain is reversed from a tensile one to a compressive one as the crack length increases during the tension loading of the brace. The behavior of crack is such

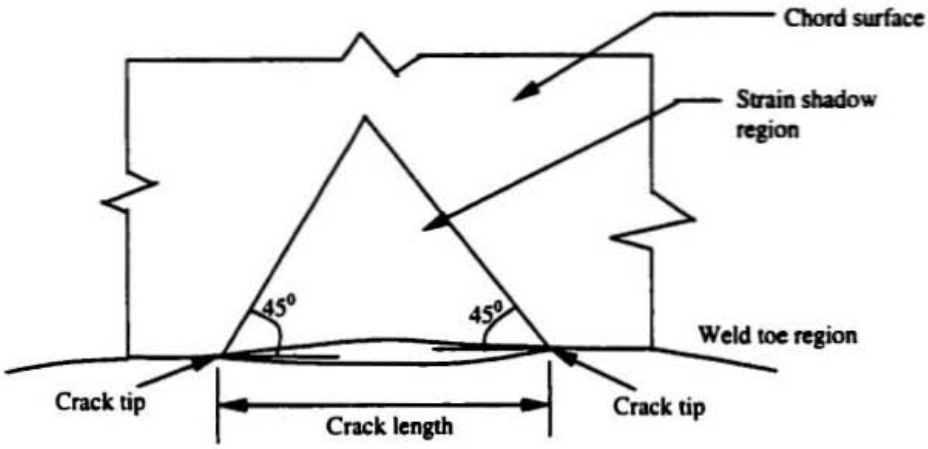

Figure 5.3: Strain shadow concept

that when it grows through the surface (which could not be modelled in this analytical examination), the load has to be transmitted through the uncracked ligament, and this will increase the strain on one side of the wall thickness and reduce on the other side. However, when crack grows through the complete wall thickness and then extends laterally along the weld toe, the surface strain decreases. This decrease will be gradual till breakthrough occurs. From the given figure it is seen that for a crack length of 1.9 times the radius of the horizontal brace, the local strain ε_{11} reduces by more than 120% while the local strain ε_{22} reduces by 90% from its uncracked state, at a point located 0.043 m away from the crack line. In the case of the horizontal brace, at a location which is 0.0325 m away from the joint intersection, it is observed that the local strains in 1- and 2-directions decrease by 95.8% and 108.257%, respectively, for the same crack lengths (Figure 5.2 (b)).

5.5 Effects of a Crack at Different Locations around the Tubular Joint Intersections of the Structure

Development of a crack at any location of the structure, would certainly influence the structural properties not only around the crack region but also far away from the crack region. According to the manner in which loads are carried by the system if any member of the system becomes weaker (through crack formulation), the load carried previously by that member would be shared by other adjacent regions and members of the structure. From fracture mechanics point of view, when a crack is developed, a new surface is created; some of the energy contained in that cracked portion is released. This released energy is stored in the uncracked portion especially, near the crack tip of the structure. In this case energy of the uncracked portion of the structure has changed due to the occurrence of the crack. Therefore, at every stage of crack growth in the structure it changes or modifies the structural deformation properties such as stresses, strains, modal parameters (natural frequencies, mode shapes and modal damping), etc. By comparing these changes between uncracked and cracked conditions, one could identify the crack in the structure. In the present study the strains at different locations of the structure have been compared for various cracks (locates at a distance of 0.03 m away from the intersection of the horizontal brace and chord member at joint 3). The various locations considered in the study are shown in Figure 5.4. The results are shown in Figures 5.5 through 5.13. Figures 5.5 through 5.8 represent the variation of strains in the local 1- and 2- directions at a point on the chord surface, 0.073 m away from the saddle point of the intersection of horizontal brace and chord member. The crack length is normalized with

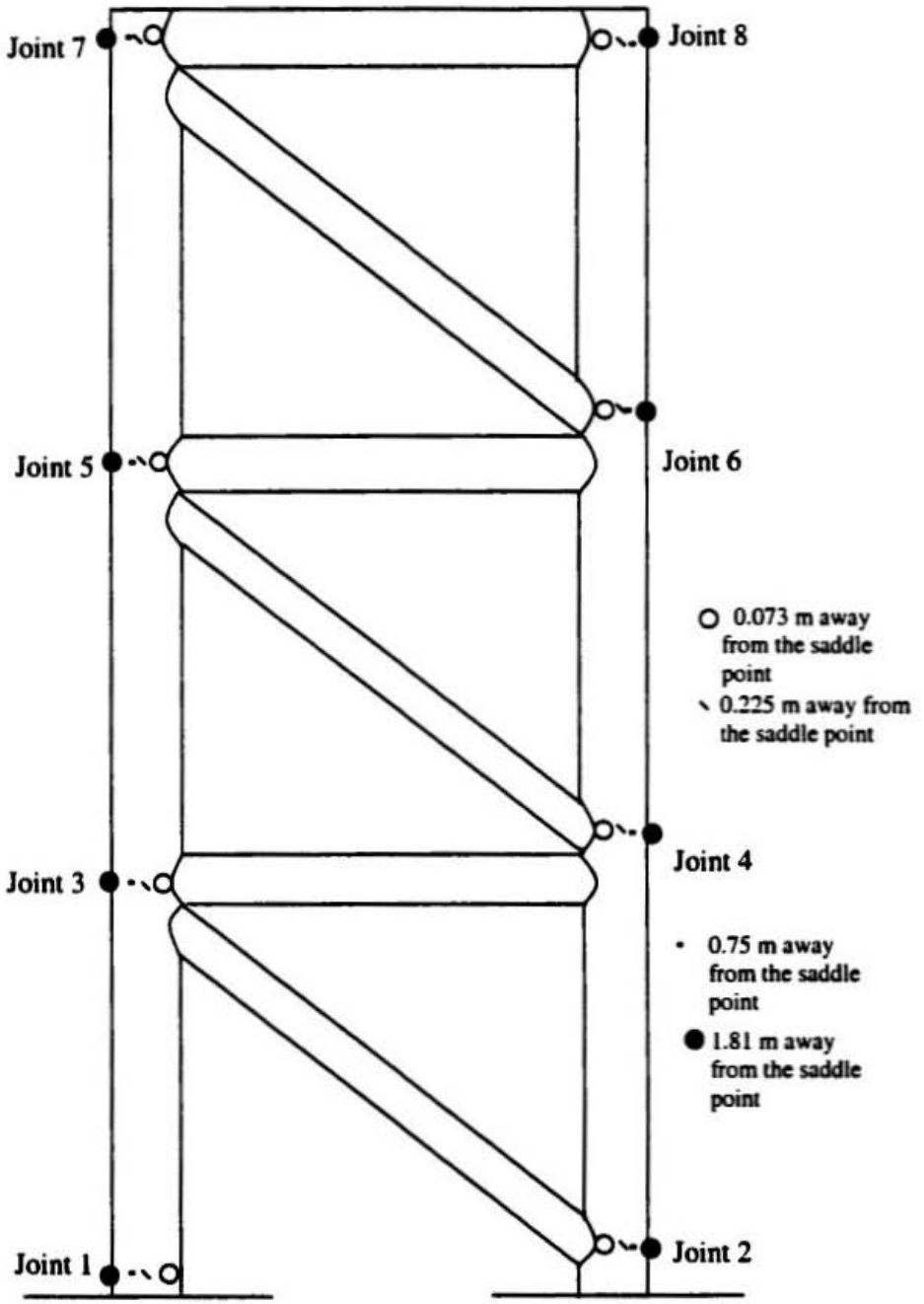

Figure 5.4: Location of points on the frame that are considered for comparison of local strains in 1- and 2-directions, between the cracked and uncracked structures.

respect to the radius of the brace member and maximum crack length is considered to be 1.9 times the brace radius. These figures also give the variation of strains that occur at other locations of the structure, which are at other joints (0.073 m away from the saddle point of the intersection on the chord surface). The locations of all points at the different joints of the frame structure, considered in this study, are shown in Figure 5.4. From these figures (Figure 5.5 to 5.8) it is seen that the point, which is near the crack location has large strain ratio than the other points, which are located far away from the crack. Considering all these points, the variation of local strain ratios in 1- ($\varepsilon_{11cr}/\varepsilon_{11ucr}$) and 2-directions ($\varepsilon_{22cr}/\varepsilon_{22ucr}$) are very large only at joint-3 (near the crack). However, the variations of local strains in 1- and 2- directions at joints 1 and 6 are appreciable; the local strain ratio in 2-direction at the same point of joint 6 varies by 16.65% due to the presence of a large crack at joint 3. At all the other joints, the changes in strain ratios are rather small. These figures also show that the local strain ratios in both the local directions decrease enormously at the point near joint 3, where the crack is present. The maximum variations of strain ratio are 123.9% in local 1-direction and 85.55% in local 2-direction (for a crack 1.9 times the radius of the brace). The reason for this is the strain releases that occur when the length of crack increases and their consequent effect near the crack is quite considerable.

The Figures 5.9 (a) and (b) show the variation of strain ratios in local 1- and 2 –directions at a point on the chord surface, around different joints intersection (see Figure 5.4), that is 0.225 m away from the intersection of horizontal brace and chord. According to these

figures it is seen that the variation of strain ratios in local 1-direction is very large at the point of interest in joint 3, but at all the other points it is much smaller. At this point (in joint 3), strain ratio in 1-direction increases to a maximum of 49.12% from its uncracked condition when the crack length considered is 1.9 times of brace radius. Also the variation of strain ratios in the local 2-direction is very large at the points of interest in joint 3 and 5. In this case, the strain ratios decrease by a maximum of 92.517% and 14.27% at joints 3 and 5, respectively. Moreover, at this point on the chord surface, the local strain in 2-direction is affected more than the local strain in 1-direction by the crack. The strains in local 2-direction decrease, due to the extension of crack in almost the same direction. However, in the region beyond the strain energy release zone (the so called "shadow" region), strain energy is stored either in local 1-direction or 2-direction. It depends on the location of the point from the crack. For this reason, the strain component ε_{22} at the corresponding points in joints 3, 5 and 7 are influenced more than at any other points of the joints.

Figures 5.10 and 5.11 show the variation of strain ratios in the local coordinate system at a point that is 0.75 m away on the chord surface (for all joints) from the saddle point of horizontal brace/chord intersection. These figures indicate that the variations of strain ratios in local 1- and 2- dirctions at joint 3 are almost similar in nature, but strain ratios in local 1-direction are influenced more than the local 2- direction by the presence of crack. The strain ratio increases to a maximum of 40.14% in local 1-direction and 6.43% in local

2-diection (when the crack length is 1.9 time the radius of brace). It should be noted that this point is around the quarter-point of the circumference from the crown intersection.

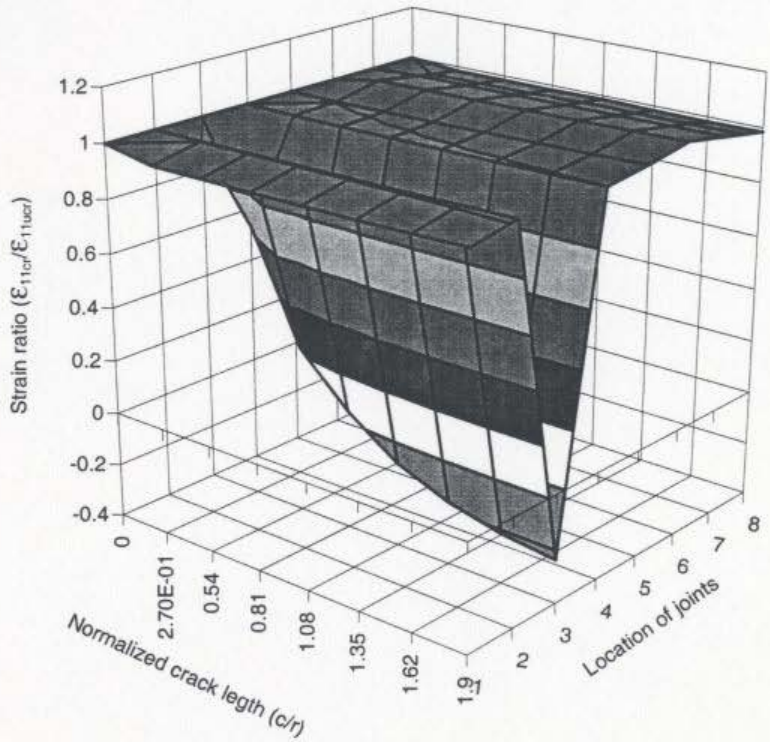

Figure 5.5: Variation of strain ratios in local 1-direction at a point on the chord surface for different crack lengths at 0.073 m away from the saddle intersection of the horizontal brace and chord.

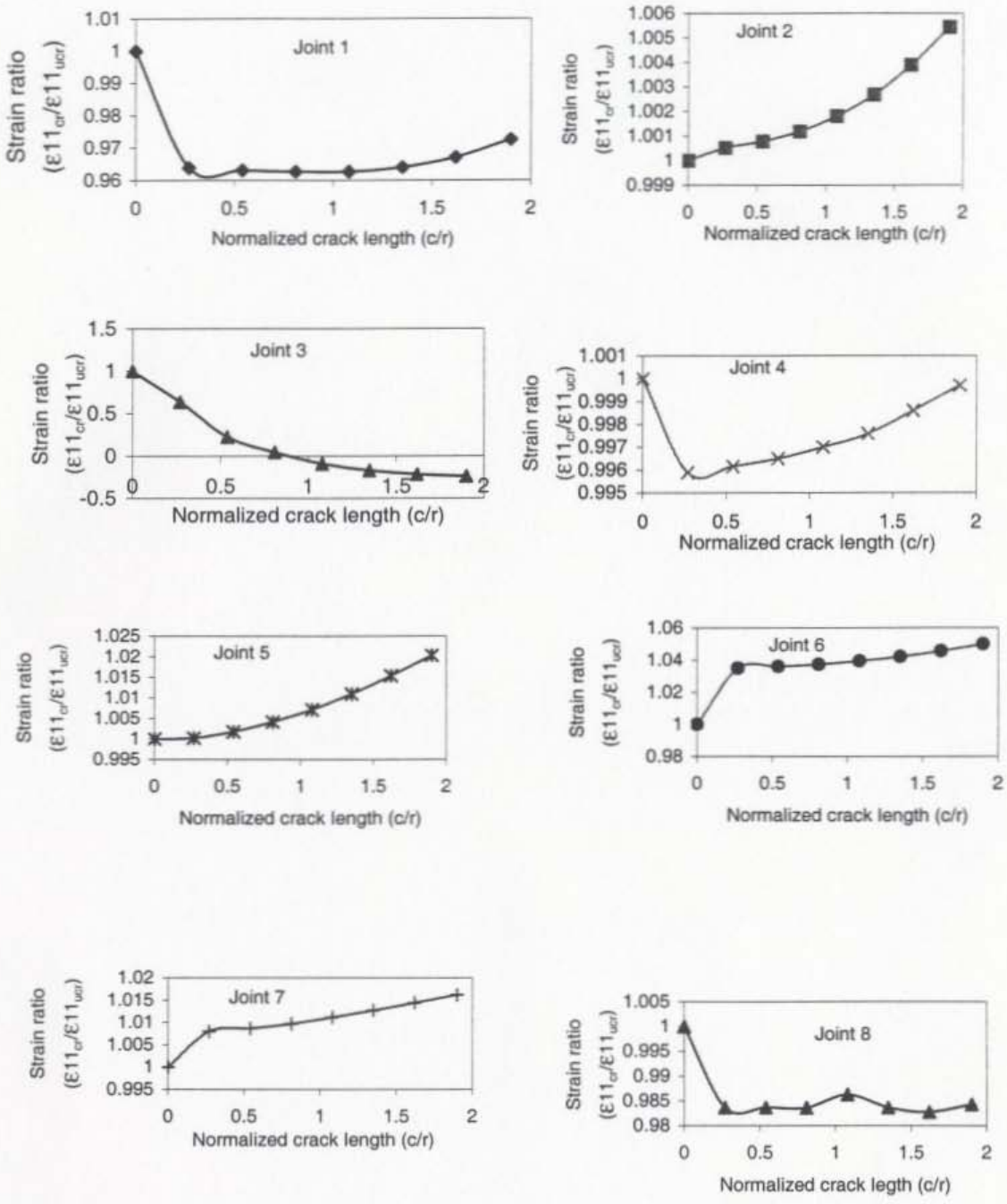

Figure 5.6: Variation of strain ratios in local 1- direction at different locations of the frame, for different crack lengths, at 0.073 m away from the saddle intersection of the horizontal brace and chord in substructure 3

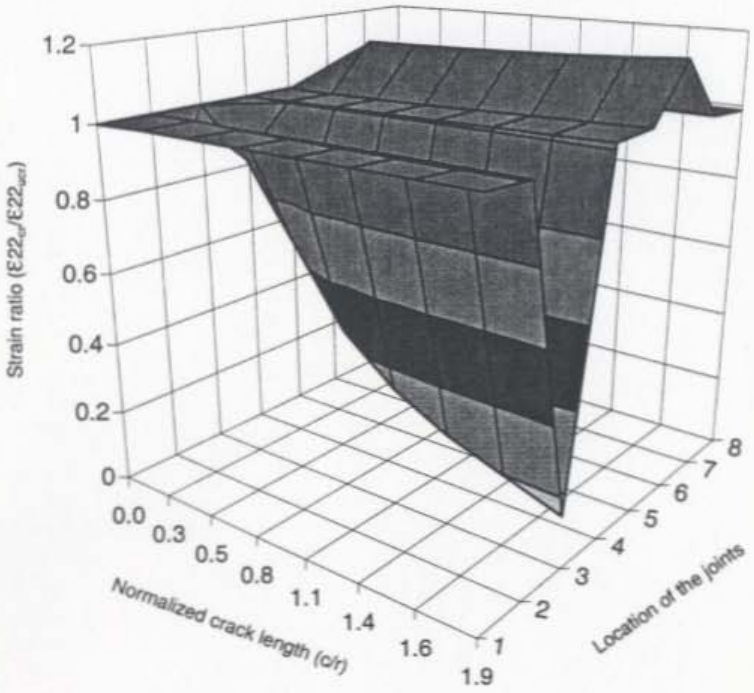

Figure 5.7: Variation of strain ratios in local 2-direction at a point on the chord surface for different length of cracks at 0.073 m away from the saddle intersection of the horizontal brace and chord.

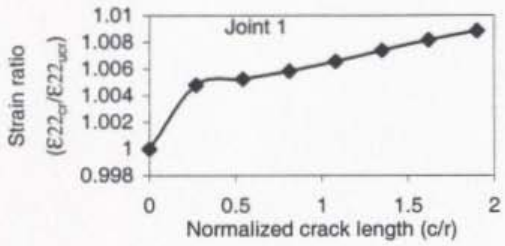

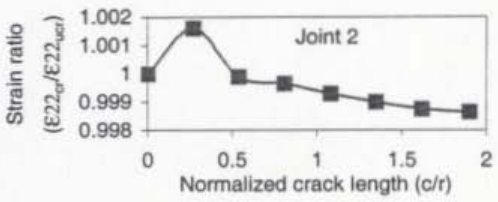

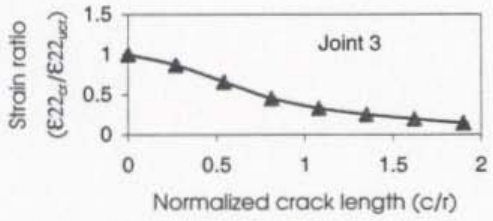

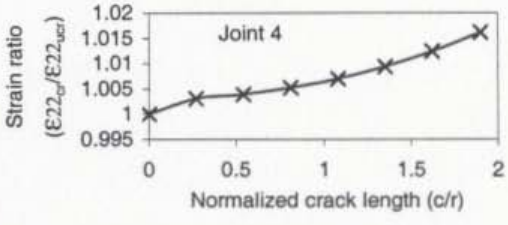

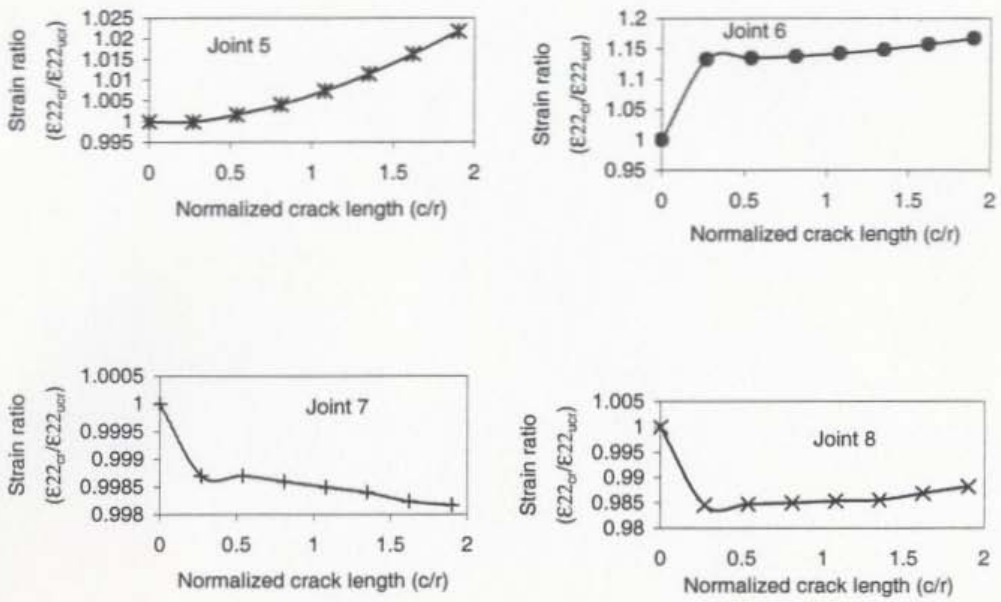

Figure 5.8: Variation of strain ratios in local 2- direction at different locations of the frame, for different crack lengths, at 0.073 m away from the saddle intersection of the horizontal brace and chord in substructure 3.

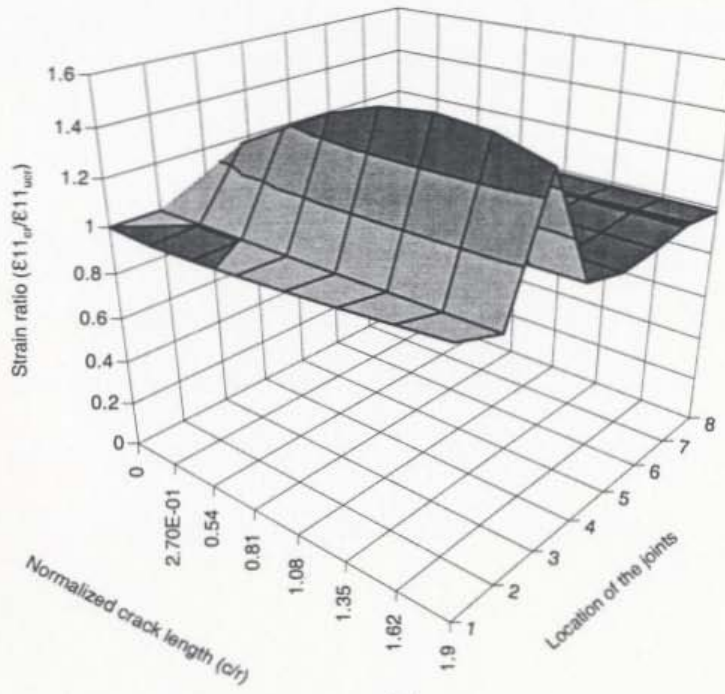

(a)

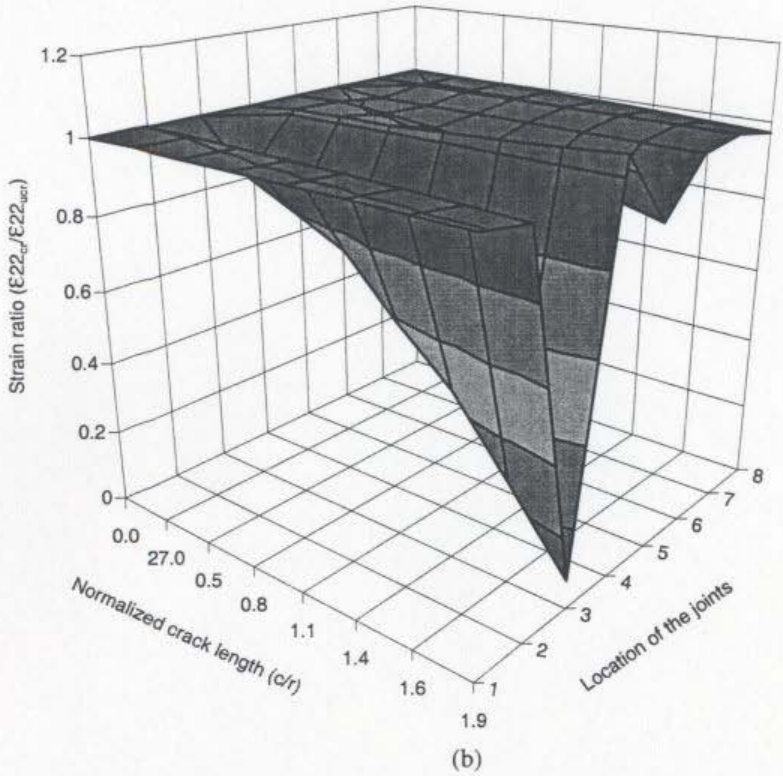

(b)

Figure 5.9 (a) and (b): Variation of strain ratios in local 1- and 2- directions on the chord surface, for different crack lengths, at 0.225 m away from the saddle intersection of the horizontal brace and chord member.

At joint 1 the strain ratios in local 1- and 2- directions decrease by a maximum of 27.64% and 0.7%, respectively. At joint 4 it increases by a maximum of 0.37% and 11.98%, respectively. At joint 5 the strain ratios in local 1-direction increases by a maximum of 4.14% and in local 2-direction decreases by a maximum of 1.93%. Hence it could be seen that the presence of crack does influence the strain values far away from the crack region as well as at far-away joints.

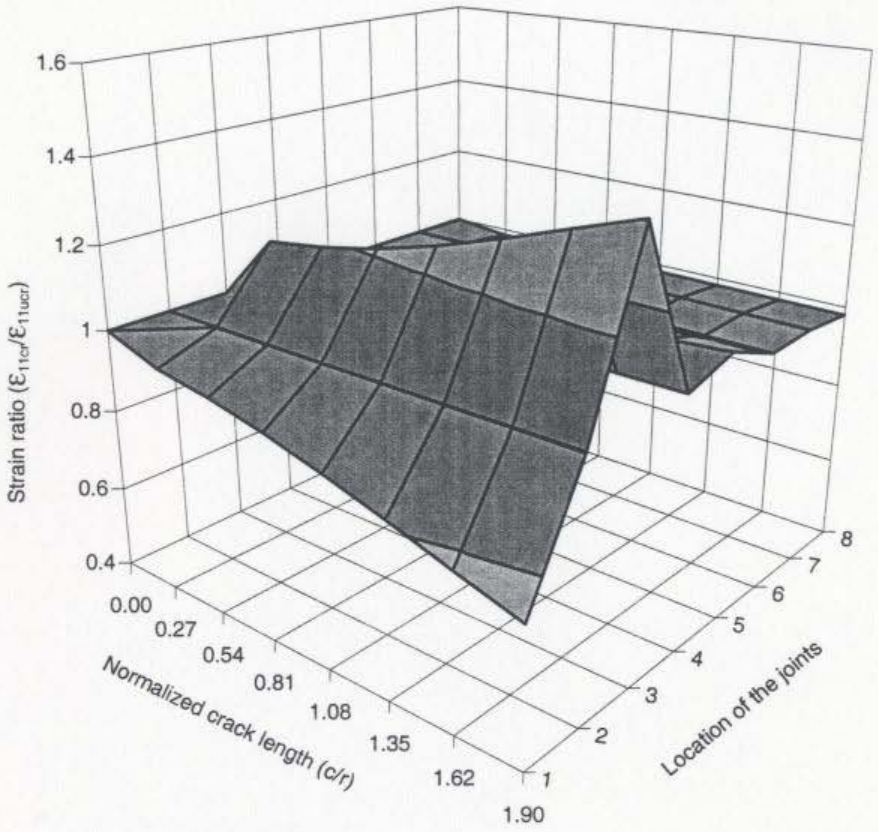

Figure 5.10: Variation of strain ratios in local 1-direction on the chord surface, for different crack lengths, at 0.75 m away from the intersection of the horizontal brace and chord member.

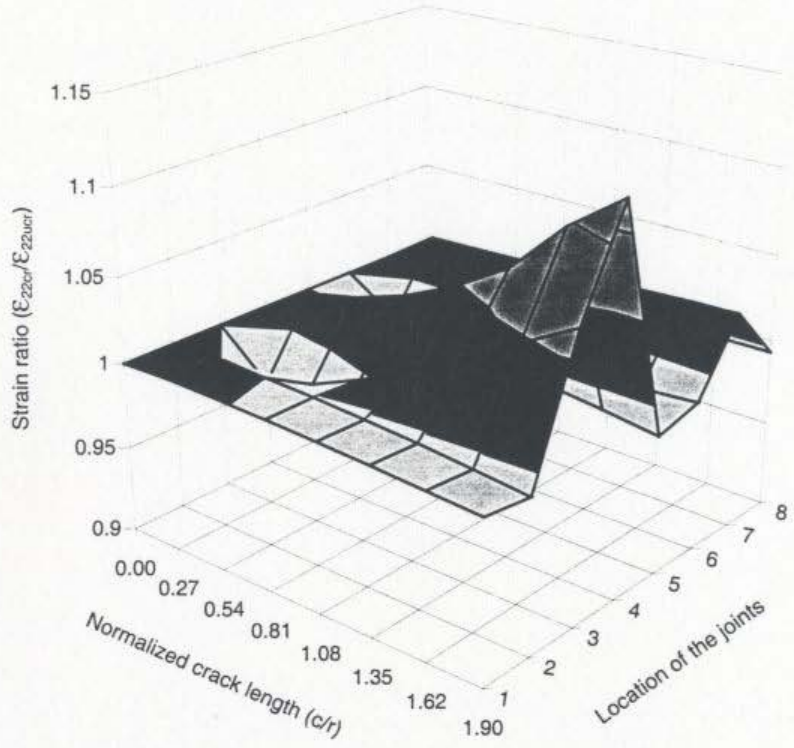

Figure 5.11: Variation of strain ratios in local 2-direction on the chord surface, for different crack lengths, at 0.75 m away from the intersection of the horizontal brace and chord member.

Figures 5.12 and 5.13 also show the variation of strain ratios at a point that is, 1.81 m (exactly opposite to the crown intersection) away, on the chord surface from the saddle point of horizontal brace/chord intersection. From these figures it is seen that the variation of strain ratios in local 1-direction is more at this location of joints 1, 3, 4 and 5. These ratios increase to a maximum of 11.39% at joint 1, 82.55% in joint 3 and 3.42% in joint 4, and decreases by a maximum of 6.6% at joint 5. However, strain ratios in local 2-direction increase by a maximum of 2.62% at joint 3 and decrease by a maximum of 1.66% and 1.04% at joints 4 and 5, respectively. It should be noted that at these points the

stress in 2- direction is considerably larger than the stress in 1- direction. Thus it can be stated that an intelligent strain gauge instrumentation of suitable locations around the critical tubular joint intersections would reveal the presence of the crack much earlier before the crack length reaches its critical failure length.

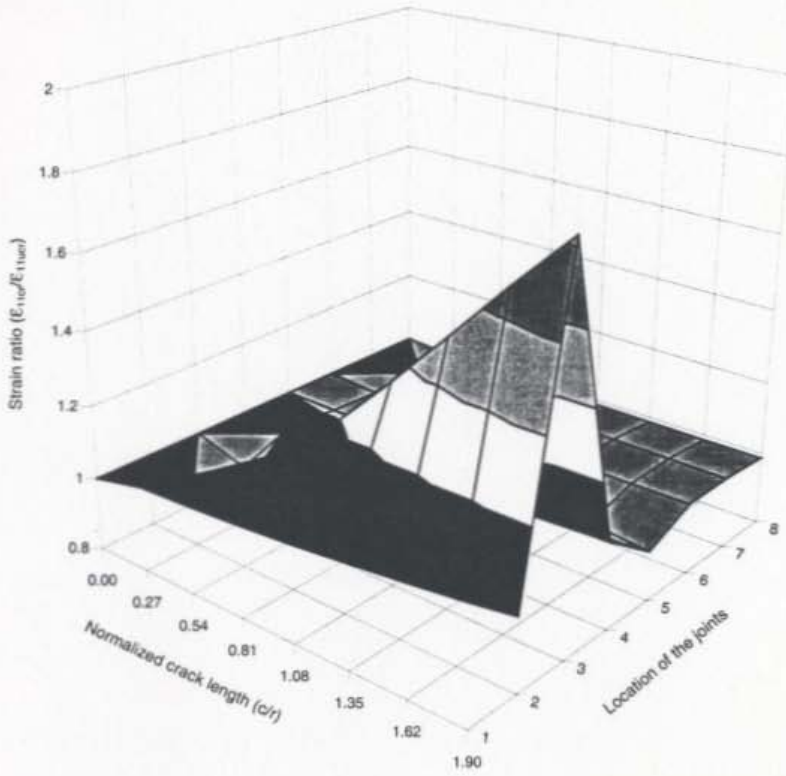

Figure 5.12: Variation of strain ratios in local 2-direction on the chord surface, for different crack lengths, at 1.81 m away from the saddle intersection of the horizontal brace and chord member.

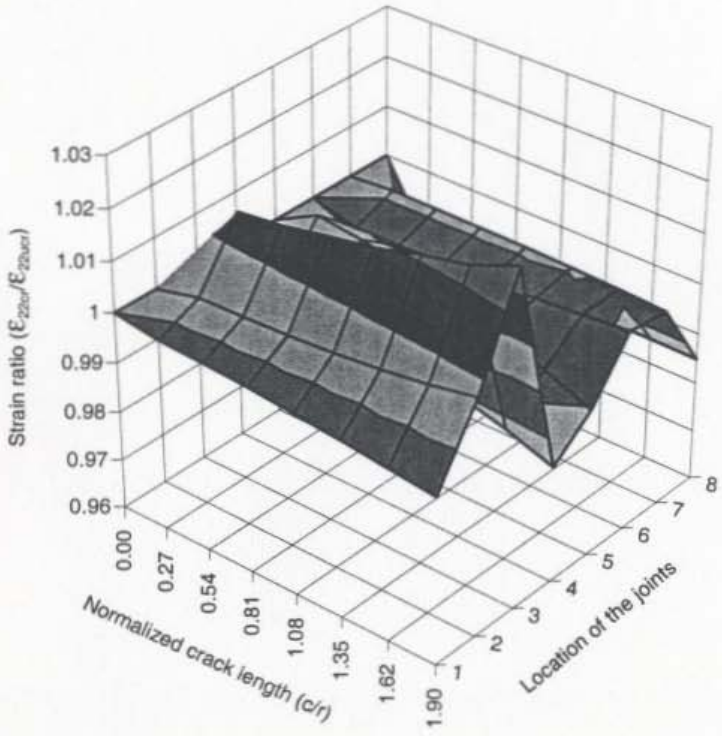

Figure 5.13: Variation of strain ratios in local 2-direction on the chord surface, for different crack lengths, at 1.81 m away from the saddle intersection of the horizontal brace and chord member.

5.6 Comparison of Strain Ratios between "Both Sides" Crack and "One Side" Crack

Since crack can be developed at any place of the joint weld toe it becomes essential to investigate the effects of crack at different locations of the joint weld toe. Hence, two symmetric cracks of equal length were considered at saddle points of the same joint on opposite sides (from crown intersection line). In order to compare the strain ratios (ε_{cr} / ε_{ucr}) in local 1- and 2- directions two points on the chord surface, that are located at 0.225

m and 1.81 m away from the saddle point of horizontal brace/chord intersection at joint 3, were taken into consideration. The results of this comparison are shown in Figures 5.14 through 5.17. From Figures 5.14(a) and (b) it is seen that the variation of strain in local 1- and 2- directions, at a point 0.225 m away from horizontal brace chord intersection in joint 3, are similar and almost the same for the case of "both sides" cracks and "one side" crack [see Figures 5.9 (a) and (b)]. The strain ratios in local 1-direction increases by a maximum of 58.8% (49.12% for one side crack) and in 2-direction decreases by a maximum of 92.2% (92.517% for one side crack) at this point in joint 3. The comparison of local strain ratios ε_{11} between one side crack and both side cracks for various locations of the structure are shown in Figure 5.15. It is observed that the strain ratios decrease at joints 2 and 4 as the length of crack increases for the "both sides" crack; but this phenomena is reversed when only "one side" crack occurs at joint 3. These changes can be utilized to identify whether the crack is on "one side" or "two sides" of the intersection. The maximum variation observed in joints 1, joint 3 and joint 4, are respectively, -1.40% (+6.94% for "one side" crack), +58.8% (+49.12% for one side crack), and -3.08% (+0.756% for "one side" crack). At all the other joints of structure, the variation of strain ratios ε_{11} is very small.

Figure 5.16 (a) and (b) show the variation of strain ratios ε_{11} and ε_{22} at a point on the chord surface that is 1.81m away from the saddle point of horizontal brace/chord intersection for "both sides" cracks. Figure 5.17 shows the comparison of results between "one side" crack and "both sides" cracks at this location. It shows a similar variation to that obtained for "one side" crack (refer Figures 5.12 and 5.13). From Figures 5.16 (a)

and (b), it is seen that strain ratios in local 1- and 2- directions increase by a maximum of 50.36% and 3.02%, respectively, at joint 3, and decreases by a maximum of 15.42% and 2.8%, respectively, at joint 5. The variation of strain ratios is almost negligible at other locations of the structure. From a comparison study of strain ratios between "both side" crack and "one side" crack at the same location of each joint of the structure, it is observed that the maximum variation of results are obtained at joints 1, 3 and 4. These variations in ε_{11} are 7.35%, 32.19% and 3.28%, respectively; insignificant differences of results are obtained at other locations of the structure. It is also observed that at joints 1, 2 and 3, the presence of crack on one side of the weld toe intersection gives a larger strain ratio than the two-side crack (see Figure 5.17). The reason for this obvious contradiction is that the small local changes produced in 1-direction strains (for "one side" crack) are neutralised by the strain releases that occur due to crack on the other side (for "two sides" cracks). From all the above analysis it is concluded that when a crack is developed at a joint intersection, strain ratios around that joint are affected more than at other joints; the crack also influences the strain ratios appreciably at other joints. Another mode of expression of the strain changes due to crack occurrence is given in Figures 5.18 and 5.19. Figure 5.18 (a) and (b) show the variation of strain ratios in local 1- and 2-directions at four locations on the chord surface at joint 3 for one side crack (the locations are at 0.073 m, 0.225 m, 0.75 m and 1.81 m away from the saddle point of horizontal brace/chord intersection). Figure 5.19 (a) & (b) show the variation of strains (in local 1- and 2- directions) at joint 3 for both side cracks. It is seen that in each case the maximum variation has occurred at a point that is located near the crack.

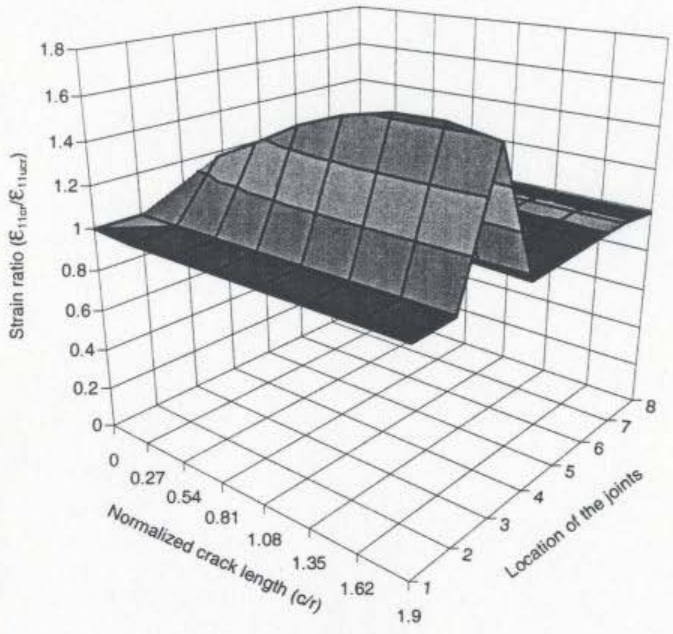

(a)

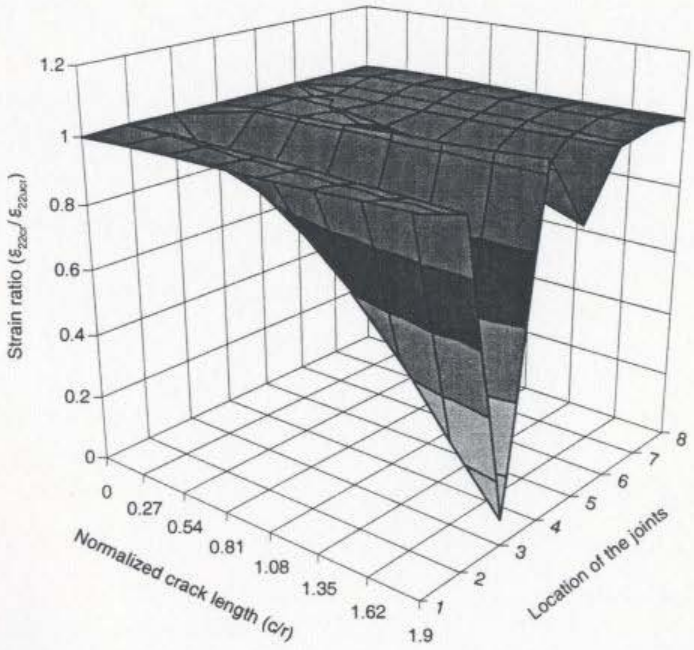

(b)

Figure 5.14 (a) and (b): Variation of strain ratios in local 1- and 2- directions at a point 0.225 m away from saddle point of horizontal brace/chord intersection in substructure 3 on chord surface (cracks on both saddle locations).

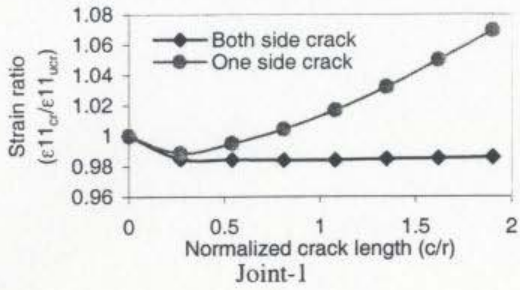

Joint-1

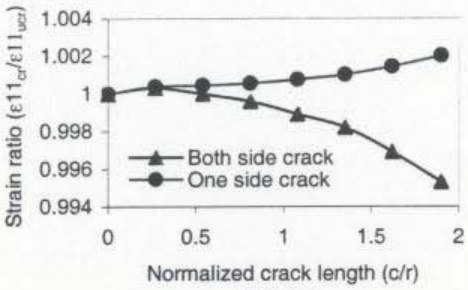

Joint-2

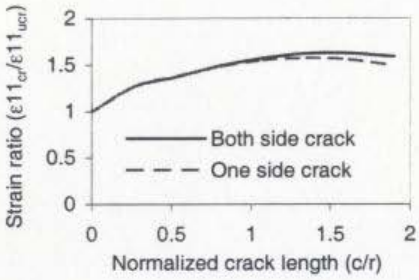

Joint-3

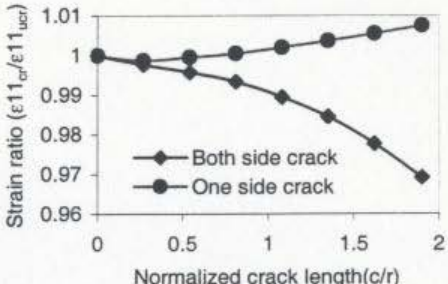

Joint-4

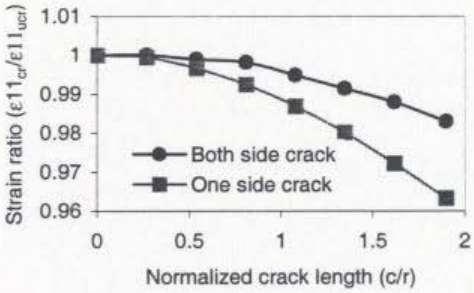

Joint-5

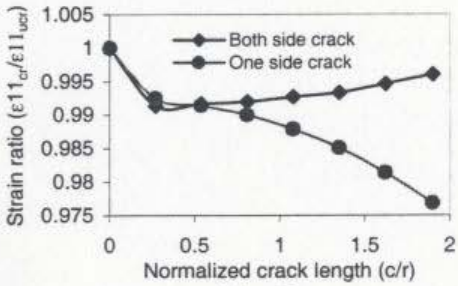

Joint-6

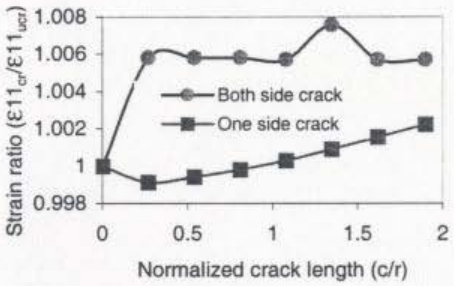

Joint-7

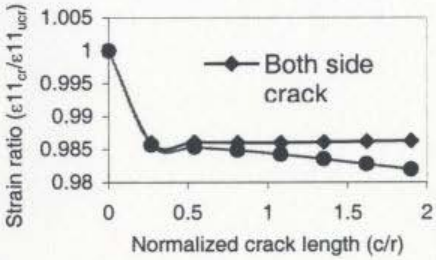

Joint-8

Figure 5.15: Comparison of strain ratios in local 1-direction at different locations of the frame between both side crack and one side crack (located at 0.03 m away from the intersection of horizontal brace and chord in substructure 3). All the points are considered at the same distance 0.225 m away from the saddle point of the corresponding joint.

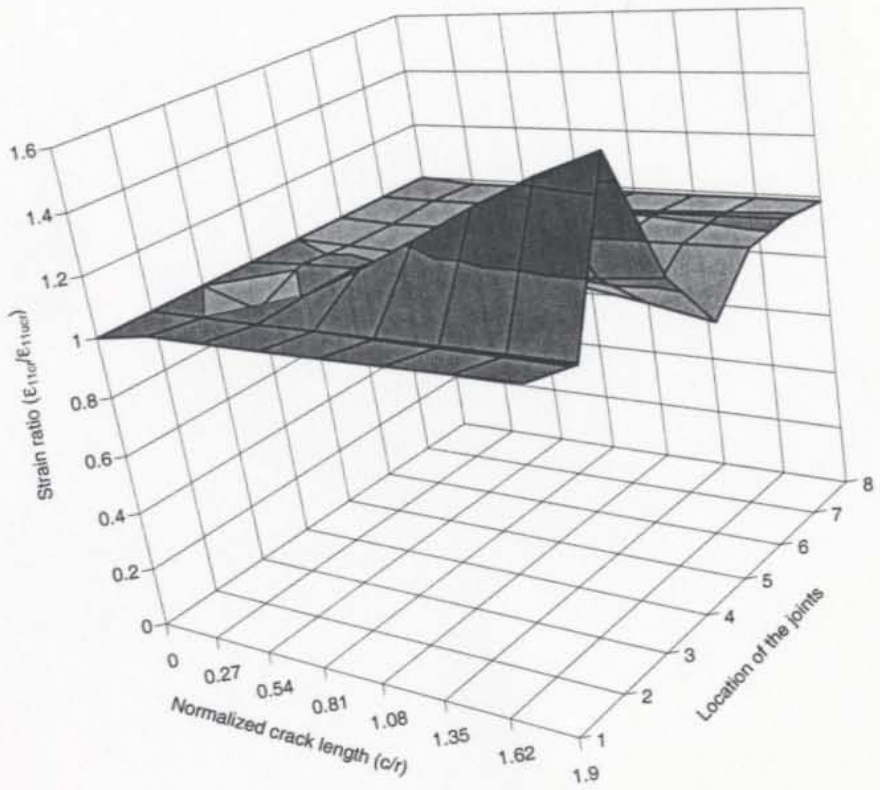
Strain ratio ($\varepsilon_{11d}/\varepsilon_{11undf}$)
1.6
1.4
1.2
1
0.8
0.6
0.4
0.2
0
0
0.27
0.54
0.81
1.08
1.35
1.62
1.9
Normalized crack length (c/r)
1
2
3
4
5
6
7
8
Location of the joints

(a)

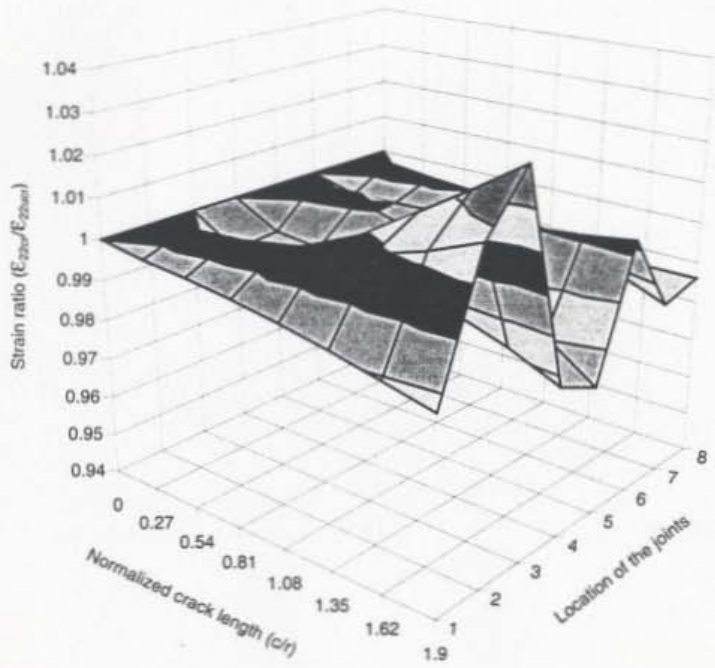

(b)

Figure 5.16 (a) and (b): Variation of strain ratios in local 1-direction and 2-direction at a point on the chord surface 1.81 m away from saddle point of horizontal brace/chord intersection for different lengths of "both sides" cracks at 0.03 m away from the intersection of joint-3.

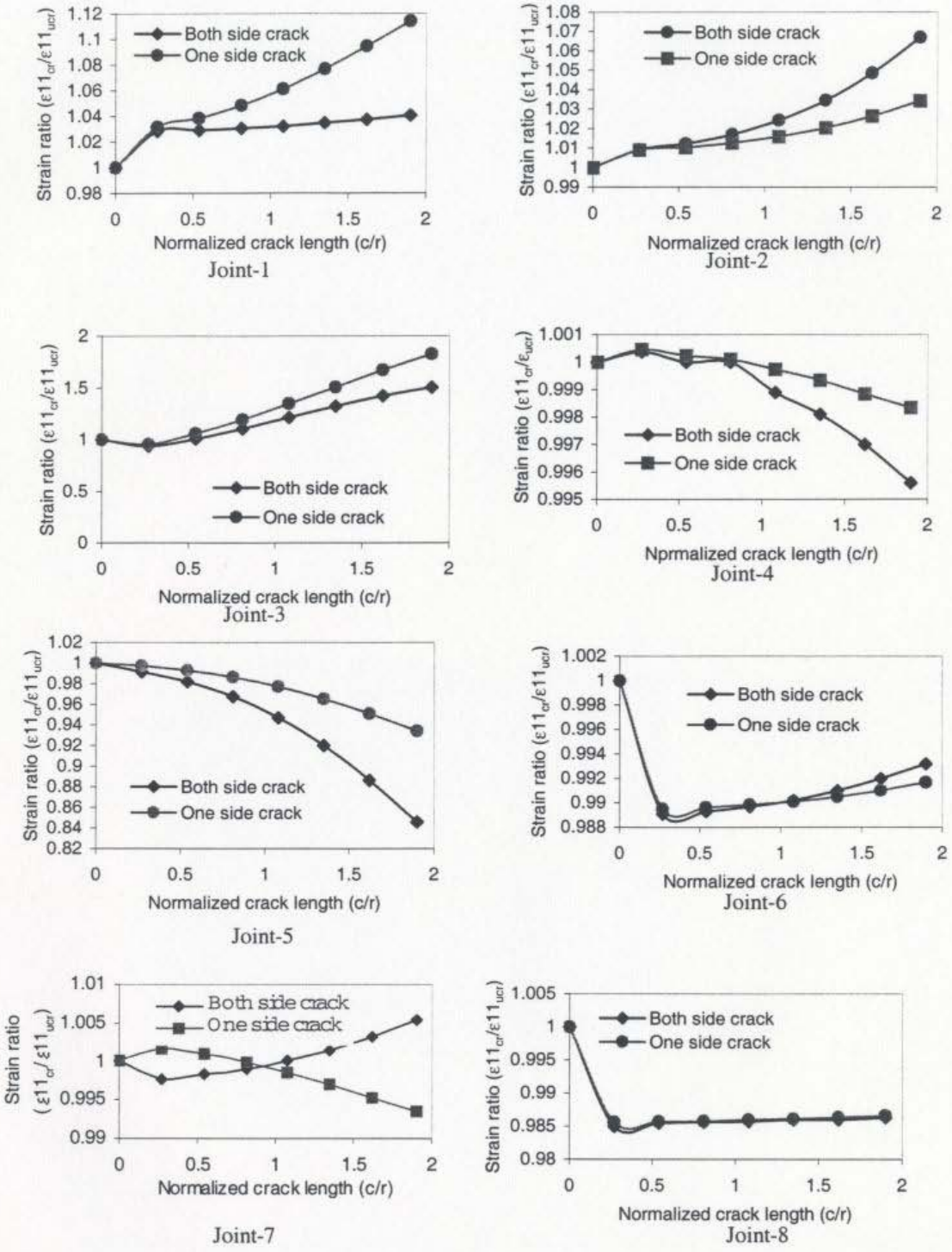

Figure 5.17: Comparison of strain ratios in local 1-direction at different locations of the frame between "both sides" crack and "one side" crack (located at 0.03 m away from the intersection of brace/chord at joint-3). (All points are considered at the same distance 1.81 m away from the saddle point in the corresponding joint).

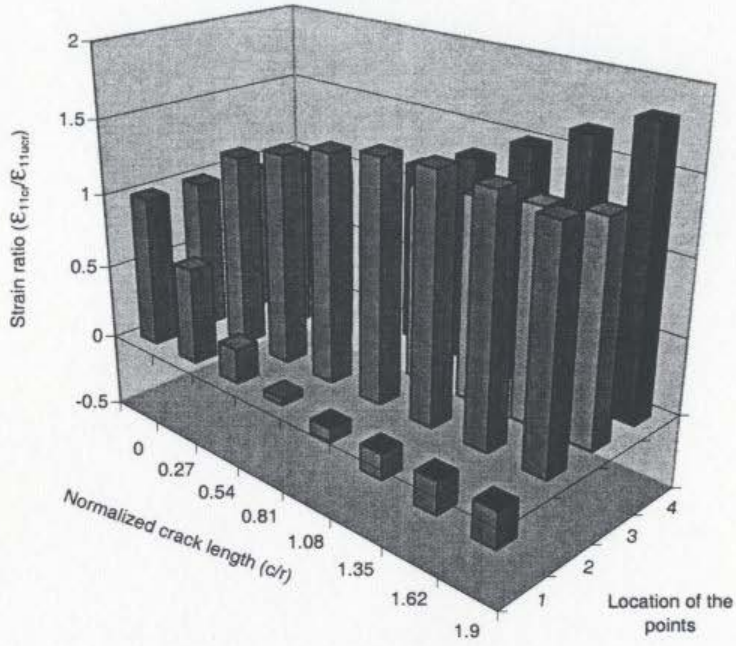

(a)

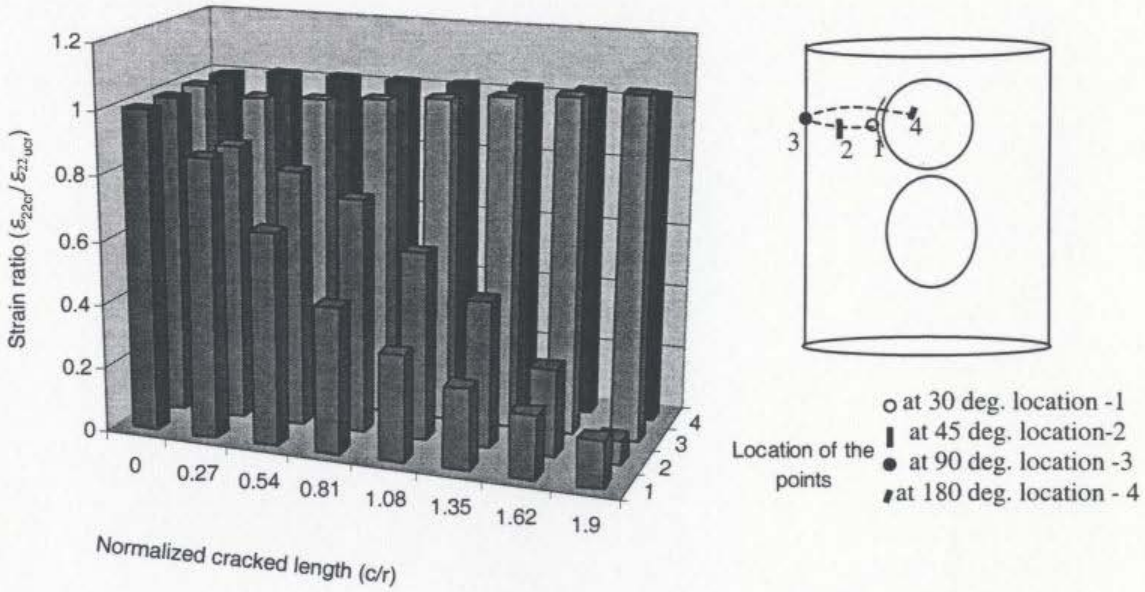

(b)

Figure 5.18 (a) and (b): Variation of strain ratios in local 1- and 2- directions at four locations on the chord, at joint 3 for "one side" cracks at joint-3.

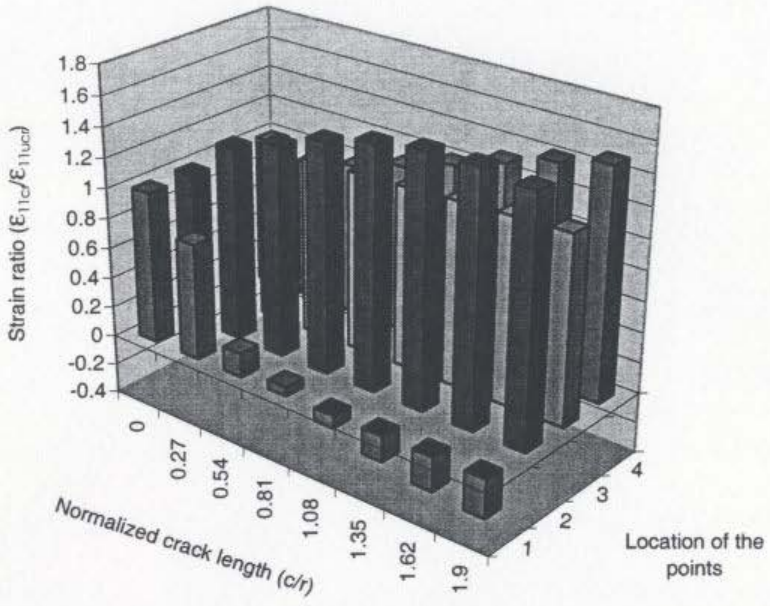

Figure 5.19 (a): Variation of strain ratios in local 1- direction at four locations on the chord at joint 3 for "both sides" cracks at joint-3.

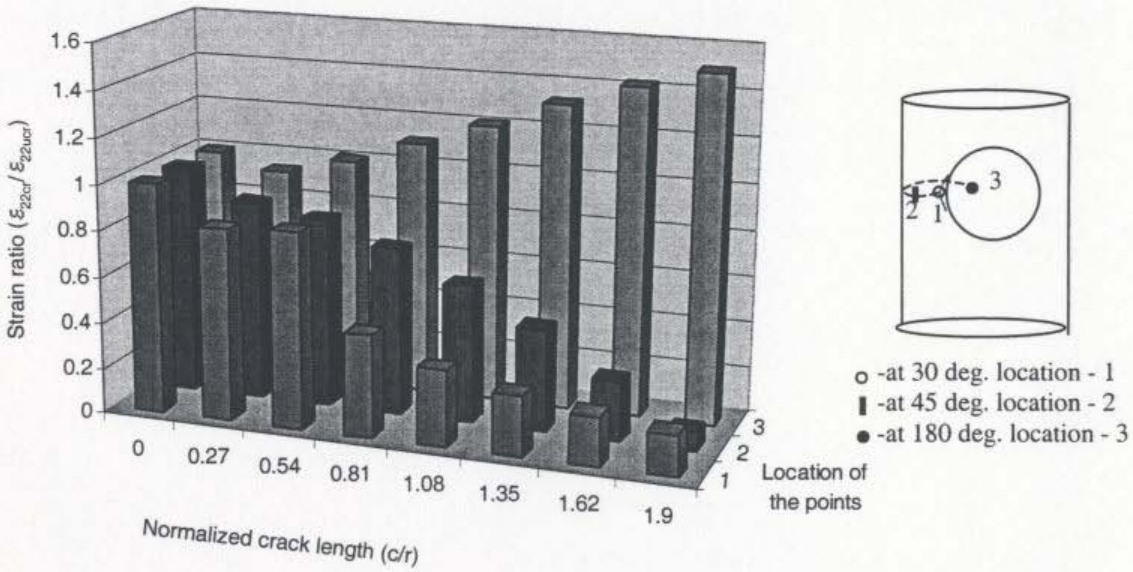

Figure 5.19 (b): Variation of strain ratios in local 2- directions at three locations (for better understanding of the variation) on the chord at joint 3 for "both sides" cracks at joint-3.

5.7 Influence on Global Responses due to Development of Crack in an Offshore Plane Frame Structure

Detection of crack in offshore structures using global parameters such as displacement, velocity, acceleration and strain is required for saving inspection period required for the purpose and wealth. By using this analysis one can find out which portion of the structure is affected by the presence of a crack. Thereafter, this region can be examined in greater detail to identify the crack properly. In the previous sections, the effect of local responses due to a crack at particular location (substructure 3) of the structure have been discussed at length. This section discusses the changes of global displacements in x-, y- and z-directions due to the presence of different length cracks at substructure 3. Figures 5.20 to 5.22 present the variation of these displacements with respect to the uncracked structure. The crack lengths considered in this study are 0.81 times and 1.9 times the brace radius. It is seen that the rate of change of displacement in all the figures is maximum within 10 to 30 m of the height of the frame. At all the other regions, this change is much smaller. Since crack is considered to be present in substructure 3 only and it is located at 20 m height of the frame, these changes indicate clearly that the crack is present around this region. This is a clear indicator for the crack presence.

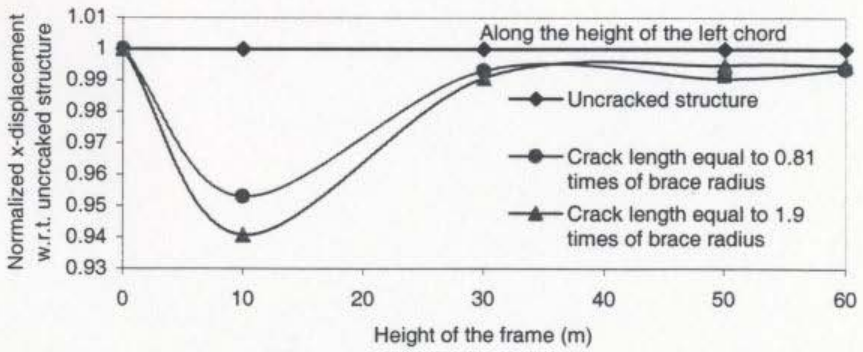

(a)

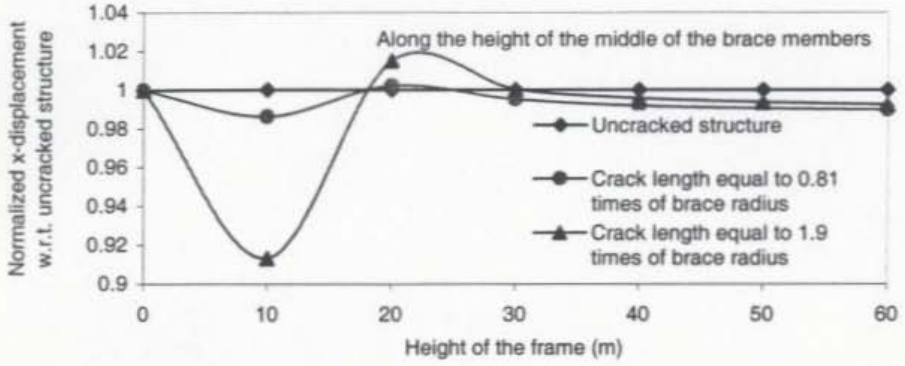

(b)

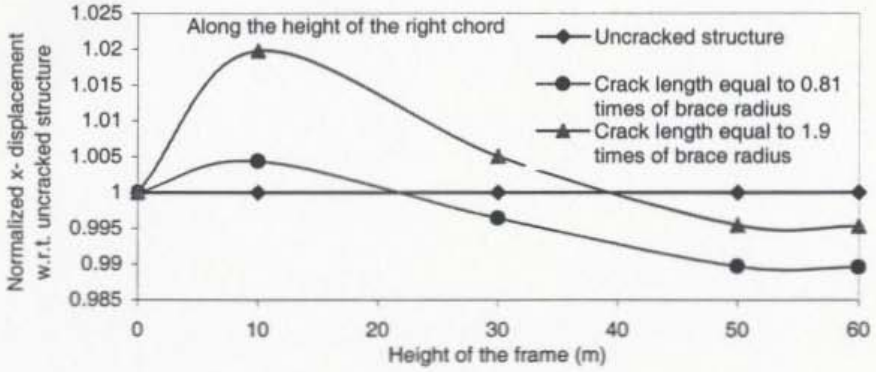

(c)

Figure 5.20 (a), (b) and (c): Comparison of global x-displacements along left chord member, middle of the braces and right chord member of the structure between uncracked and cracked structure due to crack in substructure 3.

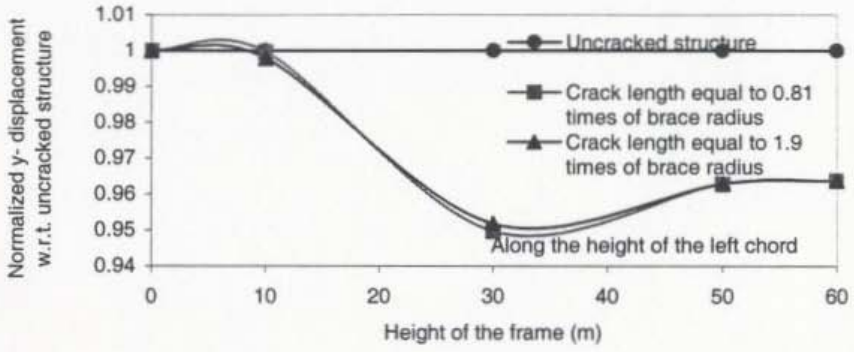

(a)

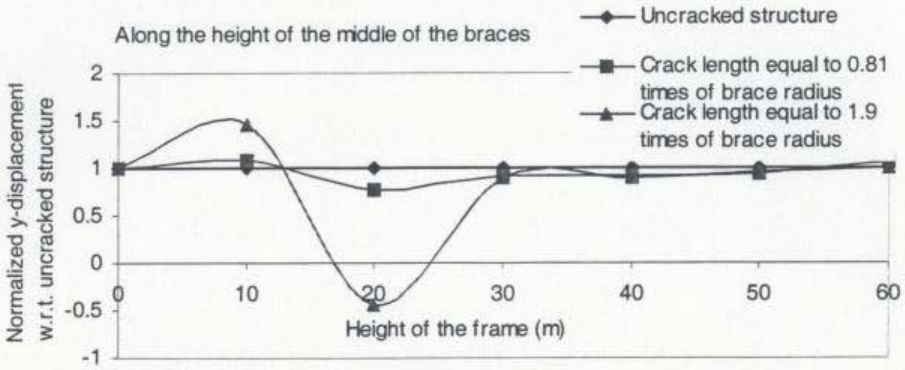

(b)

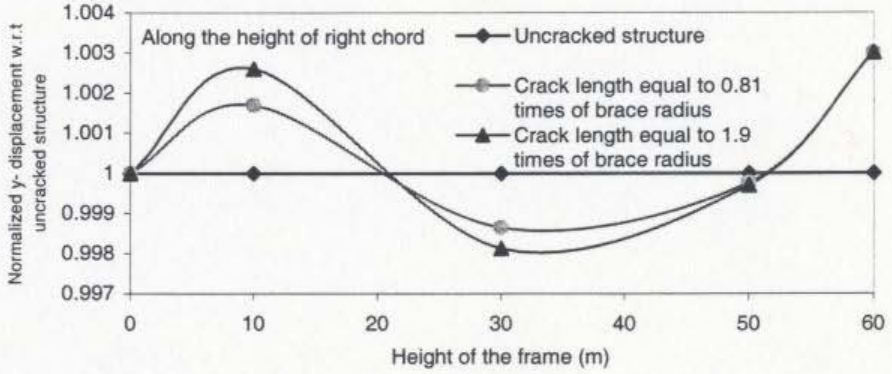

(c)

Figure 5.21 (a), (b) and (c): Comparison of global y-displacements along left chord member, middle of the braces and right chord member of the structure between uncracked and cracked structure due to crack in substructure 3.

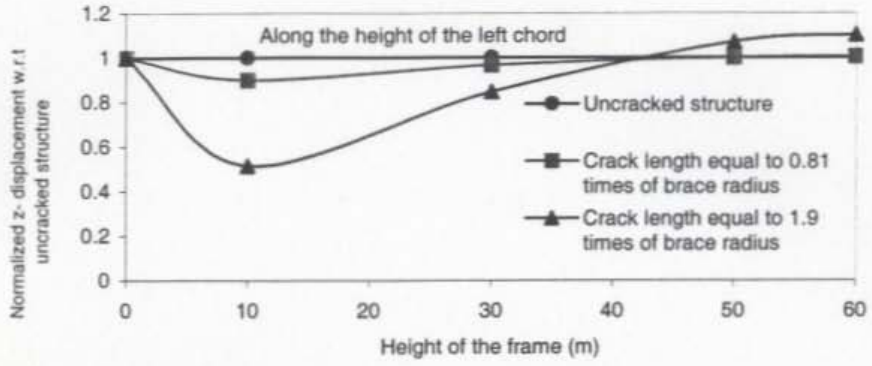

(a)

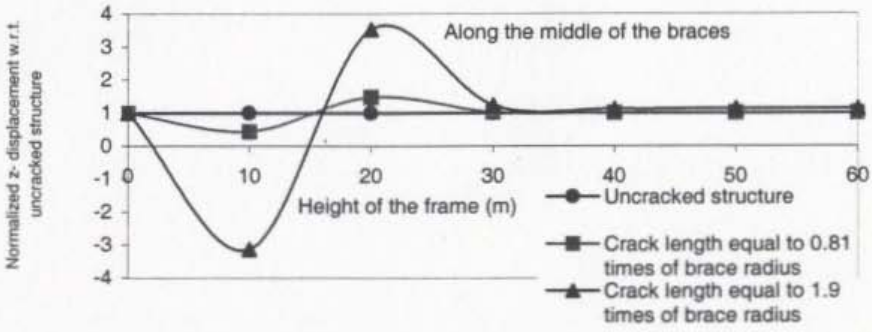

(b)

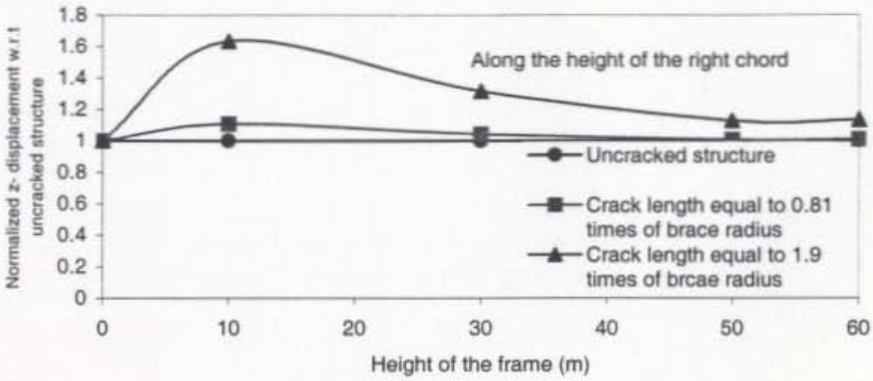

(c)

Figure 5.22 (a), (b) and (c): Comparison of global z-displacements along left chord member, middle of the braces and right chord member of the structure between uncracked and cracked structure due to crack in substructure 3.

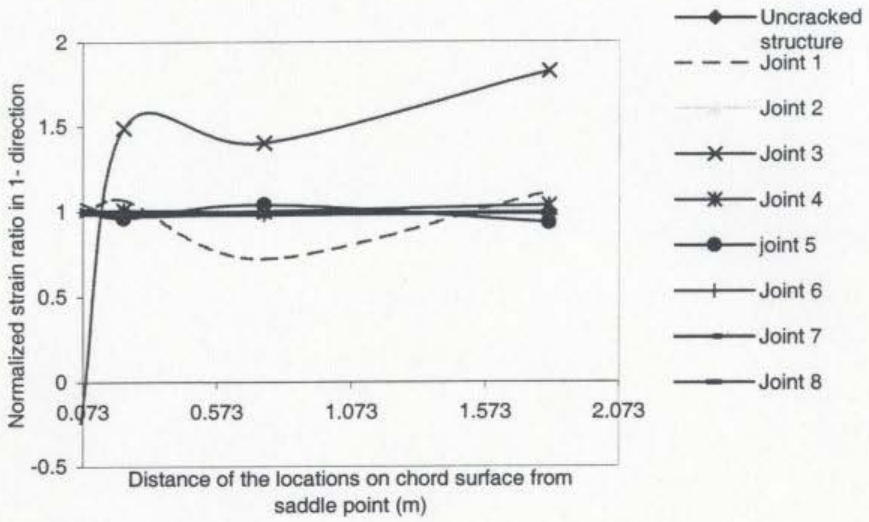

Figure 5.23: Comparison of strain ratios at different locations of the frame between uncracked and cracked structure (crack length equal to 1.9 times of brace radius) due to crack in substructure 3.

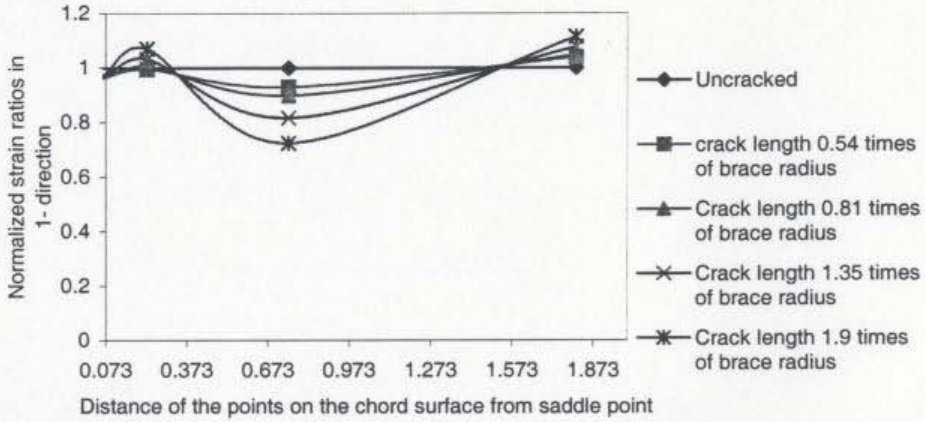

(a)

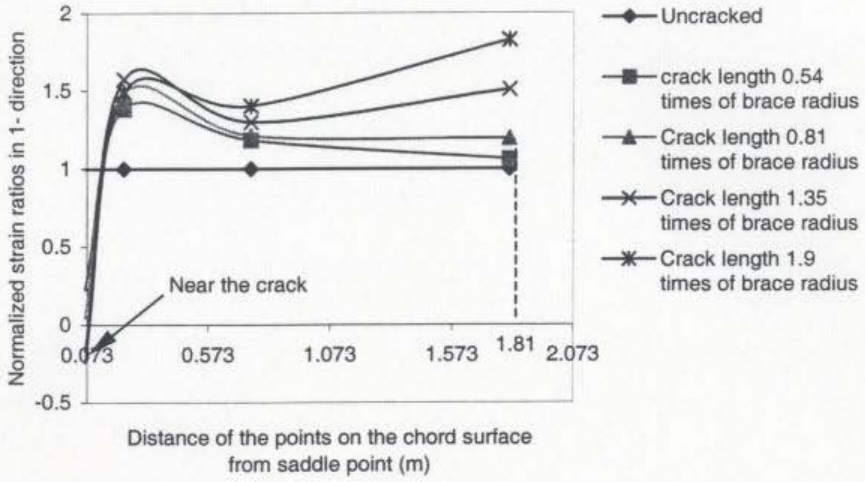

(b)

Figure 5.24: (a) Variation of strain ratios at different locations on the chord surface in joint 1 from the uncracked structure due to different lengths of crack at the critical region of substructure 3.

Figure 5.24: (b) Variation of strain ratios at different locations on the chord surface in joint 3 from the uncracked structure due to different lengths of crack at the critical region of substructure 3.

Figure 5.23 shows the variation of strain ratios at some points (0.073 m, 0.225 m, 0.75 m and 1.81 m away from the saddle point) of all the joints of the structure. This figure shows which joints were affected more by the crack in substructure 3. It is seen that joints 1 and 3 are affected more for this crack; joint 3 is affected quite a lot since the crack is located around its weld toe. Approximate location of crack within the structure could be found out by using this analysis. Figures 5.24 (a) and (b) show the variation of strain

ratios at some local points of joint 1 and joint 3. The figures show that joint 3 is affected more than joint 1. Moreover the maximum gradient of the curves occur near the origin of Figure 5.24 (a). For this reason, a detailed analysis should be performed for joint 3 to find out the exact location of the crack. It is observed that strain drop becomes large near the crack when crack length is increased gradually. At all the other points, the changes in strains are less than those at points near the crack.

5.8 Summary

The effect on local strains in 1- and 2- directions near the crack and at other locations of the entire structure due to different lengths of cracks at critical region of substructure 3 have been discussed in this chapter. The effects of crack on both sides of the intersection of those locations mentioned above, have also been shown in this study. In order to determine the probable location of crack a comparison study of the results obtained from uncracked and cracked structures at some local points of the cracked joints have been made. The differences of local strain ratios at four locations on the chord, around the cracked joint (in substructure 3), for "one side" crack and "both sides" crack have also been presented for this study. To determine the approximate location of the crack, global analysis using displacements of the substructure boundary nodes, between uncracked and cracked structures, has been carried out. This analysis would identify the approximate location of the crack.

Chapter 6

Conclusions and Recommendations

6.1 Conclusion

In order to develop a method to detect and identify cracks in steel jacket offshore platforms based on global and local responses (deformation, stress and strain), finite element method was used for numerical studies. Since the analysis of a complex large scale structure like a steel offshore platform using eight noded degenerate isoparametric shell elements would give a very large number of degrees of freedom, substructure technique was used to solve this problem. Also, a two-dimensional plane frame was considered instead of the three-dimensional space frame structure. For the whole structure, eight substructures were considered and the total degrees of freedom (DOFs) for the entire structure were obtained as 211,270. Substructure 3 alone, where the crack was located, had 36,670 DOFs. When substructuring approach was applied it reduced the DOFs to 1180.

Although this structure is subjected to a cyclic wave loading from the sea environment, the analysis was carried out by considering only a concentrated load applied at the top of the frame (for simplicity in calculations). Displacements, stresses and strains were obtained by analyzing this structure using ABAQUS finite element software. Since stress measurement is not convenient in practical cases, global displacements and local strains

approach were used to obtain information regarding the detection of cracks in an offshore structure.

The results obtained from the study are given below:

1. For the accuracy of analysis, the results obtained from substructure approach (with shell elements) were compared with those obtained using beam elements. The differences between the two analyses were within 5-10%.
2. Mesh refinement was checked by considering 24, 48 and 96 elements around the weld toe regions of brace and chord members, near the intersection. The local stress on chord member for 96 elements was 10-15% greater than those obtained with 48 elements (used in the present study for all cases in substructure 3).
3. Maximum stress (hot spot stress) in local 1-direction was developed at an angle of 88.25 and 271.75 degrees from the bottom crown and it was located at the weld toe on the uncracked chord surface of horizontal brace/chord intersection.
4. Local stresses in 1- and 2- directions decreased enormously in all the cracked elements. However, the decrease was considerable near the tip of crack.
5. Due to development of crack (crack lengths equal to 0.81 times and 1.35 times of brace radius) at the hot spot, the changes of stresses in local 1- direction were observed to be 95.411% and 116.85% near the crack (at a point 0.043m away from the crack on the chord surface). However, these changes were respectively 48.23% and 57.368% at 0.225 m away and 19.376% and 50.68% at 1.81 m away, from the horizontal brace/chord intersection (on chord surface).

6. From the comparison study of "without quarter point" nodes and "with quarter point" nodes, it was observed that if mid-side nodes of the isoparametric thin shell element were shifted to the quarter points near the crack tip, the stress singularity was modelled in a better way.
7. The principal plane angle varied by 666.21%, and 53.57% at locations 0.073 m and 0.225 m away from the saddle of horizontal brace/chord intersection on the chord surface, respectively, and by 103.08% at 1.81 m away location from the saddle point, when the crack length considered was 0.27 times of brace radius. These results show that examination of changes of principal plane angles could also be used to identify the "through-thickness" crack initiation.
8. The variation of stresses for "one side" crack of the intersection was obtained similar to those obtained from the "both sides" crack of the same joint. Also differences of results between the two cases were less than 20%.
9. Strain variations were observed to be more than 95% at a point 0.043 m away from the crack (saddle) when crack length considered was 1.9 times the brace radius. However, it was less than 60% in the far away (0.225 m, 0.75 m and 1.81 m) locations on the chord surface of the cracked joint and less than 17% at other joint locations.
10. Maximum rate of change of global displacements in a cracked structure occurred between heights of 10 m and 30 m along the left chord, middle of all braces and the right chord. This could be used to determine the approximate location of crack in a structure.

From the results of above analyses, it can be concluded that large strain changes occur near the crack region and they could be used as indicators for the detection of any kind of faults such as cracking, debonding, delamination, loosening of parts, etc. The measurement of these changes can be made by using triaxial strain gauge sensors at predetermined critical regions of the structure. In addition the slope of the displacement diagram over the whole height of the structure could also be used to affirm the presence of the crack.

6.2 Recommendations

The following additional investigations are recommended to complete the studies reported in this thesis:

1. Analyses need to be carried out considering three-dimensional space frame structure with shell elements.
2. In order to find out the exact hot spot location very fine meshes (having more than 96 elements) should be used around the intersection of all joints.
3. Preparation of model of crack using 3-D solid elements and arbitrary geometry of cracks, that usually occur in real life structures, should be considered in the analyses.
4. A non-modal crack identification methodology, using a procedure similar to the one proposed earlier by Owolabi (2001), could also be developed for this large-scale prototype structure; the cracks are to be located sequentially at the weld toe regions of eight substructures and the results processed accordingly. This will exactly identify the crack size and crack location.

5. Analyses need to be performed considering dynamic random loading.
6. During the analysis of uncracked and cracked structures, the effect due to the settlement of foundation, rotation of foundation and stacking of loads on the super-structure should also be taken into consideration.

References

ABAQUS Theory Manual, Hibbitt, Karlsson and Sorensen Inc., R. I. USA, 1999, Version 5.8.

ABAQUS Standard User's Manual, Hibbitt, Karlsson and Sorensen Inc., R. I. USA, 1999, Version 5.8, Vols. I, II

ABAQUS Post Manual, Hibbitt, Karlsson and Sorensen Inc., R. I. USA, 1999, Version 5.8.

Ahmad, S, Irons, B. M., and Zienkiewicz, O. C., 1970. "Analysis of Thick and Thin Shell Structures by Curved Finite Elements". International Journal for Numerical Methods in Engineering, Vol.2, pp. 419-451.

Barsoum, R. S., 1976. "A Degenerate Solid Element for Linear Fracture Analysis of Plate Bending and General Shells". International Journal for Numerical Methods in Engineering, Vol. 10, pp. 551-564.

Berge, S., 1996. "Fatigue Strength of Tubular Joints". Fatigue in Offshore Structures, A.A.Balkema/Rotterdam/Brookfield, Vol.2, pp. 335-358.

Bowness, D., and Lee, M. M. K., 1994. "Crack Curvature Under the Weld Toe in a Tubular Joint: A Three-Dimensional Numerical Investigation". Proceedings of the Fourth International Offshore and Polar Engineering Conference Osaka, Japan, Vol. 4, pp. 664-669.

Brahmi, K., Bouhaddi, N., and Fillod, R., 1995. "Reduction of the Junction Degrees of Freedom before Assembly in Dynamic Substructuring". Design Engineering Technical Conferences, Vol. 3, Part B.

Bucak, O., Mang, F., and Herion, S., 1993. "Development and Propagation of Cracks in Welded Hollow Section Joints under Uniaxial and Multiaxial Loading". International Conference on Offshore Mechanics and Arctic Engineering, Vol. 3, pp. 159-166.

Burdekin, F. M., 1985. "Engineering Design Against Fracture at Stress Concentrations". Material Science and Technology, Vol. 1, pp. 487-493.

Cheng, S., 1998. "Non-destructive Evaluation of Cracking in Tubular T-Joints Using Vibration Procedures". Ph. D. Thesis, Memorial University of Newfoundland St. John's, Canada, pp. 13-20.

Chen, Y., and Swamidas, A. S. J., 1993. "Change of Modal Parameters due to Crack Growth in a Tripod Tower Platform". Canadian Journal of Civil Engineering, Vol. 20, No.5, pp. 801-813.

Cook, R. D., Malkus and Plesha, M. E., 1989. "Concepts and Applications of Finite Element Analysis". 3rd Edition, John Wiley and Sons, Inc, New York.

Doherty, W. P., Wilson, E. L., and Taylor, R. L., 1969. "Stress Analysis of Axi-Symmetric Solids using Higher Order Quadrilateral Finite Elements". Structural Engineering Laboratory Report No. SESM 69-3, University of California, Berkeley.

Dover, W. D., and Rao, A. G. M., 1996. Fatigue in Offshore Structures, A.A.Balkema/Rotterdam/Brookfield, Vol. 2, pp. 336-338, 691-705.

Farrar, C. R., Baker, W. E., Bell, T. M., Cone, K. M., Darling, T. W., Duffey, T. A., Eklund, A., and Migliori, A., 1994. "Dynamic Characterization and Damage Detection in the I-40 Bridge Over the Rio Grande". Los Alamos National Laboratory report LA-12767-MS.

Fox, C. H. J., 1992. "The Location of Defects in Structures: a Comparison of the Use of Natural Frequency and Mode Shape Data". Proceedings of the 10th International Modal Analysis Conference, Vol. 1, pp. 522-528.

Gdoutos, E. E., 1993. Fracture Mechanics An Introduction, Kluwer Academic Publishers, Dordrecht / Boston / London, pp. 1-13, 15-27.

Gomes, A. J. M. A., and Silva, J. M. M. E., "Theoretical and Experimental Data on Crack Depth Effects in the Dynamic Behavior of Free-Free Beams". Proceedings of the 9th International Modal Analysis Conference, Vol. 1, pp. 274-283.

Griffith, A. A., 1920. "The Phenomena of Rupture and Flaw in Solids". Transactions, Royal Society of London, Ser. A., Vol. 221, p.163.

Haisty, B. S., and Springer, W. T., 1985. "The Longitudinal Vibration Characteristics of a Uniform Beam Containing Two Symmetric Discontinuities". Proceedings of the Society for Experimental Mechanics, Spring conference, pp. 389-393.

Haisty, B. S., and Springer, W. T., 1988. "A General Beam Element for Use in Damage Assessment of Complex Structures". Journal of Vibration, Acoustics, Stress and Reliability in Design, Vol. 110, pp. 389-394.

Harvey, Robert, L., 1994. Neural Network Principles, Prentice–Hall, Inc, pp. 2.

Henshell, R. D., and Shaw, K. G., 1975, "Crack Tip Elements are Unnecessary". International Journal for Numerical Methods in Engineering, Vol. 9, pp. 495-509.

Hinton, E., and Owen, D., R., J., 1984. Finite Element Software for Plates and Shells, Pineridge Press, Swansea, U.K., pp. 235-326.

Hughes, T. J. R., Cohen, M., and Haroun, M., 1978. "Reduced and Selective Integration Techniques in the Finite Elements Analysis of Plates". Numerical Methods in Engineering and Design, Vol. 46, pp. 203-222.

Inglis, C. E., 1913. "Stresses in a Plate due to presence of Cracks and Sharp Corners". Proceedings, Institute of Naval Architects, Vol. 60.

Johal, R. S., 2000. "An Efficient Method for Transient Data Recovery from Large DOF FE model". International Modal Analysis Conference (San Antonio, Texas), Vol. 1, pp. 208-212.

Kudva, J., Munir, N., and Tan, P., "Damage Detection in Smart Structures Using Neural Networks and Finite Element Analysis". Proceeding of ADPA/AIAA/ASME/SPIE Conference on Active Materials and Adaptive Structures, pp. 559-562.

Lie, S. T., Chiew, S. P., Lee, C. K., Wong, S. M., and Huang, Z. W., 2000. "Modelling Arbitrary Through-Thickness Crack in a Tubular T-Joint". Proceeding of the Tenth International Offshore and Polar Engineering Conference Seatle, USA, Vol. 4, pp. 53-58.

Mcguire, W., and Gallagher, R. H., 1979. Matrix Structural Analysis, John Wiley & Sons, pp. 328-340.

Nwosu, D.I., 1993. "Fatigue Strength Analysis of Offshore Tubular Welded Joints under Constant Amplitude Loading: Local Strain and Fracture Mechanics Approach". Ph.D. Thesis, Memorial University of Newfoundland St. John's, Canada, pp. 90-96, 121-124, 139-149.

Owolabi, G. M., 2001. "Crack Identification Procedures in Beam Using Experimental Modal Analysis". Master's thesis, Memorial University of Newfoundland St. John's, Canada, 132 p.

Pandey, A. K., Biswas, M., and Samman, M. M., 1991. "Damage Detection from Changes in Curvature Mode shapes". Journal of Sound and Vibration, Vol. 145, No. 2, pp. 321-332.

Paranavitana, S., 1996. "Symmetric and Asymmetric Crack Development in Tubular T-joints". Master's Thesis, Memorial University of Newfoundland St. John's, Canada, 89 p.

Parks, D. N., Lockett, R., and Brockenbrough, J. R., 1981. "Stress-Intensity Factors for Surface Cracks in Plates and Cylindrical Shells using Line-Spring Finite Elements". Proceedings of the Winter Annual Meeting, ASME, Washington, D.C., pp. 279-285.

Przemieniecki, J. S., 1968. Theory of Matrix Structural Analysis, McGraw-Hill Book Company, pp. 231-263.

Qian, R. J., 1996. "Applying Strain Energy Density Factor Theory to Propagation Estimating of Surface Crack in Tubular T-Joints". Engineering Fracture Mechanics, Vol. 53, No. 6, pp. 849-858.

Reddy, D. V., and Arockiasamy, M., 1991. Offshore Structures, Krieger Publishing Company, Malabar, Florida, Vol. I, pp. 1-65.

Rice, J. R. and Levy, N., 1972b. "The Part-through Surface Crack in an Elastic Plate". Journal of Applied Mechanics, Vol. 39, pp. 185-194.

Roitman, N., Batista, R. C., Magluta, C., Viero, P. F., and Sarquis, F. M., 1991. "Identification of Structural Damages in Fixed Offshore Platforms". Proceeding of the 1st International Offshore and Polar Engineering Conference, Vol. IV, pp. 77-83.

Sih, G. C., and Hagendorf, H. C., 1977. "On Cracks in Shells with Shear Deformation". Mechanics of Fracture, Vol. 3, pp. 201-229.

Springer, W. T., Lawrence, K. L. and Lawley, T. J., 1987. "The effect of a Symmetric Discontinuity on Adjacent Material in a Longitudinally Vibrating Uniform Beam". Experimental Mechanics, Vol. 27, pp. 168-171.

Swamidas, A. S. J., and Chen, Y., 1992. "Damage Detection in a Tripod Tower Platform (TTP) Using Modal Analysis". Proceeding of ASME Conference on Offshore Mechanics and Arctic Engineering, Vol. I-B, pp. 577-583.

Thomson, W. T., and Madison, W., 1949. "Vibration of Slender Bars with Discontinuities in Stiffness". Journal of Applied Mechanics, Vol. 17, pp. 203-207.

Wang, B., Kurobane, Y., and Makino, Y., 1997. "Damage Criterion and Ultimate Strength for Tubular Joints". Proceedings of the Seventh International Offshore and Polar Engineering Conference, Vol. 4, pp. 132-138.

Wang, B., and Hu, N., 2000. "Study of Spherical Shell with a surface Crack by the Line-Spring Model". Engineering Structures, Vol. 22, pp. 1006-1012.

Williams, W. L., 1961. "The Bending Stress Distribution at the Base of a Stationary Crack". Journal of Applied Mechanics, Transaction ASME Series E, Vol. 82, pp. 78-82.

Yang, J. C. S., Dagalakis, N. G., and Hirt, M., 1980. "Application of the Random Decrement Technique in the Detection of an Induced Crack on an Offshore Platform Model". Computational Methods for Offshore Structures, ASME Publication, AMD, Vol. 37, pp. 55-67.

Yun, C. B., and Bahng, E. Y., 2000. "Substructure Identification Using Neural Networks". Computers and Structures, Vol. 77, pp. 41-52.

Zienkiewicz, O. C., Taylor, R. L. and Too, J. M., 1971. "Reduced Integration Technique in General Analysis of Plates and Shells". International Journal for Numerical Methods in Engineering, Vol. 3, pp. 275-290.

Zubaydi, A., 2001. "Use of Neural Networks for the Identification of Damage in Ship Structures". Ph.D. Thesis, Memorial University of Newfoundland St. John's, Canada.

Appendix

Shape Functions (Nwosu 1993)

i	N_i	$\frac{\delta N_i}{\delta \xi}$	$\frac{\delta N_i}{\delta \eta}$
1	$1/4(1-\xi)(1-\eta)(-\xi-\eta-1)$	$1/4(2\xi+\eta)(1-\eta)$	$1/4(1-\xi)(2\eta+\xi)$
2	$1/4(1+\xi)(1-\eta)(\xi-\eta-1)$	$1/4(2\xi-\eta)(1-\eta)$	$1/4(1+\xi)(2\eta-\xi)$
3	$1/4(1+\xi)(1+\eta)(\xi+\eta-1)$	$1/4(2\xi+\eta)(1+\eta)$	$1/4(1+\xi)(2\eta+\xi)$
4	$1/4(1-\xi)(1+\eta)(-\xi+\eta-1)$	$1/4(2\xi-\eta)(1+\eta)$	$1/4(1-\xi)(2\eta-\xi)$
5	$1/2(1-\xi^2)(1-\eta)$	$-\xi(1-\eta)$	$-1/2(1-\xi^2)$
6	$1/2(1+\xi)(1-\eta^2)$	$1/2(1-\eta^2)$	$-(1+\xi)\eta$
7	$1/2(1-\xi^2)(1+\eta)$	$-\xi(1+\eta)$	$1/2(1-\xi^2)$
8	$1/2(1-\xi)(1-\eta^2)$	$-1/2(1-\eta^2)$	$-(1-\xi)\eta$

Assuming,

$$\xi_0 = \xi\xi_i, \qquad \eta_0 = \eta\eta_i \tag{A.1}$$

The shape function can be written as in the following form,

$$N_i = \frac{1}{4}(1+\xi_0)(1+\eta_0) \tag{A.2}$$

This form permits to write down all the shape functions in one expression. These are:

1. Corner node with $\xi i = \pm 1$ and $\eta i = \pm 1$

$$N_i = \frac{1}{4}(1+\xi_0)(1+\eta_0)(\xi_0+\eta_0-1) \tag{A.3}$$

2. Mid-side nodes with (ξ_i, η_i) equate to $(0, \pm 1)$ and $(\pm 1, 0)$

$$\xi_i=0, \quad N_i = \frac{1}{2}(1-\xi^2)(1+\eta_0) \tag{A.4}$$

$$\eta_i=0, \quad N_i = \frac{1}{2}(1+\xi_0)(1-\eta^2) \tag{A.5}$$